Transport properties of InAs Nanowhiskers

Master Thesis
to obtain the degree of Master of Science Physics

at Fachbereich Physik
Universität Duisburg-Essen

submitted by
Vadim Migunov
from Sarov, Russian Federation

May 2009

Contents

Abstract

The transport properties of InAs nanowhiskers with different atomic structures have been investigated by in-situ transmission electron microscope equipped with scanning tunneling microscope unit. This novel technique allows studing transport properties of a single nanoscale object and correlating them directly with the observed atomic structure. The experiments on transport properties of InAs nanowhiskers prepared by metal organic chemical vapor deposition show that:

1. the resistivity of wires with Wurtzite atomic structure is lower than the resistivity of wires with mixture of Wurtzite and Zinc Blende atomic structures,
2. the transport properties strongly depend on electron beam irradiation – irradiated sample shows less conductivity,
3. the resistivity depends on mechanical deformations – deformed nanowires are non-conductive.

The resistance measurements were also performed in presence of magnetic field (about 1 T) but the current-voltage data for both cases (with and without magnetic field) found to be the same.

The special part of the study is dedicated to electrical properties of the interface between the InAs nanowire and the gold cap. It was shown that the interface play an important role in the electronic transport through the nanowires, it increases the resistivity and probably results in non-ohmic transport behavior.

Chapter 1. Introduction

Introduction

InAs is a very interesting semiconducting material, which has potential applications in high-speed circuits and other special devices, like superconductor/normal conductor/superconductor Josephson junction devices [1]-[3] and dilute magnetic semiconductor devices. [4]-[5] Also InAs nanowires are especially interesting because they exhibit a lower effective electron mass, a higher carrier mobility, a larger energy level separation, a higher efficiency, and lower threshold [6] at room temperature in comparison to other semiconductor nanowires. From device point of view, they could be applied in electronic and optoelectronic devices based on nanowires and superlattices. The nanowires have been found to be very attractive due to their potential for low-power and high speed applications [7],[8]. They also allow epitaxial combination with a variety of semiconducting materials [9] (for example indium phosphite, germanium, galium, silicon), even for large lattice mismatches [10] (up to 12% in case of InAs/Si). Because of the small contact area between the wire and the substrate (here GaN), the former can relax easily and remains virtually free of dislocations in the volume [11]. Furthermore, semiconductor nanowires are of great interest for basic studies since they represent one-dimensional structures in terms of electronic transport [12] at wires diameters of 1 to 100 nm [13].

Electrical measurements of nanowhiskers are often made after a multistep preparation process, including electron beam lithography, metal deposition, etching and lift-off techniques. Each process step is a source of uncertainties and errors such as wires deformations or additional doping with contact material. Several groups studied electronic transport properties of indium arsenide nanowires prepared by the above mentioned techniques [14]-[18], and obtained sometimes conflicting results [17]-[18], most probably due to different wires structures.

The experimental investigation of electronic transport processes and their correlation with the atomic structure of the same wires was the aim of this work. In this thesis I use a novel technique: a combined Scanning Tunneling Microscopy and Transmission Electron Microscopy study in one apparatus will be presented. The technique provides the possibility to study electronic transport properties of a single as prepared nanostructure (here nanowhiskers) and simultaneously the structural properties.

Chapter 2. Theoretical background

2.1 InAs bulk properties

Indium (III) arsenide has been well studied (for a review see [19]) and represents a commonly used semiconductor material. Bulk InAs has a cubic Zinc Blende structure (figure 2-1) with the lattice constant a = 6.058 Angstrom, and easily forms alloy with Ga, Sb or Al. The melting point is 1215 K.

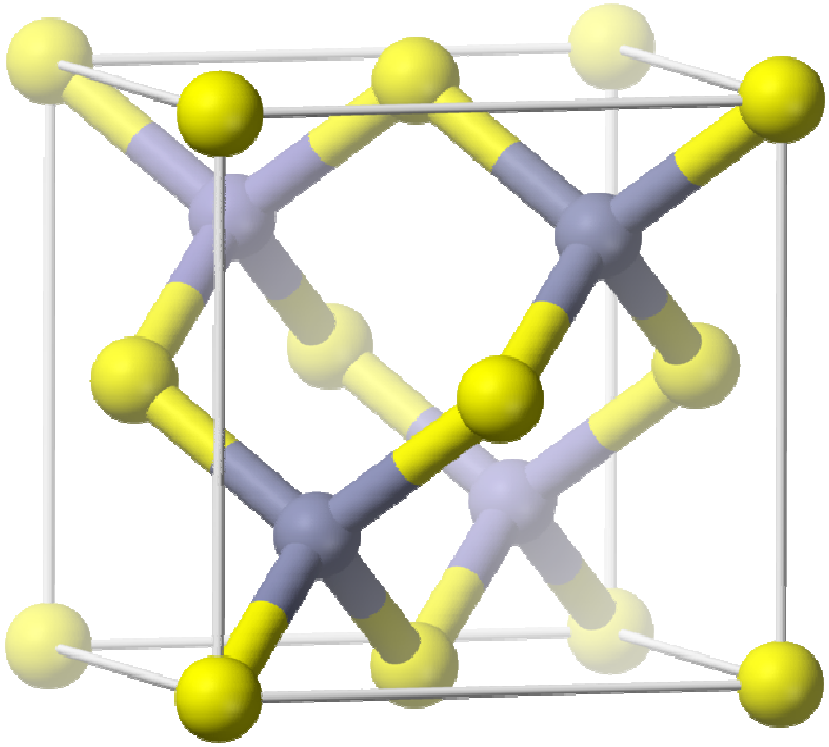

Figure 2-1. Cubic Zinc Blende structure. In case of InAs, In^{3+} atoms are yellow and As^{3-} atoms are grey.

Indium arsenide has a band gap of 0.354 eV. The intrinsic carrier concentration of $1 \cdot 10^{15}$ cm^{-3} yields an intrinsic resistivity of 0.16 Ohm·cm. The electronic band structure is shown in figure 2-2 [19]. The indirect band gap of 1.08 eV and 1.37 eV at the L and X points results in different electrical properties in different crystallographic directions.

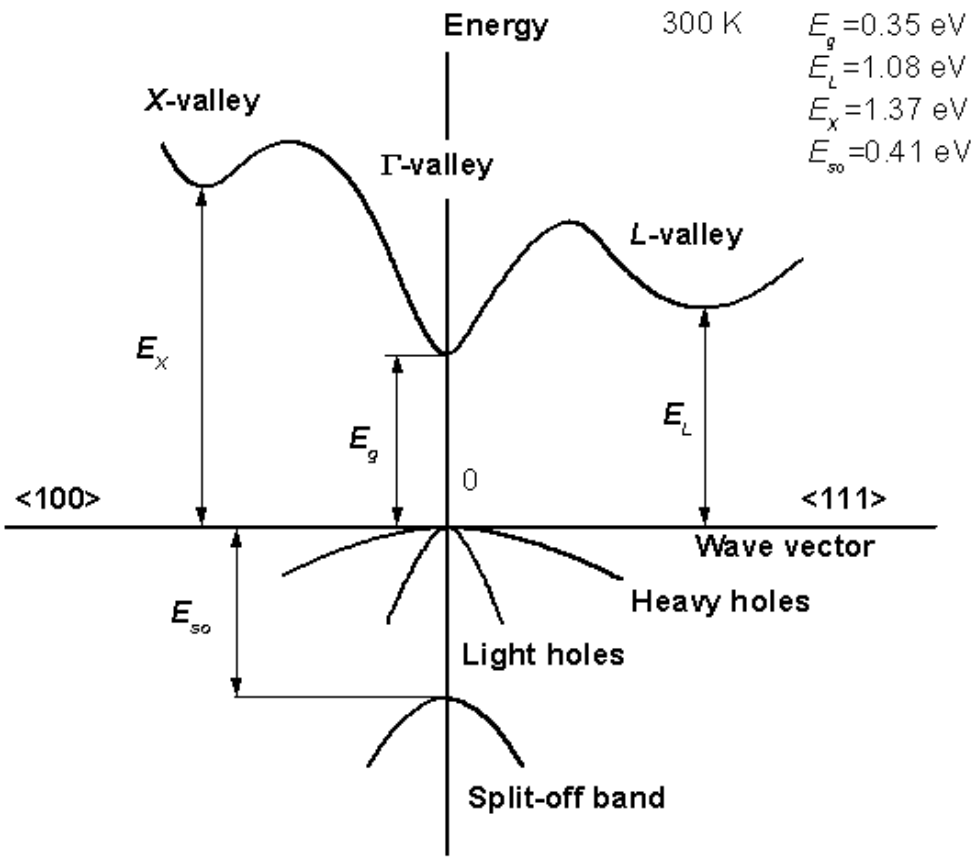

Figure 2-2. Band structure of InAs along two different crystallographic directions - <100> to the left and <111> to the right. Characteristic energies for room temperature are presented at the top. (From ref. [19])

Charge accumulation at the InAs surface is supposed to play the biggest role in the electron transport process of InAs nanowires [17]. This effect appears due to a peculiar tendency of InAs to adjust its energy bands in such a way that the Fermi level becomes located above the conduction band minimum (CBM) [20]. At InAs surface a larger adsorbate-induced conductivity change can be observed. The charge accumulation layer was first observed by Schottky barrier measurements [21]-[22], and later confirmed by electron tunneling [23]-[25] and electron spectroscopy measurements [20], [26], [27]. The charge accumulation layer creates a natural 2-dimensional electron gas at InAs surfaces [20], [25]. Since the 2-dimensional electron gas is located immediately below the surface, surface band bending in InAs has been produced even by submonolayers of adsorbates [28], [29]. To reduce the surface effects usually different kinds of surfaces passivation are used. [15], [31], [32]. Most often passivation of the surface with ammonium polysulfide, $(NH4)_2S_x$ is used. Particularly this method has been found to remove contaminations and natural oxides from the InAs surface, and to provide a passivation layer with covalently

bonded sulfur atoms. It leads to environmental stability and semiconducting behavior of the surface.

2.2 InAs nanowires

The physics of InAs nanowires has been intensely studied over the last decade. Different synthesis methods were developed [33]-[39], which are shortly summarized in the following

1. Vapor Liquid Solid method (VLS).
   Metal Organic Chemical Vapor Deposition (MOCVD). The method is based on the catalytic decomposition of organic precursors (like arsine and trimethylindium) in the presence of a catalyst, mostly nanoparticles (for example gold). First, catalyst gold nanoparticles are deposited on an InAs substrate, and the sample is heated up usually above the melting point of the particles. The particles are saturated with In and As from the substrate and the organic precursors (most often tertiarybutylarsine, trimethylindium are used) flowing through the chamber. The precursors thermally decompose at a pressure of about 100 mbar and mix with the catalyst gold particle in the liquid state – that is form an eutecticum – and then crystallize. In this method it is easy to control the diameter of the wires by changing the diameter of the Au particles and the length of the wires by changing the exposure time to the precursors. Several different types of precursors have been used sequentially to produce composite wires like InGaAs/InAs [33]. A wire diameter of 10 nm could be obtained with this method.
   It is also possible to grow wires by the VLS approach by annealing of an InAs wafer plated with gold film from both sides. This wafer is placed in a molybdenum sample holder mounted on a heated graphite platform. It takes about 1 hour for wires to grow at a temperature of T = 923 K and no toxic chemicals (no precursors) need to be used in the synthesis. This method seems to be the best for the fabrication of nanowhiskers for industrial manufacturing processes [39].
2. Formation of InAs nanowires at giant step edges on vicinal (110) GaAs surfaces by molecular beam epitaxy. In this method wires grow not perpendicular to the substrate, but parallel to the substrate surface [34], [35]. First, a surface with large terraces separated by high steps is prepared by molecular beam epitaxy of $Al_{0.5}In_{0.5}As$, which is deposited on a GaAs substrate. The steps are periodically aligned and extend over several micrometers along the [-110] direction. Aluminium content of the AlInAs layers decreases as the layer thickness increases at the step edges [35]. Subsequently several monolayers of

InAs are grown by Molecular Beam Epitaxy on the stepped surface. As a result, InAs nanowires with a length of several hundred nanometers forms at the step edges (figure 2-3).

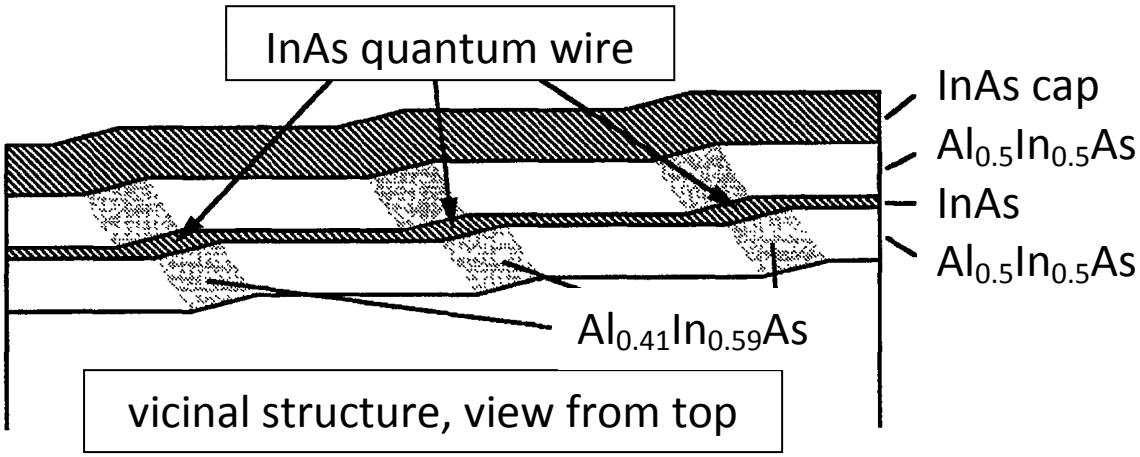

Figure 2-3. Scheme (adapted from [35]) of formation of InAs nanowires at the giant step edges on vinicial GaAs surface. Ga should be replaced on In in the picture in case of fabrication of InAs nanowires [34].

3. Fabrication of wires in a porous glass matrix. In this method InAs is grown in a nanochannel glass which contains regularly formed open channels with diameters of 50 nm and 360 nm (were used in ref [38]) and length of 40 microns. The wires are formed in the glass channels due to the reaction of organometallic compound (trialkylindium) with arsine.

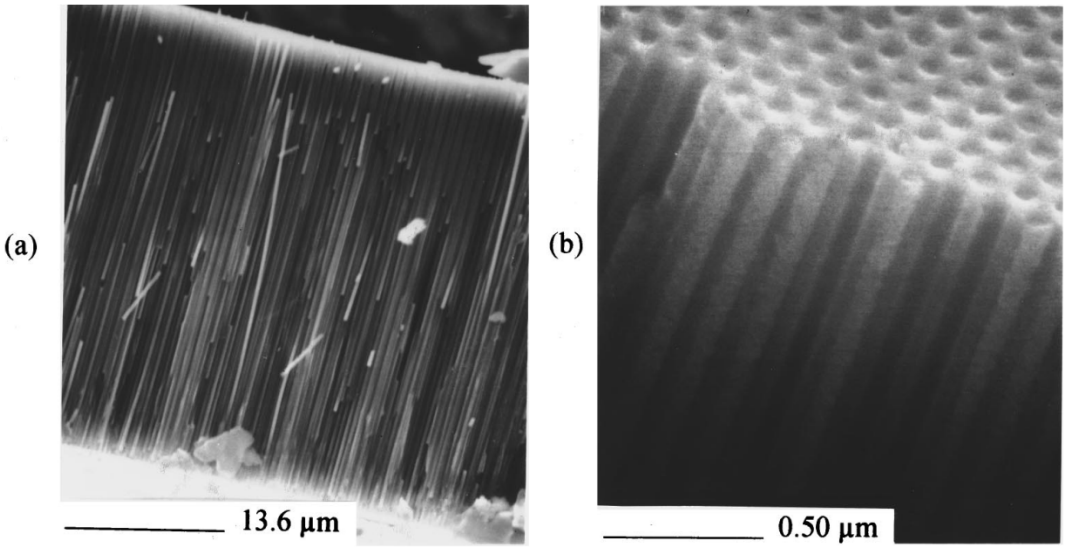

Figure 2-4. Cross-sectional SEM image (taken from [38]) of InAs nanowhiskers fabricated in a nanochannel glass with diameters a) 360 nm and b) 50 nm.

Transport properties of InAs Nanowhiskers

As a result a high density array of uniformly shaped parallel InAs polycrystalline nanowires in a glass matrix are fabricated (figure 2-4) [38]. The biggest problem of the method is the glass which complicates further studies of the wires. Also the surfaces of the nanowires are modified due to the interface with the glass.

For all the different synthesis methods structural studies were made. Coexistence of cubic Zinc Blende and hexagonal Wurtzite atomic structure was found and appear quite often in the wires [40]. The Wurtzite atomic structure usually appears in wires grown by VLS. The growth directions are [-12-10] and [111]. There were no other structures observed. There are also two common defects present in the wires: stacking-faults [41] and rotation twins [14], [42]. The defects are expected to influence the electric transport properties of the wires. Most probably they will act as additional scattering sources and decrease the mobility of the carriers. Relative to these assumptions it is interesting to review the electronic structure of the wires. The electronic structure calculations were made for two different growth directions – [111] and [100] ([43], [44]). The band structure of [100]-orientated InAs nanowires with a square cross section of 13x13 nm^2 is shown in figure 2-5 [44].

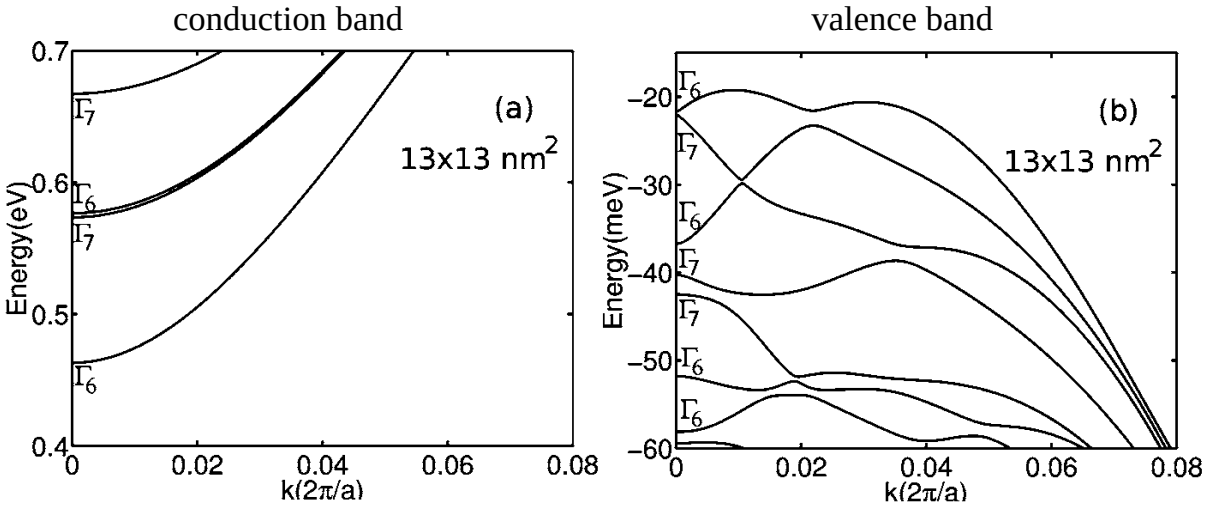

Figure 2-5. Band structure of [100]-oriented InAs nanowire with a square cross section of 13x13 nm^2 (calculated by [44]). The symmetries of the band state at the Γ point are marked according to the double valued irreducible representations, Γ_6 and Γ_7, of the D_{2d} point group. The conduction band shows good parabolic dispersion around the Γ point. Due to spin-orbit coupling the second and third conduction bands are not degenerate. The valence bands of the nanowires show rich and complex structures.

In the case of [100]-oriented InAs NW the band gap value exceeds the bulk value – 0.46 eV against 0.354 eV, respectively. In both cases the conduction bands shows a parabolic dispersion around the Γ point (figures 2-2 and 2-5). The energy separation

between the two bands is, however, small but distinguishable. The valence bands of the square nanowires show complex structures: strong nonparabolicity, anticrossings, and a double-maximum structure in the highest valence band [44]. Figure 2-6 shows the band structure of [111]-oriented InAs nanowires of different diameters [43].

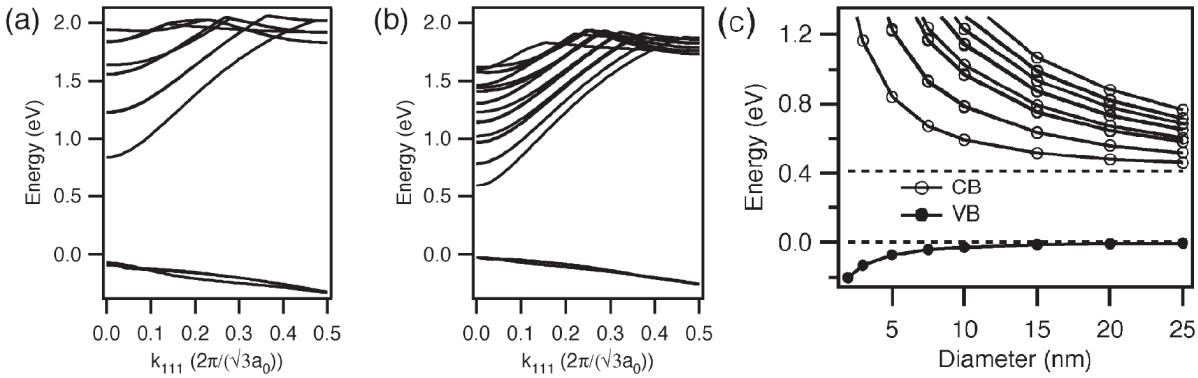

Figure 2-6. Calculated [43] conduction and valence subbands for a (a) 5- and (b) 10-nm diameter [111]-oriented InAs wire. (c) Conduction and valence subband energies at the Γ point as a function of the wire diameter. The dashed lines are the bulk position of the valence and conduction band.

The results of the calculations show that the band gap increases with decreasing nanowire diameter. For the wires with a diameter of more than 250 nm bulk-like behavior is expected [43]. Using those band structure calculation results the authors have calculated the drive current and mean carrier velocity as a function of the gate voltage for metal oxide semiconductor field-effect transistor (MOSFET) based on InAs nanowires with different diameters (figure 2-7).

The I-V curves show the expected behavior – less current through the wires with smaller diameter. This effect is due to increased electron scattering at the wire surface [43].

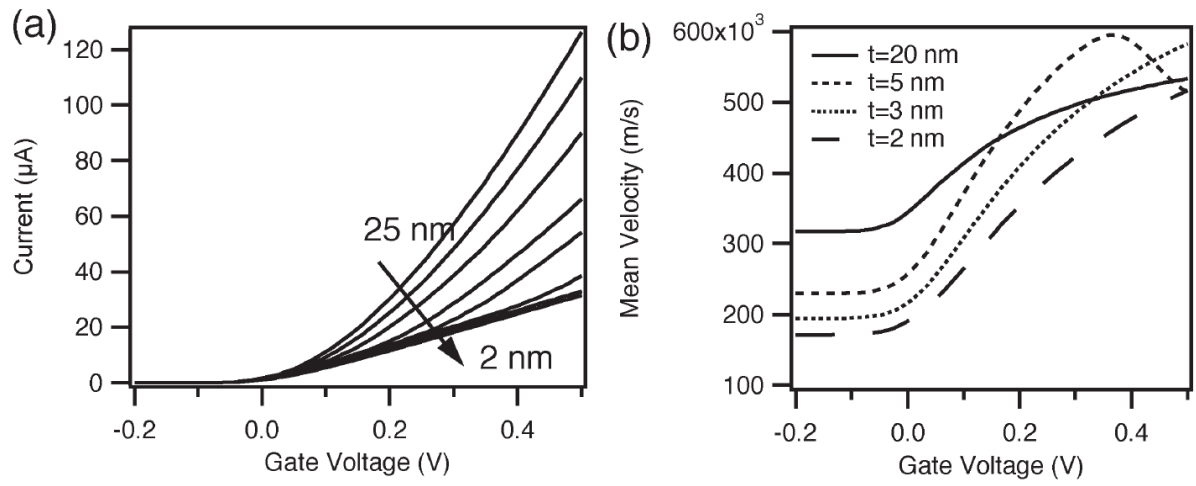

Figure 2-7. (a) Calculated [43] I-V characteristics for [111]-oriented InAs nanowires with different diameters (t). (b) Simulated mean velocities as a function of the gate voltage. The dip in the velocity for t = 5 nm arises from carriers starting to populate the second subband, with corresponding small kinetic energies.

Additional surface/interface and passivation studies were motivated by complications at the interfaces to the electrical contacts [14]. It was found that surface passivation with sulfur atoms stabilizes the surface and reduces the surface electron states.

The morphology of surface of the InAs nanowires grown by MOCVD was investigated by STM [45]. Two types of facets of Wurtzite {11-20} facets and {10-10} facets were found to be the most common. Surface defects and impurities were observed which give rise to localized states in the band gap of InAs, even leading to the appearance of a 2-Dimensional Electron Gas like in the bulk material.

Photoluminescence (PL) has been observed in InAs nanowires [46]. The wires could be used for optoelectronic devices and detection of biomolecules [13], [47]-[50]. In the case of InAs-InP core-shell nanowires the PL energy can be increased up to 0.8 eV [51].

There have also been several studies concerning the thermoelectric properties of InAs nanowires. Temperature dependences of electrical and thermal conductivity and Seebeck coefficient were measured for lithographically prepared InAs (figure 2-8) [52]. Here one did find a strong temperature dependence of the electrical conductivity near the room temperature. The wire conductivity increases two times increasing the temperature 60 degrees only. This strong dependence can result in nonlinear I-V dependences near the room temperature due to ohmic heating of the wire. The Seebeck effect should not influence measured in this work properties due to the maximal Seebeck coefficient is about -64 μV. The thermal conductivity is about 10 times less than in the bulk InAs, this can probably result in local heating of the wire

especially in presence of atomic defects. These facts had been taken into account in all electrical measurements that were performed near the room temperature in the presented work.

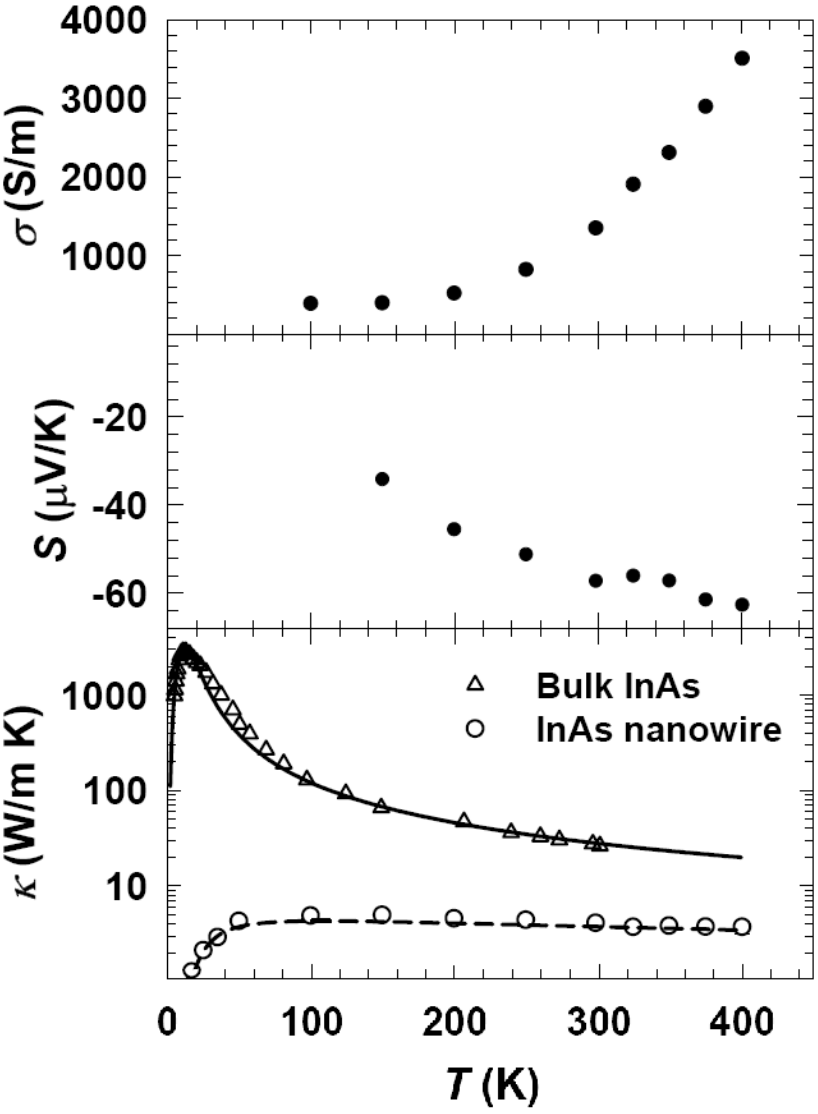

Figure 2-8. Electrical conductivity σ, Seebeck coefficient S and thermal conductivity κ, of a 150 nm wide, 40 nm thick etched InAs nanowire as a function of temperature obtained in [52]. In the κ-T plots, the open circles are the experimental results for the nanowire, the open triangles are the bulk values reported by Guillou and Albany [53], and the dashed and solid lines are the calculation results for the nanowire and bulk, respectively.

Mostly, experimental studies have been focused on the electrical properties of field effect transistors based on InAs nanowires [54], [55]. Concerning nanowires themselves, just few tries to study the correlation of electrical properties and morphology (diameter, length) directly were undertaken [15]-[16], [56]. There were found that the nanowire conductivity increases with decreasing diameter down to

30 nm. Figure 2-9 shows dependence of carrier density on the nanowire diameter [56]. The carrier concentration decreases with increasing nanowire diameter. This is due to the presence of a charge accumulation layer at the InAs surface. The experimental result was confirmed in the same study with a numerical simulation [56].

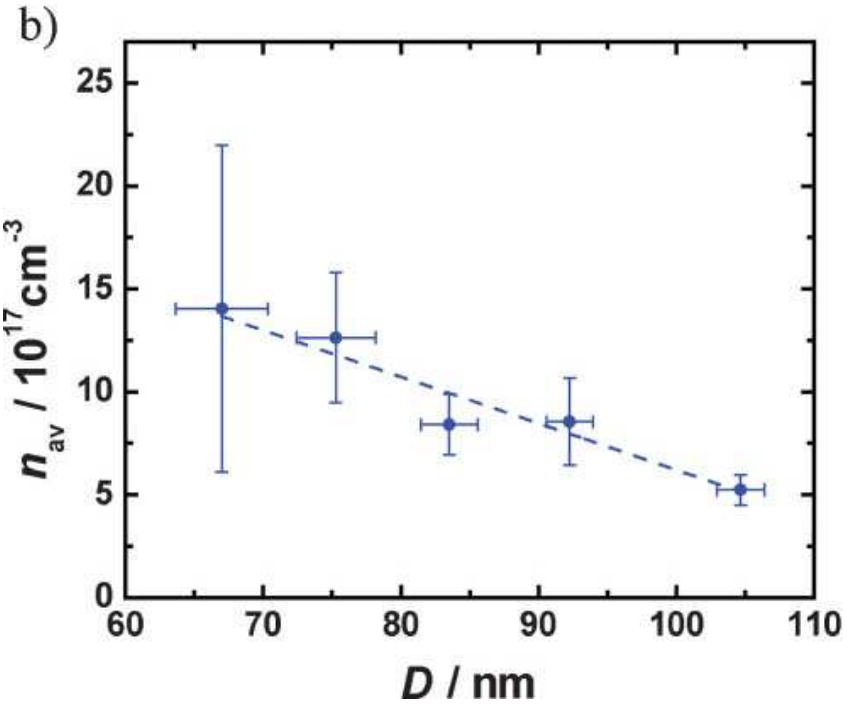

Figure 2-9. Carrier density of InAs nanowire as a function of the wire diameter. Dashed line is a linear fit. The data were measured by a 4-point electrical measurement (the picture is taken from [56]).

Two regimes of transport behavior were observed by length dependent resistance measurements: ballistic transport and conventional drift transport (figure 2-10) [57], [16]. The nanowires were grown by MOCVD method on Si (001) substrate. To perform the electrical measurements, authors made two Ti /Al ohmic contacts on InAs nanowire and applied some bias voltage between them. Placing conductive Atomic Force Microscopy (cAFM) tip on the wire between the contacts, wire resistance as a function of distance to the contact were measured [57]. Was found that the wire resistance is independent on the wire length (*L*) for lengths below 200 nm (ballistic regime) and linearly increases with increasing *L* for the lengths above 200 nm (conventional drift regime). It confirms the assumption that for distances up to a few mean free paths of electrons the resistance increases more with increasing *L* much slower than in the case of drift transport regime [57].

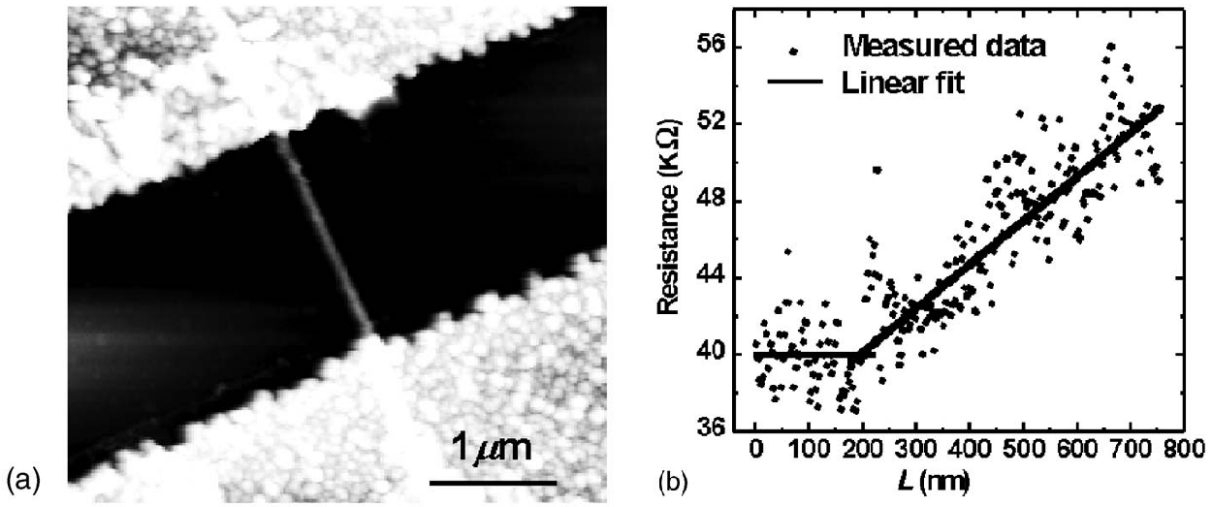

Figure 2-10. (a) AFM topography image of InAs nanowire and Ti/Al Ohmic contacts. (b) Resistance measured by cAFM as a function of tip-contact distance L (symbols), with linear fits for the ballistic transport regime (below 200 nm), where the resistance is independent of L, and the drift transport regime (above 200 nm), where the resistance increases linearly with increasing L. Linear I-V dependences were observed for both cases up to 0.5V (both pictures are taken from [57]).

Correlations of the crystalline structure of the nanowires and electrical properties of the field effect transistors built on these nanowires were observed [52], [54]. The I-V curves for wires with two different types of structure were recorded. It was shown that the conductivity of the nanowires with a pure Zinc Blende structure is higher than that for the wires possessing Wurtzite/Zinc Blende structure with stacking faults (figure 2-11). Most probably for wires with mixed Wurtzite/Zinc Blende structure the stacking faults act like an additional source of electron scattering [52].

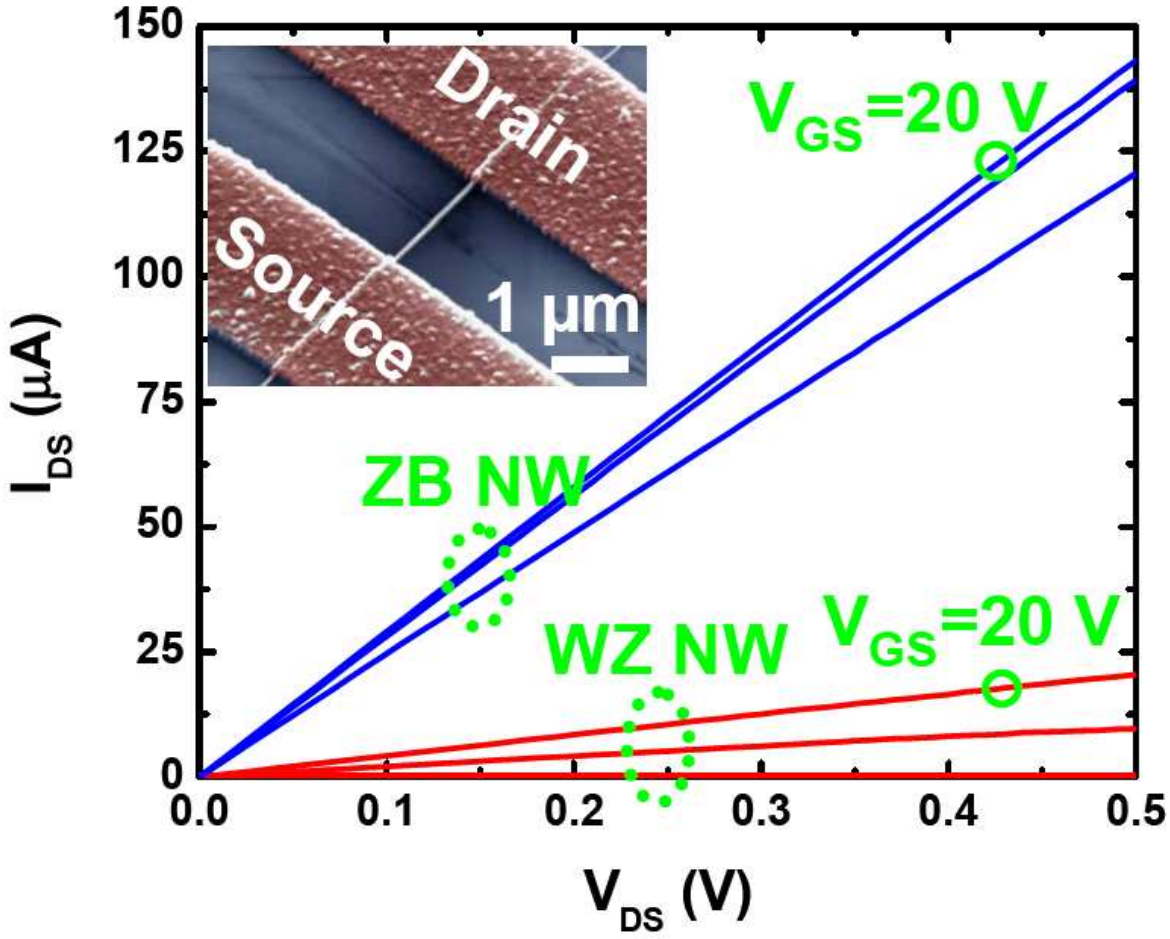

Figure 2-11. I-V curves for InAs nanowires (NW) fabricated by OMVPE method (adopted from [54]). Blue lines are for wires grown along <110> direction with Zinc Blende (ZB) atomic structure. Red lines are for wires grown along the <0001>/<111> direction with mixture of Wurtzite (WZ) and Zinc Blende atomic structures. The I-V characteristics were measured with three different gate voltages in both cases: 20V, 0V, -20V.

Scanning Tunneling Microscopy has become an established method to study transport properties of nanostructures and -wires [58], [59]. It offers the advantage over the traditional 4 point contact technique with lithographically prepared contacts to study as-prepared nanowires, without cutting them from the substrate. On the other hand – since it presents a two point contact method – the interface properties must be well understood and characterized. Here, the combination with transmission electron microscopy yields an interesting approach.

Transmission Electron Microscopy allows investigation of composition, morphology and structure with atomic precision. Using an STM setup in-situ in TEM one can study transport properties of a single nanoscale object and correlate them directly with the observed atomic structure. In this work the experimental setup will be described and tested for nanowires with different structures. Such a combination of STM and TEM

techniques is a reliable way to systematically study the correlation of atomic structure and transport properties of nanowires.

2.3 Basics of Transmission Electron Microscopy.

In transmission electron microscope high energy electron beam (e.g. 200 keV) interacting with atoms of an ultrathin (C < 200 nm) specimen. High resolution images with atom column resolution can be achieved. The resolving power of the microscope is limited by diffraction and can be described by the Rayleigh criterion which gives the minimal resolvable separation d_0:

$$d_0 = \frac{0.61\,\lambda}{n\,sin\alpha}$$

where λ is wavelength of the illuminator (here electrons), α is a half-angle subtended by the microscope objective at the object, n is refractive index [60]. The attainable resolution of a transmission electron microscope is mainly determined by the properties of the objective lens. A resolution of 0.78 Angstrom in Si [112] ([61]) for example has been demonstrated.

When the electron beam is directed to a thin solid sample the electrons can go through undeviated or can be scattered. Only when the sample is sufficiently thin (below 200 nm, different for different materials) a fraction of the electron beam can be transmitted. Figure 2-12 shows various interactions of an electron beam with a solid target. The difference in scattering power gives the image contrast in Transmission Electron Microscopy. Images containing phase information can also be obtained from crystalline and non-crystalline samples using special imaging modes [62].

The number of scattered electrons into a certain spatial region depends on the scattering angle. The number of detected electrons is given by the aperture of the imaging lenses. A parallel electron beam is going through the sample situated in the object plane of the microscope. The transmitted beam passes through the objective lens and an image formed at the image plane on the fluorescent screen. The aperture can be inserted in the back focal plane of the lens. It is usually used to limit semi-angular aperture of the lens.

Consider a monochromatic electron beam incident perpendicularly on a solid specimen under idealized conditions:

1. The specimen is thin enough that electrons are transmitted.
2. The sample contains atoms of one kind only which are randomly arranged.

3. Electrons scatter elastically and incoherently.
4. Scattering events are random [62].

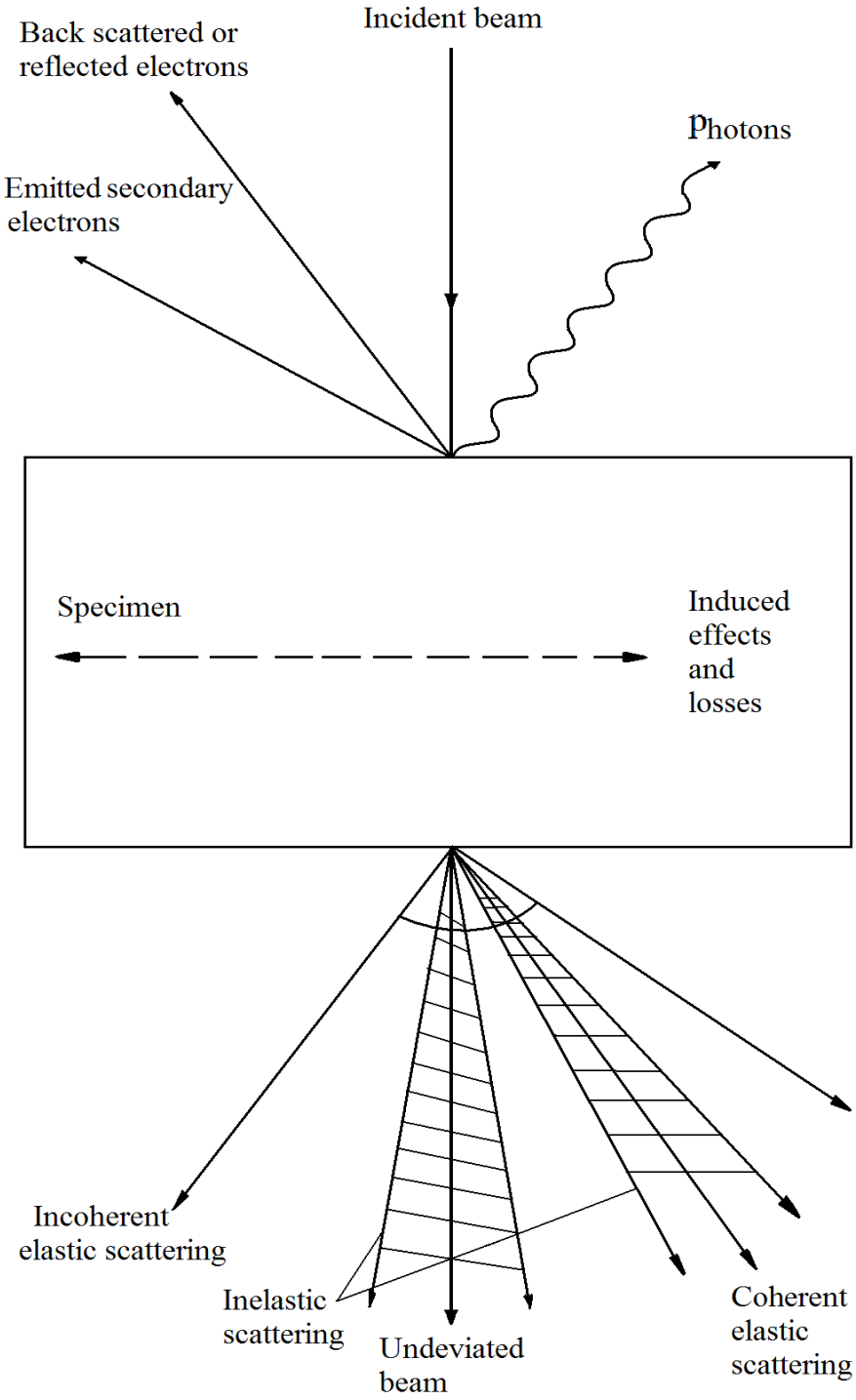

Figure 2-12. A scheme of various interactions of an electron beam with a solid target. The interactions pertinent to the various modes of electron microscopy are indicated [62].

By analogy with photon optics, total transmitted intensity can be written as [62]:

$$I = I_0 e^{-\sigma_s t}$$

where t is the thickness of the specimen, and I_0 is the incident beam intensity and σ_S is the total scattering cross section of the material. σ_S depends on the scattering cross section of the atom, σ_a [62]:

$$\sigma_S = N\sigma_a = \frac{N_0\ \rho\ \sigma_a}{A}$$

where N is a number of atoms in volume unit, N_0 is Avogadro's number, ρ and A are density and atomic weight of the material respectively. It has experimentally been found that the value of σ_a / A is nearly constant for different electron energies for a given material. That means that the product ρt (also known as "mass thickness") determines the transmitted intensity. Thicker regions of the specimen, or regions with higher atomic number will appear dark whilst regions with no sample in the beam path appear bright – this mode is called "bright field" and can be used to study morphology (shape and size) of nanoparticles or nanowires.

Another technique used in TEM is electron diffraction. Coherently elastically scattered electrons form the diffraction patterns. To understand some details about the process, consider a monoenergetic electron beam incident on a crystal specimen. Arrays of atoms in crystal planes act as reflectors of the beam. Constructive interference from parallel planes occurs when the angle of incidence and reflection θ satisfy Bragg's law:

$$2d_{hkl}\ sin\theta_{hkl} = n\lambda_k$$

where d is the lattice spacing between atomic planes, λ is the wave length of the electron beam, and n is an integer [60]. h, k, l are the Miller indices [61]. If the parallel electron beam in TEM falls on a crystal at the angle θ which satisfies Bragg's Law (called *Bragg angle*), and the fluorescent screen placed at a distance L from the crystal the diffracted beam will be displaced from the undeviated beam by a value R given by (angle θ is very small):

$$R = L\ tan2\theta_{hkl} = 2\theta_{hkl}L$$

Combining it with Bragg's law one obtains:

$$d_{hkl} = \frac{\lambda L}{R_{hkl}}$$

for first order (*n=1*) diffraction, and d-spacing of crystalline specimens can be calculated. Usually L and λ are not determined separately, but grouped together as $\lambda \cdot L$ (so-called camera constant). The camera constant is determined experimentally using a standard specimen with known lattice spacing.

If polycrystalline sample is used instead of single crystalline sample, a diffraction pattern will be formed due to the crystallites satisfying the Bragg relation and the diffracted rays will form cones whose surfaces intersect the screen and show diffraction rings of radius R_{hkl}.

High Resolution Transmission Electron Microscopy (HRTEM) as opposed to conventional microscopy does not use amplitudes, i.e. absorption by the sample, for image formation. Instead, contrast arises from the interference in the image plane of the electron wave with itself. The images are mostly formed due to the differences in the phase of electron waves. This mechanism of the image formation is called phase contrast. The phase contrast provides an improved sensitivity for the analysis of the atomic structure of thin specimens [63].

2.4 Basics of Scanning Tunneling Microscopy.

Five scientific and technical achievements and ideas form the basis for the success of Scanning Tunneling Microscopy (STM) [64] as invented in 1981 by Binnig and Rohrer.

1. The principle of quantum mechanical tunneling.
2. Achievement of controlled motion over small distances using piezoelectrics.
3. The principle of negative feedback.
4. Vibration isolation.
5. Electronic data collection.

I will only describe the basic principle of quantum mechanical tunneling. Electron tunneling across the vacuum barrier between STM tip and conductive sample could be observed if the bias voltage is applied between the two. If the potential barrier too thick, no electron can travel through it. At distances of few Angstroms electrons can tunnel through the barrier. Using Schrödinger's equation of quantum mechanics one can calculate how the tunneling current increases with decreasing separation between two metals [64], [65]:

$$-\frac{\hbar^2}{2m}\frac{\partial^2\psi_n(z)}{\partial z^2} + U(z)\psi_n(z) = E\psi_n(z),$$

where $\hbar$ is Plank's constant, *U(z)* potential barrier function form, ψ is an electron wave function, *m* is the electron mass, *E* is the electron energy eigen values. The following solution is given:

$\psi_n(z) = \psi_n(0)e^{\pm \kappa z}$, where $\kappa = \frac{\sqrt{2m(U-E)}}{\hbar}$

and the tunneling probability can be estimated as:

$P \propto |\psi_n(0)|^2 e^{-2\kappa W}$, where *W* is barrier width (distance between the metals)

The tunneling current through the barrier is given by:

$I \propto \sum_{E_f - eV}^{E_f} |\psi_n(0)|^2 e^{-2\kappa W}$, where E_f is the Fermi energy and *V* is the applied bias voltage.

The sum of the probability over energies between $(E_f - eV)$ and eV gives the number of states available per unit volume, thereby finding the local density of states (LDOS) near the Fermi level [65]. The LDOS at energy *E* in an interval ϵ is given by:

$$\rho_s(z, E) = \frac{1}{\epsilon} \sum_{E-\epsilon}^{E} |\psi_n(z)|^2 .$$

and the current is given by:

$$I \propto V \rho_s(0, E_f) e^{-2\kappa W} .$$

The tunneling current is proportional to the applied bias voltage as well as to the density of states at the Fermi level, and decreases exponentially with increasing distance between tip and sample.

In modern STM setups (figure 2-13) the resolution of a piezo driving the tip reaches sub-Ångstrom resolution. Tip approaches the sample at tunneling distance. A bias voltage is applied to the sample and the tunneling current between the tip and the sample is measured. Keeping the tunneling current constant by a feedback loop and changing only the tip to sample distance, the STM can be used to image the surface topography with atomic resolution. It also can be used in Scanning Tunneling Spectroscopy mode. In this case *dI/dV* is measured, which is proportional to the Local Density of States near the Fermi level at the sample surface.

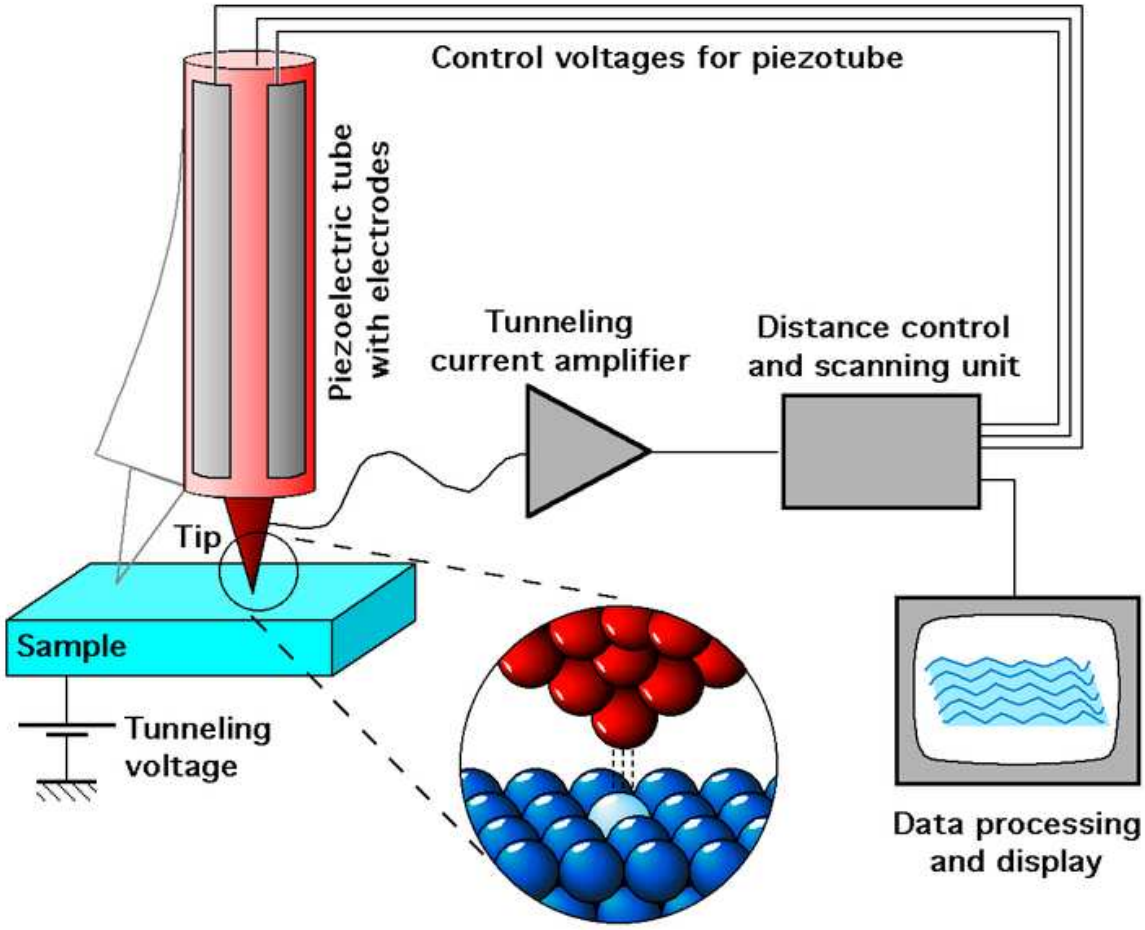

Figure 2-13. Principal scheme of STM setup. Piezoelectrically driven tip approaches the sample. A bias voltage is applied to the sample. The tunneling current is observed at a distance of few Ångstroms between the tips first atom and sample atoms. Using a feedback loop the current is kept constant by varying the tip to sample distance. This distance variation gives the topography of the sample.

In the present work the STM was used in non-scanning contact and not in tunneling mode due to complicity of the resistance extraction from tunneling spectra. In this case the tip is in the direct contact with the sample surface. By changing the bias voltage, the voltage-current characteristics can be measured. Since the wire has a gold particle on the top contact between the tip and the wire will be ohmic and can be described by usual contact theory.

2.5 Electrical resistance at interfaces

For all solid materials the area of a true contact is just a small fraction of the nominal contact area. At the interface between two solids, the electrical current lines bundle together to pass through small contact areas called “a-spots” [67]. The electrical current flows through the “a-spots” as it is shown schematically in figure 2-14.

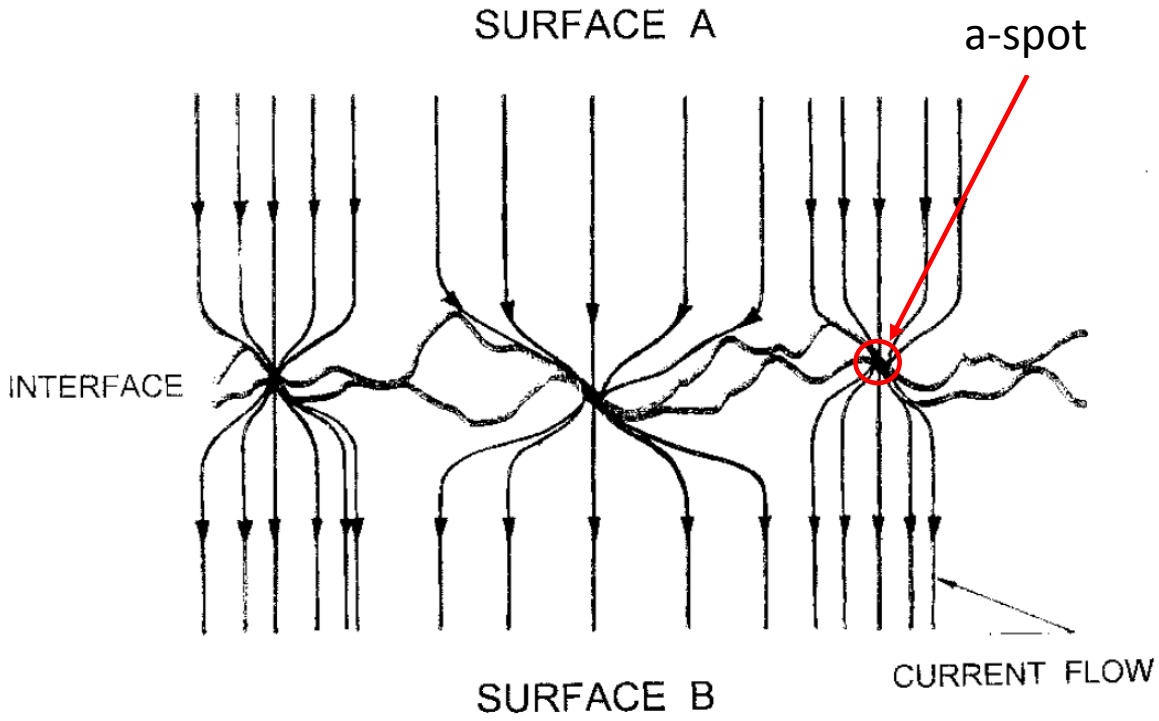

Figure 2-14. Schematic diagram of a bulk electrical interface. The top surface is "surface A", the bottom is "surface B". Arrows show current lines which are constricted at microscopic contact areas called "a-spots". (The picture is adopted from [67].)

Due to this constriction, less volume of the material contributes to electrical conductivity and electrical resistance of the system increases to a value called contact resistance [68].

According a classic contact theory a contact resistance R_C, is given by:

$$R_C = \frac{\rho}{2a} \quad (1)$$

where ρ and a are the resistivity of materials A and B thought to be identical and the a-spot radius, respectively. For cylindrical conductor of radius R the contact resistance is described by equation (1) if $a/R < 0.7$ [68]. One should note that when the a-spot diameter is larger than the free mean path (l), the conduction process remains diffusive. If the spot size is comparable or less than the mean electron free path, the electrons pass across the contact spots ballistically and this process cannot be described by the classic theory any more [69]. Sharvin [70] has shown that for the case of the ballistic transport the contact resistance can be calculated as

$$R_S = \frac{4\rho l}{3\pi a^2} \quad (2)$$

where l – free mean path, ρ is a resistivity of the material and R_S is called Sharvin resistance. ρ can be written as [69]

$$\rho = \frac{mv_F}{ne^2 l} \quad (3)$$

where m is the electron mass, v_F is the Fermi velocity, n is the free electron density and e is electron charge. Substitution of equation (3) into (2) yields

$$R_S = \frac{\left(\frac{4mv_F}{3\pi ne^2}\right)}{a^2} = \frac{C}{a^2} \quad (4)$$

where C is a constant dependent only on the electronic properties of the conductor. The Sharvin resistance given by (4) is temperature independent [69].

For the case when $a > l$ the total contact can be modeled by two serial resistances: classical contact resistance(1) and Sharvin resistance (4)

$$R_C = \frac{\rho}{2a} + \frac{C}{a^2} \quad (5)$$

The equation (5) is used to estimate the contribution of the tip-wire contact resistance to total measured resistance. To probe InAs nanowires the best idea is to use a gold tip in order to achieve the lowest contact resistance with the gold particle placed on the top of the wire. For such a contact due to the good mobility of gold surface atoms and contact spot diameter of about 30 nm can be achieved. Using the following values

ρ = 2.2 10^{-8} Ohm m, gold electrical resistivity

a = 15 nm, a-spot radius

C = 3.58 10^{16} Ohm m^2, gold constant for Sharvin resistance [69].

the contact resistance R_C = 2.3 Ohm can be calculated.

Actually the particle consists not only of gold but also 20% of Indium, but it does not change the result significantly. Most literature provides values of several kilo ohms [17], [18], for the InAs nanowires, therefore contact tip-wire resistance is negligible and does not have to be taken into account. Another significant contribution to the total measured resistance is the intrinsic gold particle-nanowire interface as discussed in following. One cans estimate the gold-InAs interface resistance using the same theory. It will be done in the next section.

2.6 Contact resistance of gold-InAs interface

In electron transport behavior surface effects become important when the dimensions are the nanoscale. Surface electron states of two different types appear in semiconductors due to imperfection of the surface and the breaking of the symmetry. They have been investigated experimentally and classified according to the relaxation time (τ) of the electronic states. Fast states which τ up to several milliseconds are generally considered to lie close to interface since they rapidly exchange charge with the conduction and valence bands. Slow states with relaxation times of seconds and more lie directly at the interface or within an oxide layer at the semiconductor surface [71]. For metal-semiconductor contacts the existence of non-ohmic electrical transport behavior is quite common due to banding of the conduction band bottom.

Figure 2-15 left shows the energy diagram of a metal and a semiconductor which are first separated. E_{Fm}.(E_{Fs}.) is the Fermi energy of the metal (semiconductor). W_m (W_s) is the work function of the metal (semiconductor).

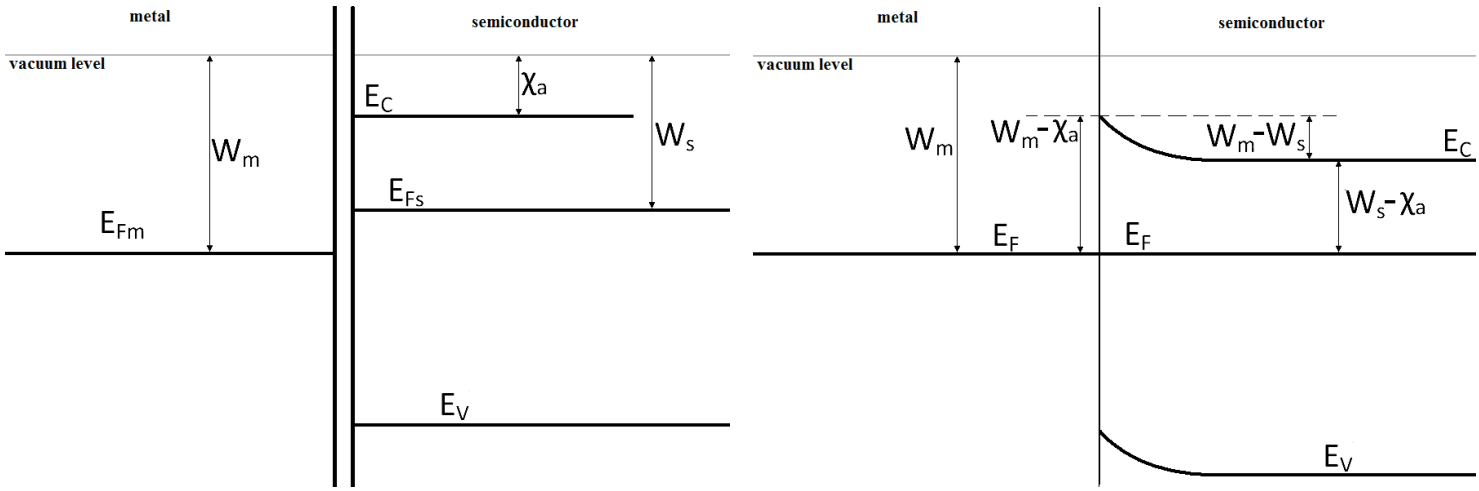

Figure 2-15. Energy diagrams of a metal and a semiconductor before contact (left) and after contact (right). Far from the surface of the semiconductor, the bottom of the conduction band shifts to maintain the same distance to the Fermi level as before the contact. At the surface, the bottom of the conduction band bends upwards to maintain the initial value.

The electron affinity χ_a is the energy difference between the vacuum level and the bottom of the conduction band of the semiconductor. If the metal and the semiconductor are in direct contact a redistribution of charge takes place: electrons from the semiconductor move to the metal in order to make the chemical potentials

(Fermi energies E_{Fm}.and E_{Fs}) the same on both sides of the interface as shown in figure 2-15 right. The semiconductor Fermi level decreases by (W_m - W_s). Far from the semiconductor surface the bottom of the conduction band (E_C) moves by the same amount to keep the same distance to the Fermi level (W_s - χ_a). At the metal-semiconductor interface the bottom of the conduction band bends upwards to keep the initial value, so that its separation from the Fermi level will be at a value of (W_m - χ_a). The top of the valence band (E_V) also moves downwards and bends at the interface upwards following the bottom of the conduction band [71]. The energy barrier at the metal-semiconductor interface at zero electrical field is (W_m - χ_a) and called a *Schottky barrier* if the semiconductor contains donor or acceptor ions in the contact region and a *Mott barrier* if the semiconductor is intrinsic [72].

Let us consider the Au-InAs interface: what type of contact is expected at the gold-InAs nanowire interface?

Generally, the work function of bulk gold is about 5.1-5.47 eV and the electron affinity of bulk InAs is 4.9 eV. Using these values the barrier height is determined to be about 0.2-0.57 eV. But one should not forget about size effects appearing in nanoscale objects. For InAs nanowires no electron affinity measurements or simulations have been reported to my knowledge. Furthermore, in this study InAs nanowires synthesized by the VLS method using catalytic gold nanoparticles are discussed. In this case – as discussed later – gold in the particle mixes with indium. There is evidence for a composition gradient at the Au nanoparticle-InAs nanowire interface; also the presence of some amount of As cannot be excluded. The interface electronic properties in this case are hardly predictable and should be investigated experimentally.

According to a standard contact theory (reviewed in the previous section) the gold-InAs interface resistance could be roughly estimated using following equation:

$$R_C = \frac{\rho_1 + \rho_2}{4a} + R_S \quad (1)$$

where ρ_1 and ρ_2 are the resistivities of gold and InAs nanowires respective, a is radius of the interface cross section, R_S is the Sharvin's resistance given by:

$$R_S = \frac{4m v_F}{3\pi n e^2 a^2}$$

here m is electron mass, v_F is the Fermi velocity, n is the free electron density and e is electron charge.

Using table values for m, e, ρ_1; a = 25 nm; $\nu_F \approx 5 \cdot 10^5$ m/s from reference [43]; $n \approx 15 \cdot 10^{17}$ cm^{-3} from reference [56] and $\rho_2 \approx 5 \cdot 10^{-3}$ Ohm*cm according to reference [15] the resistances $R_S \approx 8$ kOhm and $R_C \approx 8.5$ kOhm were calculated. The estimate contact resistance is on order of magnitude below the specific resistances were measured in present work (described in chapters 5 and 6).

In the next chapter the experimental method and setup used in the study will be discussed. The setup of in-situ STM in TEM and all sample preparation procedures will be described. Afterwards all attention will be concentrated on the experimental study of structural and transport properties of InAs nanowires grown by the VLS approach.

Chapter 3. Experimental techniques and apparatus

3.1 Scanning Tunneling Microscopy-Transmission Electron Microscopy (STM-TEM) Setup

In this chapter I will discuss the apparatus to study the correlation of electrical and structural properties of InAs nanowhiskers in-situ. This apparatus combines two well-known methods: TEM and STM. The commercial STM (sold by "Nanofactory Instruments AB") is placed in the end piece of a conventional TEM sample holder (figure 3-1), so that the sample can be positioned in the TEM directly under the electron beam. All electric connections are made on the back side of the sample holder. Additional electronics and a computer are used to control the STM.

Figure 3-1. STM-TEM sample holder sold by Nanofactory. A mini STM is installed in the TEM sample holder (figure 3-2). On the left hand side are the electrical feedthroughs to control the STM.

The STM tip is mounted into the „hat" (figure 3-2). The hat is mounted onto a sapphire ball with the possibility to slide from it. The ball is attached to the piezo tube that can move in three directions. Using fine movement of the piezo we can achieve fine movement of the hat with the tip, and using pulses we obtain coarse movement of the tip by slip-and-slide action of the hat. The sample (a wire next to the tip in the figure) is mounted into a special sample holder in front of the tip. The holder is an aluminum oxide plate (perpendicular to the figure plane) with a tube mounted on it. Wires can be inserted in the tube. On the other side of the plate four contact pads are located.

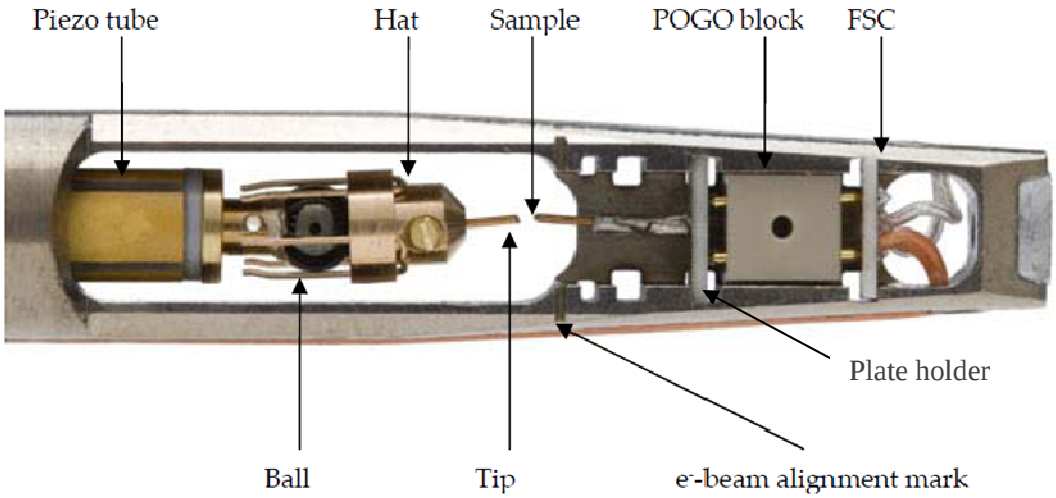

Figure 3-2. STM-TEM sample holders end piece. STM parts are described. The electron beam of the TEM is incident perpendicular to the figure plane. The tip is held with two screws inside the hat. The hat has legs to mount it onto the sapphire ball. The ball is fixed to the piezo tube which moves in three dimensions. In front of the tip is a sample wire inserted into the aluminum oxide plate holder. (Manufacture's picture)

The "POGO" block (see figure 3-2) is used to hold the plate holder and to contact the pads providing the connection to the electronics. In the STM mode only one contact pad is used to apply a bias voltage to the sample. For different sample types different plate holders can be used. The STM sample holder is designed especially for TEM usage but it can be used in air also. As was described in section 2.4 for any STM it is important to achieve good vibration isolation. Any TEM has its own vibration isolation so in the case of the in-situ STM any special damping system is not needed. Using the setup in air, however, it is necessary to avoid vibrations. A homemade damping system was used and will be described later.

3.2 Tip preparation for STM-TEM

In the case of STM-TEM measurement there are some special requirements for optimum performance of the tip. First, any STM tip must have a clean surface to have no uncontrolled influence on the electrical properties of the whole system. Second, tips for STM-TEM probing should be quite sharp (less than 100 nm in diameter). The sharpness is required since it is necessary to focus the electron beam of the TEM on the STM tip while positioning the tip. And the last requirement is the tip's mechanical stability; it should "survive" a crash into the sample or the application of a big bias voltage. To obtain really sharp tips, the best way is to use chemical etching as a preparation method instead of cutting (as for example done for PtIr) [73]. The well established method to produce tips is the etching of a tungsten wire. In the case of

tungsten one could easily obtain very sharp tips (about 20 nm in diameter) using a DC current in the etching process (figure 3-3) as described bellow.

Tungsten polycrystalline wires with a diameter of 0.25 mm were used. The wire was inserted into the etching setup so that 12 mm of wire were outside the setup (figure 3-3). The free end of the wire was dipped into 1.3 Mol/l solution of sodium hydroxide. A meniscus as indicated in figure 3-3 appears at the surface of the solution which plays a significant role in the etching process. At the bottom of the solution a stainless steel counter-electrode was placed. An etching voltage of about 4.2 V has to be applied between the wire and the electrode. Bubbles rising from the bottom confirm the etching process. The bubbles can disturb the meniscus and cause a failure of the etching process.

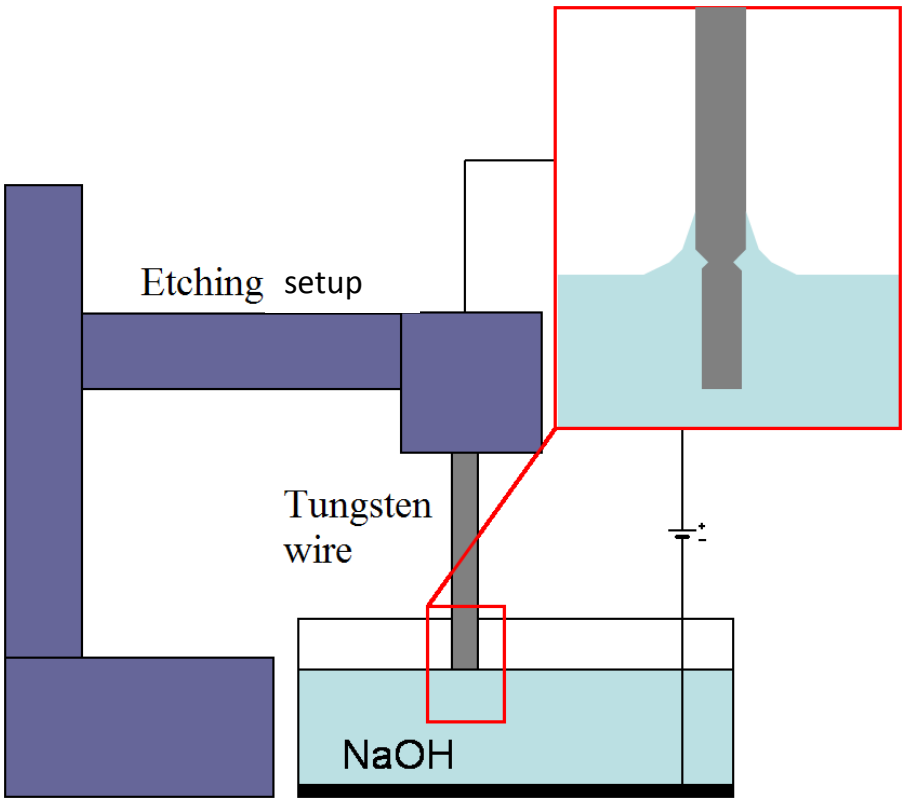

Figure 3-3. Scheme of tungsten tip preparation by DC etching in NaOH. The tungsten wire is installed in the etching setup. The other end of the wire is dipped into a 1.3 Mol/l NaOH solution. The position of the wire can be adjusted.

Due to the meniscus a small part of the wire at the surface of the solution is etched more quickly, and the wire end plunges into the solution after a few minutes (inset of figure 3-3). The etching current should be switched off immediately after the drop-off

to prevent the overetching of the tip. The power supply was equipped with a self-switching scheme that turns the supply off at the drop-off moment. After the etching process was finished the tip should be cleaned in three steps: first, cleaning in distilled water; second cleaning in ethanol; and distilled water again. Using the described method very sharp tungsten tips were produced. To characterize the tips Scanning Electron Microscopy (SEM) images were recorded (figure 3-4).

The SEM images showed that the tip apex is very sharp: less than 20 nm in diameter. Furthermore, they have a very suitable STM shape – a short needle part which results in higher stability and less vibration. In the high magnification picture (figure 3-4b) some residuals of the chemicals can be noticed. Thus the cleaning procedure was changed to very intensive rinsing only in distilled water.

The first experiments showed that the tungsten tips have a natural oxide layer on the surface. This layer modifies the tip's surface electron states and hampers the current flow to the sample. To work with tungsten tips an in-situ cleaning procedure was established. To clean the surface the *field emission* of the tip was used. This did not yield satisfactory results (see chapter 3.6). Since tungsten could not be used another material was tested. The general requirements were surface purity and better contact resistance with the gold nanoparticles which are situated on the top of the InAs nanowires. Gold was chosen as a tip material, which have several important advantages:

1. Gold forms no oxide layer at the surface.
2. Gold atoms have a high interdiffusion rate at room temperature that helps to form better electrical contacts.

There is, however, one significant disadvantage of gold tips: the tip can be easily blunted by crashing into the sample or by a big bias voltage.

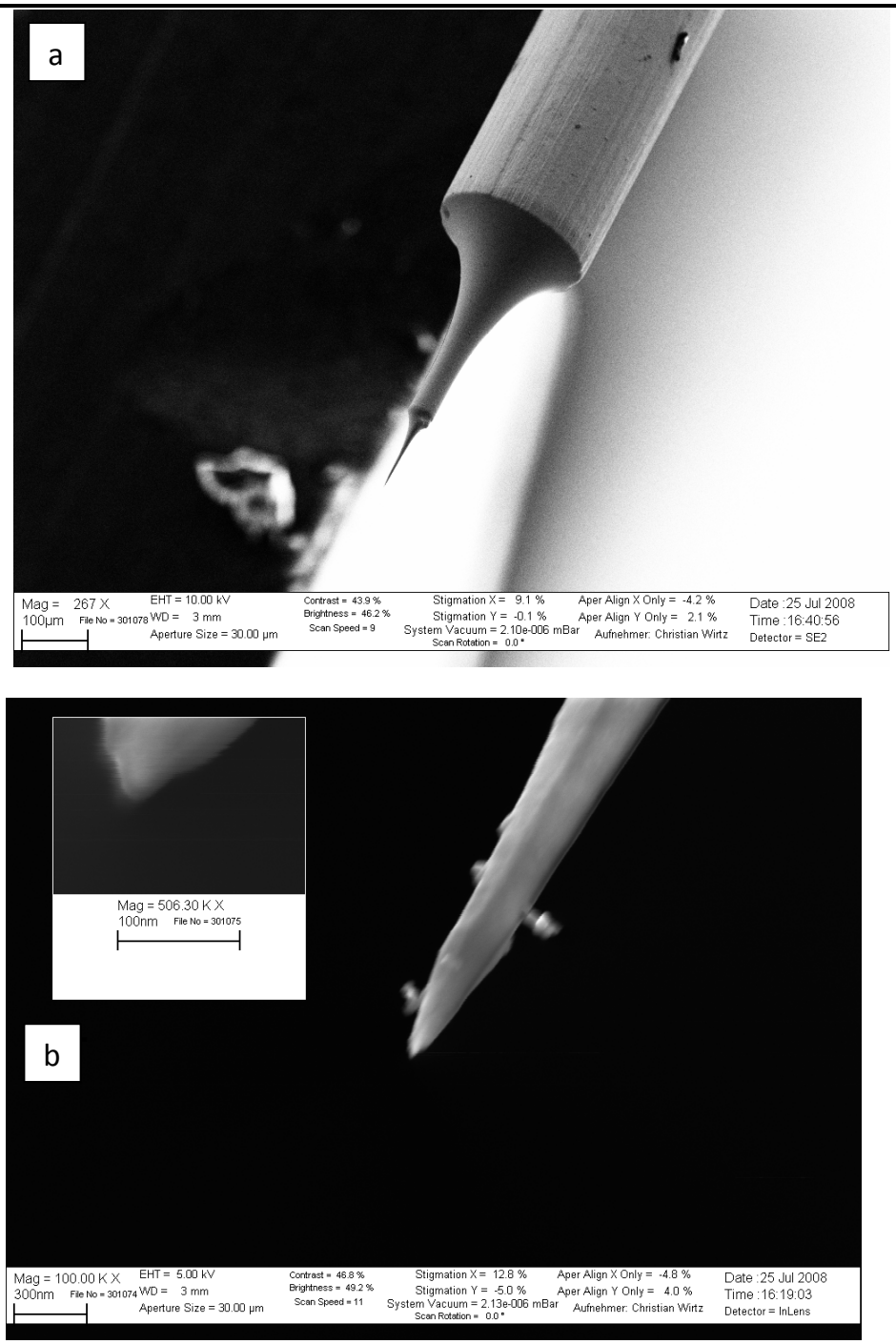

Figure 3-4. Typical SEM images of tungsten DC etched tip: a) low magnification and b) High magnification. The diameter of the end of the tip is about 20 nm.

Etching of gold is very difficult and requires some luck in the process [74]. To obtain sharp tips it is not enough just to find the suitable etching solution and applied voltage. Success appears only from time to time due to different reasons. First, more bubbles form in the solution than in the case of tungsten wire etching. The other reason is the softness of the material. The gold is so soft that small distortions of its

surface can blunt the tip. One possibility to prepare gold tips is AC etching of a gold wire in concentrated perchloric acid. First, the gold wire's end is covered by nail polish to protect the end piece from being etched (figure 3-5). Then wire is inserted into perchloric acid. A platinum electrode instead of the stainless steel electrode is placed at the bottom of the glass. Then AC voltage is applied to the wire and electrode. The sharpest tips were fabricated applying 5 V at 6 kHz with a DC offset of 2.5 V.

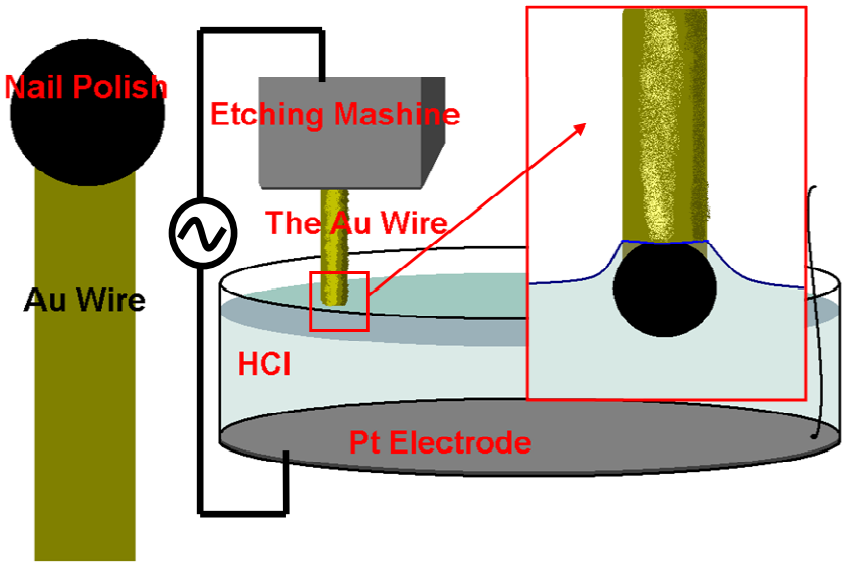

Figure 3-5. Scheme of gold tip preparation by AC etching of a gold wire in concentrated perchloric acid. A droplet of nail polish should be spread on the end of the gold wire. The wire is installed in the etching setup and its end is dipped into the glass filled with perchloric acid. At the bottom of the glass a platinum electrode is placed. An alternating bias voltage is applied between the electrode and the wire.

Using this method very sharp gold tips can be fabricated. However, some complications appear during the etching process. First, there are a lot of bubbles during the etching process. The bubbles perturb the acid surface and the meniscus. Second the current should be switched off immediately after etching is completed. For AC current no special switching devices were used and the current was switched off manually. Nevertheless, some sharp gold tips with a diameter of about 35 nm were produced (figure 3-6).

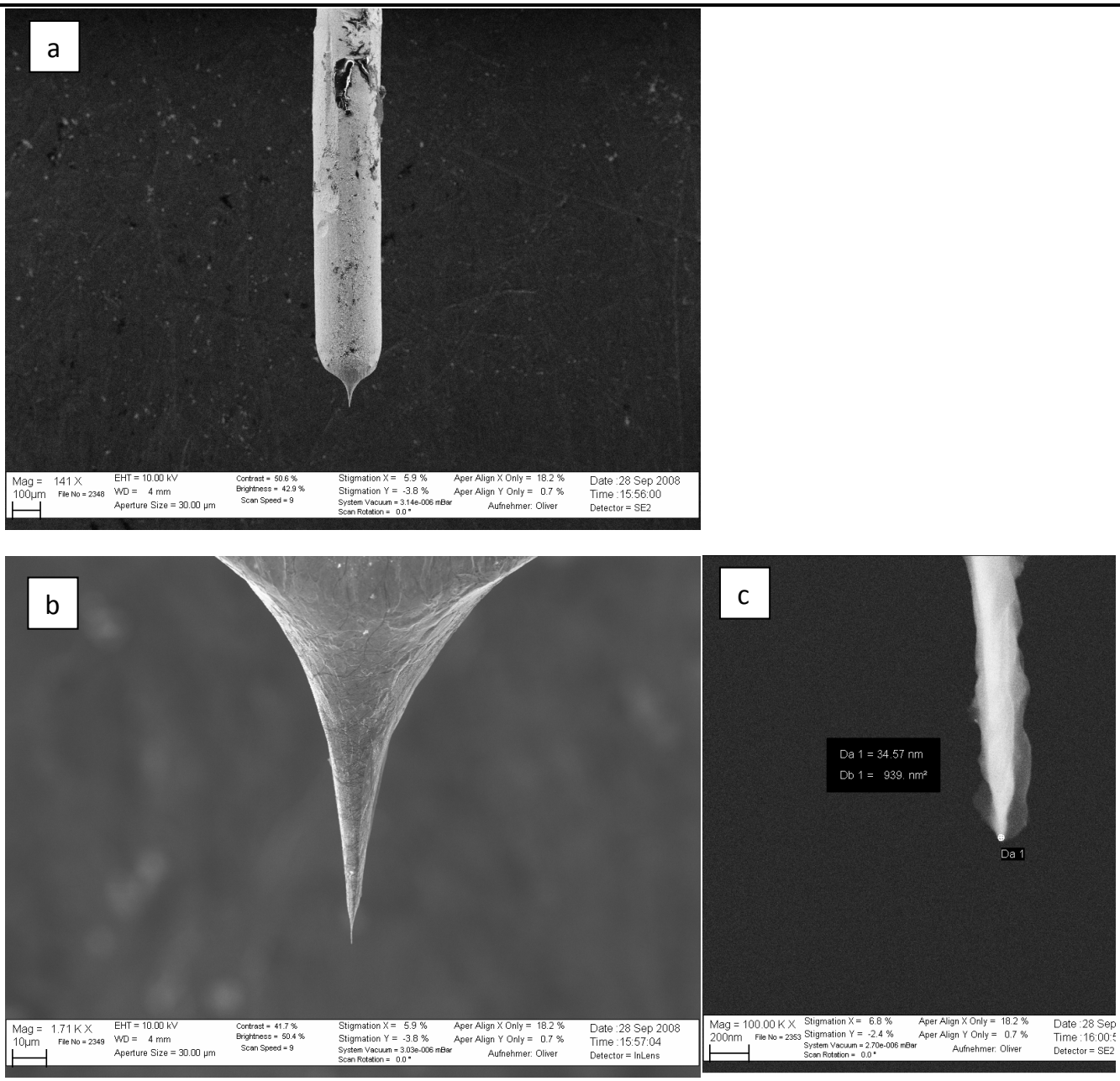

Figure 3-6. Typical SEM images of a gold AC etched tip: a) low magnification, b) medium magnification and c) high magnification. The diameter of the end of the tip is about 35 nm.

Unfortunately, the first tries inside the TEM with the AC etched gold tips showed lots of surface contaminations probably due to the nail polish. Consequently, another method to produce sharp and clean gold STM tips was used, that is DC etching in potassium chloride. The etching process is similar to the DC etching of tungsten tips. In this case, the gold wire with diameter of 0.25 mm was used. It was installed into etching setup and the end of the wire was dipped into a glass filled with saturated solution of potassium chloride (KCl instead of NaOH in figure 3-3), the platinum electrode was used. After several minutes of etching with 2.5 V DC voltage, a clean

and rather sharp tip was produced. The gold tip produced with DC etching was not as sharp as AC-etched one. The smallest diameter was about 80 nm that is still suitable for STM-TEM probing (figure 3-7).

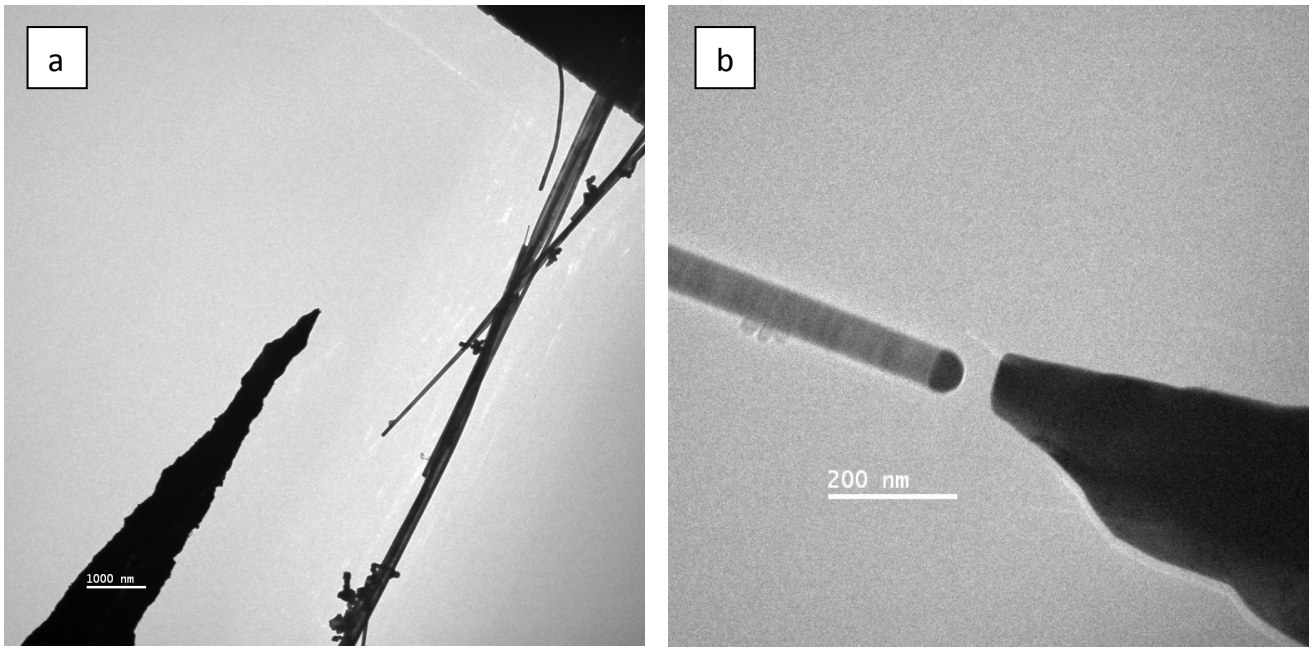

Figure 3-7. Gold DC etched tip approaching an InAs nanowire, TEM images. A) Low magnification. B) High magnification, the tip end diameter is about 80 nm. A diameter of the InAs nanowire is about 50 nm. Due to electron density difference which results in the TEM contrast difference, the gold nanoparticle is visible at the top of the wire.

In a next step some tests with the STM setup were done in air. It is to confirm that with the STM reasonable results could be achieved.

3.3 STM tests in air

Experimental conditions like the humidity, air flow, tip and sample surfaces, vibrations, obviously, are very important during the STM measurements. There are different experiment conditions inside the TEM and outside. Nevertheless, it is essential to prepare the setup on air before using it inside TEM. For this purpose, a graphite sample and a tungsten tip were prepared. The graphite plate was glued to the wire and cleaned with adhesive tape. The sample was installed into the STM-TEM sample holder and several I-V curves were recorded (figure 3-8).

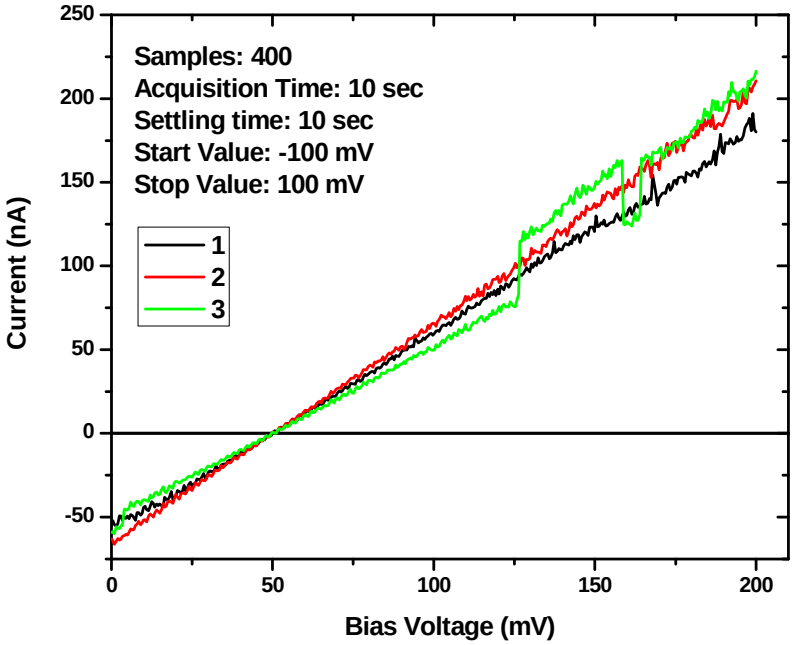

Figure 3-8. I-V curve of the graphite plate measured with a tungsten STM tip in air. Measurement parameters are given. The samples value is a number of points were taken to record each curve. The I-V curves are linear as it is expected for a conductor. The difference in the curves appears due to the difference in the tip to sample distance which was varying because of vibrations. Jumps in the green curve appear due to sudden vibrations. The experiment was made at the room temperature and it is supposed to be the same for all I-V curves due to long settling time. The apparent bias voltage offset 50 mV could be corrected later.

The I-V curves are linear as it is expected for a conductor. Also some unexpected jumps appear, most probably, due to mechanical or acoustic vibrations. In the first experiment a calibration problem was found that gave a bias voltage offset of about 50 mV. The problem was solved by adjusting the control parameters of the control unit.

3.4 STM surface topography imaging

Besides the TEM imaging, the TEM-STM technique provides a possibility to get additional information on sample surface topography using the STM imaging mode. To be sure that the setup works in the imaging mode as well, additional tests of the setup in air were carried out. Several tries to scan the surface of a gold film with different tips were made. Finally, surface topography images were obtained with a PtIr tip (figure 3-9) which is supposed to be the best for STM imaging in air.

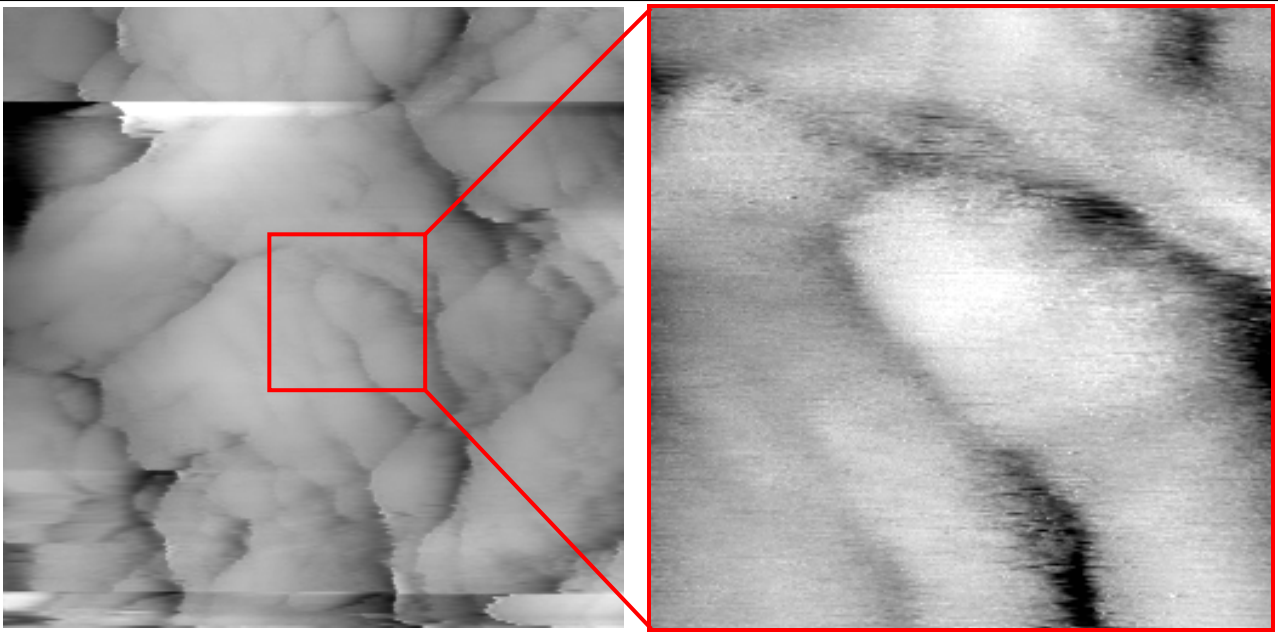

Figure 3-9. A STM topography image of a gold film surface. Left picture is 200x200 nm size, and right is 50x50 nm. The total height difference of the structure is 30 nm for the region on the left picture and 3.7 nm – right picture. The film has granular surface with a lateral grain size of between 15 and 50 nanometers.

One can see a granular structure of the surface that is typical for sputtered polycrystalline gold films. Here we can conclude that, with our STM setup, reasonable quality surface imaging can be achieved even in air. The image quality is far from perfect, most probably due to vibrations. To protect the system from vibrations a damping system consisting of a heavy granite plate on rubber pads was used. On top of the plate the STM setup was placed. Unfortunately, acoustic waves were also disturbing the measurements. To solve the problem the setup was covered with a special box made of absorbing foam material. This improved the situation but did not result in considerable suppression of the vibrations. For time reasons it was decided not to make further upgrades in air and move the experiment directly to the TEM. The TEM is specially built to suppress the vibrations which can disturb the TEM imaging. In this case mechanical vibrations are negligibly small. Care needs to be taken when using large bias voltages. Strong electronic noise can cause a movement of the tip to the sample and melt the tip due to the sudden large current.

Thus all preparations of the setup were done in air. Several tests were carried out showing that the STM setup produces reliable results: in spectroscopy and imaging modes. The rest of the chapter is devoted to the combined STM-TEM experiments. A special procedure of sample preparations and experimental conditions will be described.

3.5 Sample preparation for STM-TEM probing

There are two main requirements for the STM-TEM sample: 1) a sample should be conductive to achieve a current between the sample and the tip; 2) the sample should be visible in TEM. That means that one should make thin enough, and it should be placed on a good conducting substrate. We have found a special way to prepare samples for nanoparticles studies (figure 3-10) and for nanowires studies (figure 3-11).

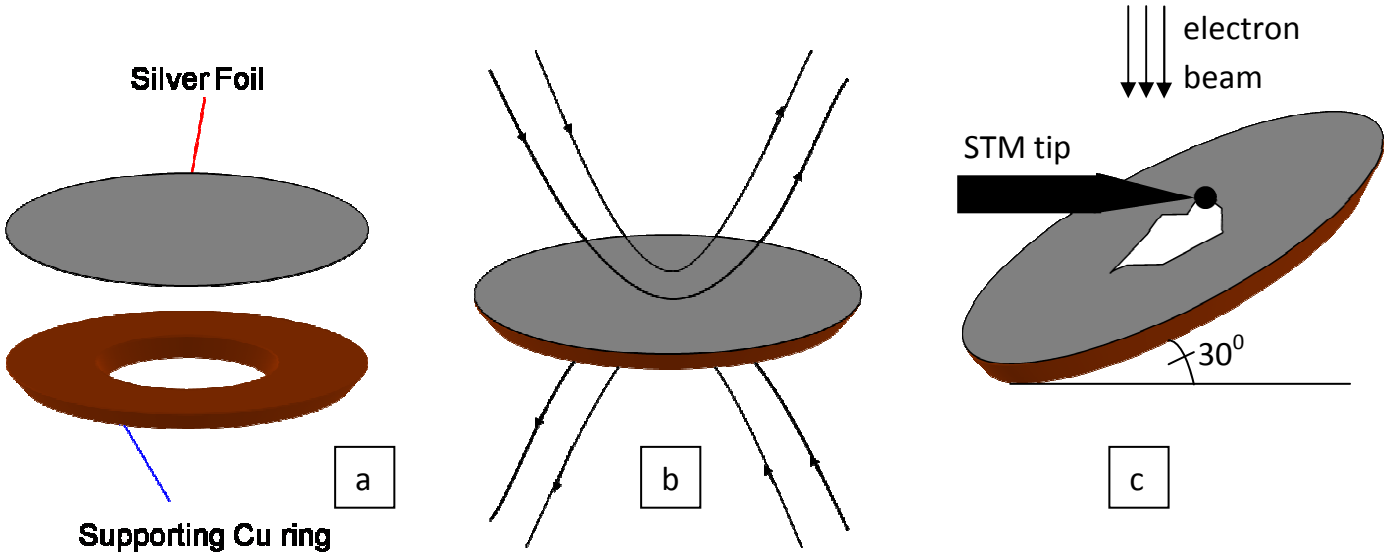

Figure 3-10. Preparation of a STM-TEM sample for nanoparticles studies. A silver foil and copper supporting ring are glued together (picture a). Then a hole in the foil is made using ion beam milling (picture b). Afterwards, nanoparticles are deposited on the edges of the hole and they can be probed with an STM tip and the sample. At the same time the sample is suitable for TEM imaging (picture c).

To prepare the nanoparticle sample which will be suitable for STM-TEM probing one glues a supporting copper ring with diameter of 3 mm and a 0.025 mm thick silver foil disc with the same diameter (figure 3-10a) together. A little hole is drilled in the centre of the foil with ion beam milling (figure 3-10b). The thickness gradient around the hole gives areas which are transparent for the electron beam. Then one deposits nanoparticles to be studied on the edge of the hole, installs the sample into the STM-TEM holder with an angle of about 30^0 and probes the particles with the STM tip (figure 3-10c). Here all two requirements for STM-TEM probing (conductance of the sample and absence of its shadow on the object) are fulfilled.

To measure a nanowire sample with the STM-TEM setup the following procedure was used: 1) a substrate with epitaxially grown InAs nanowhiskers perpendicular to the

surface was glued to the edge of a plate as schematically shown in a figure 3-11a; 2) a copper wire is attached to the substrate using conductive silver glue. The copper wire should be fixed to the substrate at an angle of 45^{o} with respect to the substrate plane thus making the wires at the substrate edge visible in the TEM (figure 3-11b).

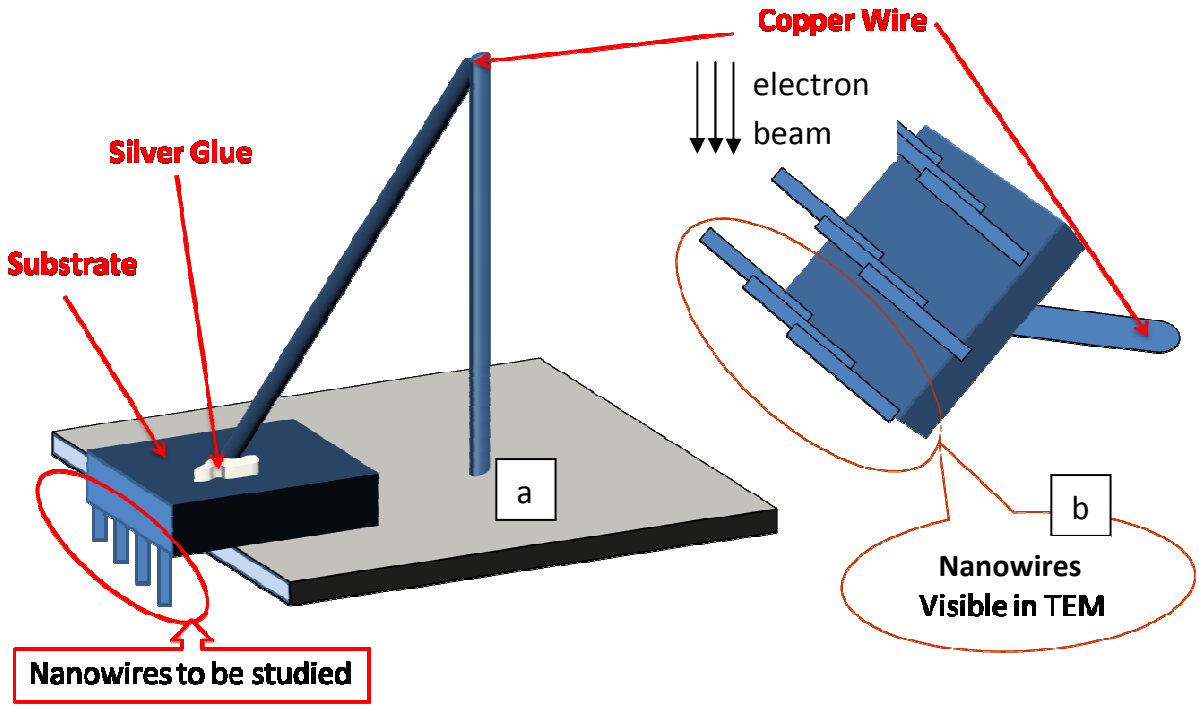

Figure 3-11. Preparation of the STM-TEM sample for epitaxial nanowires.

It should be noted that the substrate conductivity has to be much higher than that of the objects to be probed with the STM. Therefore the InAs nanowires were grown on the p-doped substrate.

3.6 Magnetic field calibration inside Philips CM12 TEM

Measuring electrical properties in-situ in a TEM requires the analysis of any electrical and magnetic fields in the object plane. Any TEM equipped with magnetic objective lens will have magnetic field at the sample position. This can influence the measurements and has to be taken into account. Special experiments were carried out to measure the magnetic field in the microscope at the sample position (figure 3-12).

The setup was built on the standard plate holder (figure 3-2). The plate holder has four blank contact pads which were soldered with a special alloy to the copper wires

and to the Hall sensor which was mounted into the STM-TEM sample holder in that way, that the sensor is located at the usual sample position.

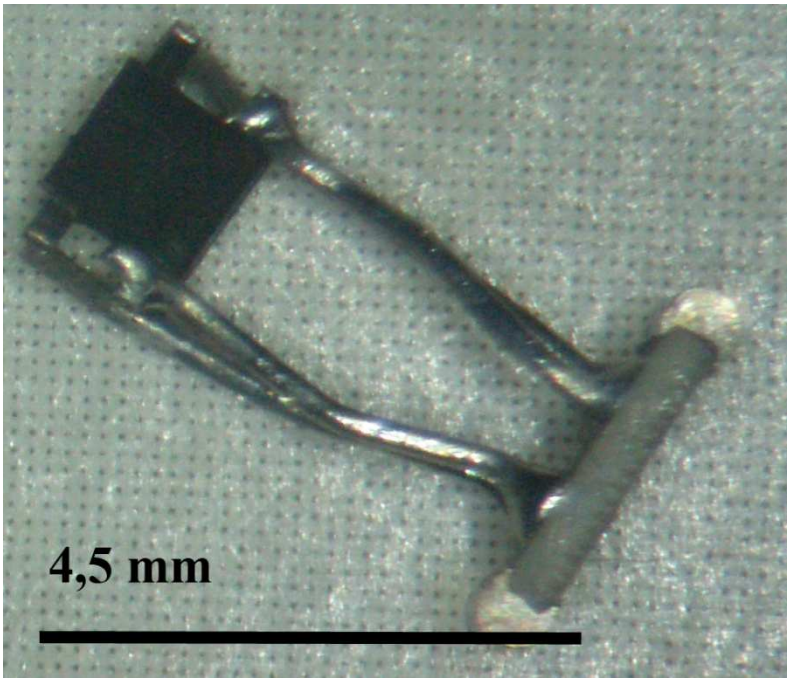

Figure 3-12. The Halls sensor mounted on an aluminum oxide plate with four copper wires.

The magnetic field values for different magnifications and sample positions after calibration of the Hall sensor (figure 3-13) are given in table 3-1.

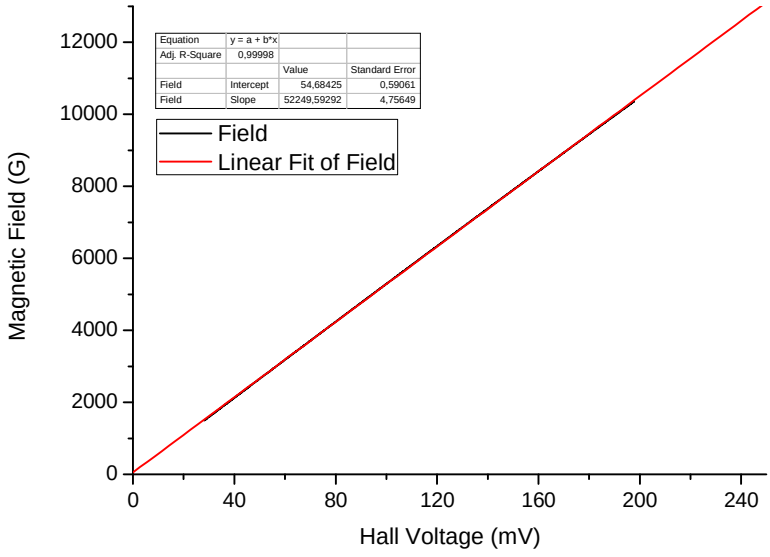

Figure 3-13. Calibration curve for the Hall sensor used for TEM magnetic field measurements. The sensor shows good linearity for magnetic fields up to 1.3 Tesla.

Table 3-1. Magnetic field measured in Philips CM12 TEM at the sample position.					
Magnification mode	Range	Magnification	Obj. Lens Current, mA	Hall Voltage (-), mV	**Field, G**
LM	31:2050	31	293	12.847	**726**
		300		12.86	**727**
		2050		12.881	**728**
M	2650:4400	2650	4128	183.575	**9646**
SA	5600:380k	5600	4102	182.362	**9583**
		175k		182.39	**9584**
		300k		182.4	**9585**
M	510k:660k	510k	4098	181.935	**9561**

The magnetic field depends on the objective lens current. The current is different in different magnification modes. For Low Magnification (LM) was measured field of about 700 G. In the other magnification modes the sample experiences a magnetic field of approximately 10 kG. The field is homogeneous as confirmed by moving the sensor in all three dimensions a few hundreds of microns. The presence of the magnetic field in the microscope gives us a possibility to carry out, for example magnetoresistance measurements in-situ probing the transport properties at different magnification modes.

3.6 Field emission and carbon contamination

Tips obtained by electrochemical etching process need a further cleaning step as their surface is covered with contaminants which cannot be removed by rinsing in water, acetone or ethanol. An oxide layer (mainly WO_3) develops on the tungsten tip during electrochemical etching. Contaminants will cause instabilities in the tunneling junction, thus increasing the noise level. Being irradiated by the high energy electron beam of the microscope organic contaminants are decomposed and a thick carbon layer forms at the tip/sample surface. Surface carbon contamination caused by the electron beam irradiation of organic residuals at the sample surface can complicate the STM measurements. Passivation of the sample/tip surface results in changes of the electronic density of states (DOS), causing difficulties in the probing of the sample by tunneling current. The presence of an insulating oxide layer can lead to a tip crash, since the resistance of this layer is greater than the tunneling gap resistance corresponding to the set current and the tip will never touch the sample surface before the desired current will be reached.

To remove the oxide layer a lot of methods were reported in the literature, such as an ion-milling, self-sputtering, annealing of the tip in vacuum, annealing of the tip in an electrical field with a high gradient or annealing of the tip in an oxygen atmosphere. The listed above procedures give good results but they cannot be used

in the STM-TEM setup in the conventional transmission electron microscope. A special in-situ cleaning setup is needed and was tested successfully.

To reduce the contaminations in our setup two procedures were examined: plasma cleaning and field emission. Conventional TEM plasma cleaning in a mixture of argon and oxygen gases was applied to the sample holder with the tip and sample mounted before inserting it into the microscope. The plasma cleaning is a well-known effective method to remove carbon and carbon-contaminated substances from surfaces. In the present work the plasma cleaning was performed three times for 10 seconds in Fischione Instruments Plasma Cleaner, but it could not be used for tungsten tips which are turned out to be strongly damaged after the plasma cleaning (figure 3-14). The plasma cleaning did not remove the oxide layer and even resulted in further oxidation. Also, one should not forget that the chemically reactive plasma can modify the nanowire surface especially in the case of semiconductor nanowires.

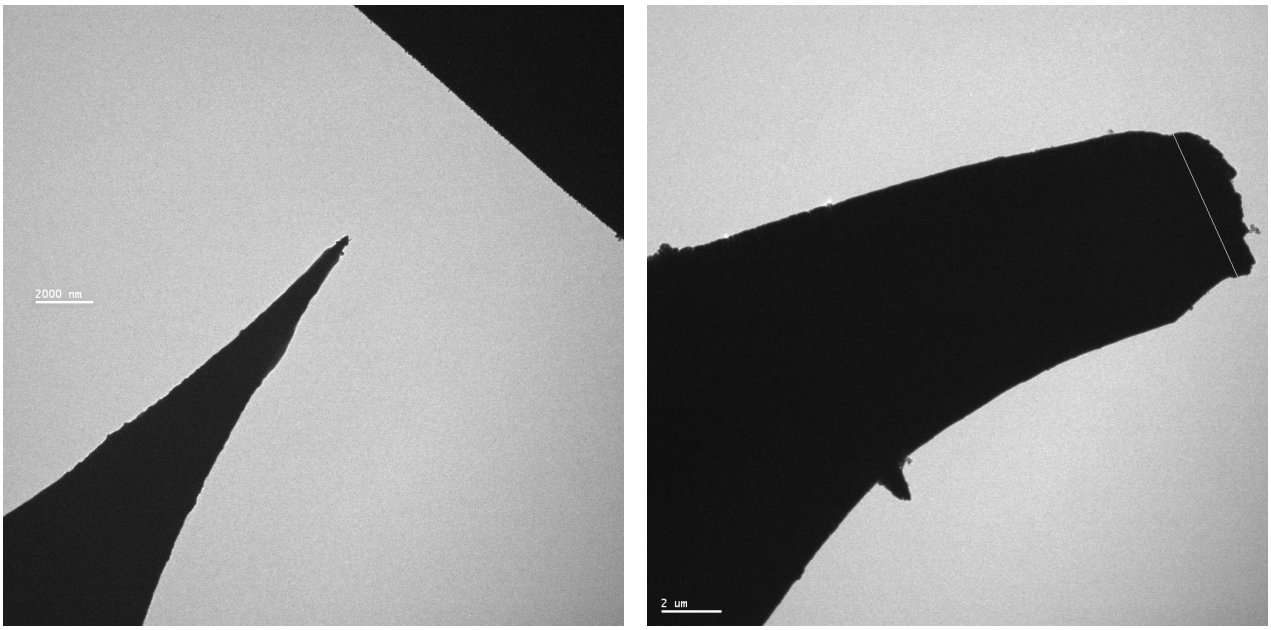

Figure 3-14. Tungsten tip before plasma cleaning (left) and after plasma cleaning (right). The diameter increases more than 100 times.

Nevertheless, the plasma cleaning procedure was used for gold tips and improvement of contact formation at the gold nanoparticles-tip interface was reached.

The other possibility to clean the tip is to apply very high biases of up to 140V. This high bias regime causes Field Emission of electrons from the tip. It is the only method to modify the tip in-situ.

STM experts usually say that it is possible to modify shape of tips by emitting electrons from the sample to the tip [75]. In this case electron migration causes the transfer of some amount of material in the direction opposite to the electron current. That results in growth of the sharp tip. It could turn out to be a good opportunity to increase the sharpness of the tip in-situ and more tests are needed in the future. The next chapter introduces the main topic of the study – InAs nanowhiskers grown by MOCVD method. In particular, synthesis, morphology and structure will be described.

Chapter 4. InAs nanowhiskers: synthesis and structure

4.1 Growth of InAs nanowhiskers by vapor liquid solid epitaxy

There are a couple of methods to synthesize the whiskers as described in section 2.2.

Here, the following method was used. The InAs nanowhiskers were prepared using the vapor liquid solid approach of growth by Metal Organic Chemical Vapor Decomposition (MOCVD) in the group of Prof. F.-J. Tegude (Universitaet Duisburg-Essen). On an InAs (001) B substrate ("B" means the substrate surface terminated with As atoms [76]) colloidal nanoparticles with a diameter of 50 nm were first deposited. The particles were annealed at 620 ^{o}C for 10 minutes under nitrogen and trimethylindium flow in order to form an Au-In interface. Afterwards wires were grown for 10 minutes at 400 ^{o}C by low-pressure MOCVD with nitrogen as carrier gas and tertiarybutylarsine, trimethylindium as group-V and group-III precursors respectively. The precursors flowed at constant V/III ratio R = 6 [77]. The InAs nanowhiskers grew with a diameter of about 50 nm and a length of 5 to 10 microns. In figure 4.1 the growth chamber is shown.

Figure 4-1. Setup for InAs nanowhiskers growth consisting of an evacuated glass chamber. Inside the chamber the InAs substrate with the gold nanoparticles was placed. The precursors flow through the chamber. (The picture is provided by the group of Prof. Tegude.)

4.2 Morphology of the InAs nanowires

The morphology of the nanowhiskers was characterized by SEM and TEM. The wires have a length of (6±1) µm and diameter of (55±5) nm. The small diameter variation is

due to the narrow size distribution of the colloidal gold nanoparticles which were used in the synthesis. As seen in the SEM image (figure 4-2) most of the wires grow along the (001) direction – perpendicular to the substrate. But some grow with an angle to the substrate, and the question arises, if the different growth correlates with a different morphology and structure of the individual wires.

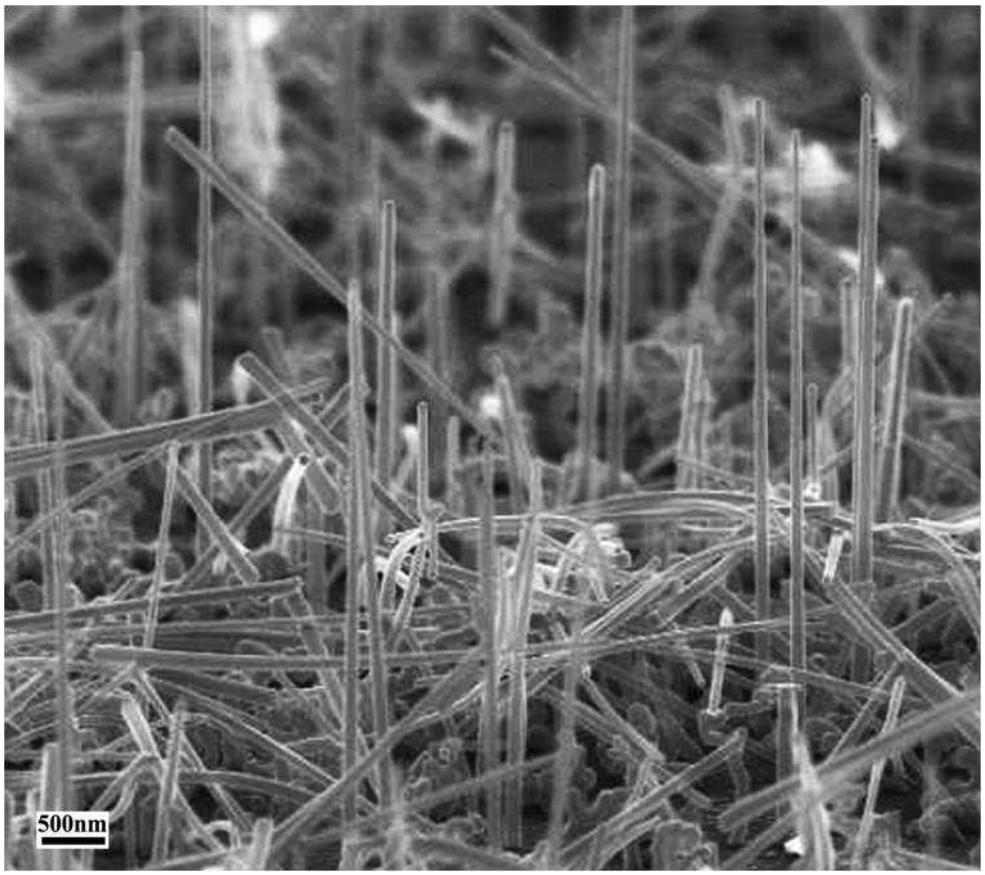

Figure 4-2. Typical SEM image (Group of Prof. Tegude) of InAs nanowhiskers. Each wire has a constant diameter over its length. The gold particle on top of the wires can be seen. Some wires are growing not perpendicular to the substrate [17].

4.3 Structure of InAs nanowhiskers

Structural studies were performed with high resolution TEM, energy filtered TEM (EFTEM), scanning TEM (STEM), energy dispersive X-Ray spectroscopy (EDXS), fast Fourier transformation of HRTEM images (FFT) by Dr. Zi-An Li (Universitaet Duisburg-Essen). Due to the synthesis process it is interesting to investigate the interface between the gold nanoparticle and the InAs nanowire. Elemental mapping by Energy Filtered Transmission Electron Microscopy was investigated. In this technique only electrons in a narrow energy window which is tuned to electronic inner-shell

excitations of the element of interest are used to form an EFTEM image [78], [79]. The In and As distributions in the wires are shown in figure 4-3.

Analyzing the element specific images we can conclude that indium is alloyed with gold in the particle at the end of the wire. It also forms a shell around the particle. To prove this conclusion a combination of Scanning Transmission Electron Microscopy and Electron Dispersive X-Ray Spectroscopy was used. The electron beam of the TEM was focused as much as possible (like in usual STEM mode) and scanned along the wire's growth direction. During the scan X-Rays were detected.

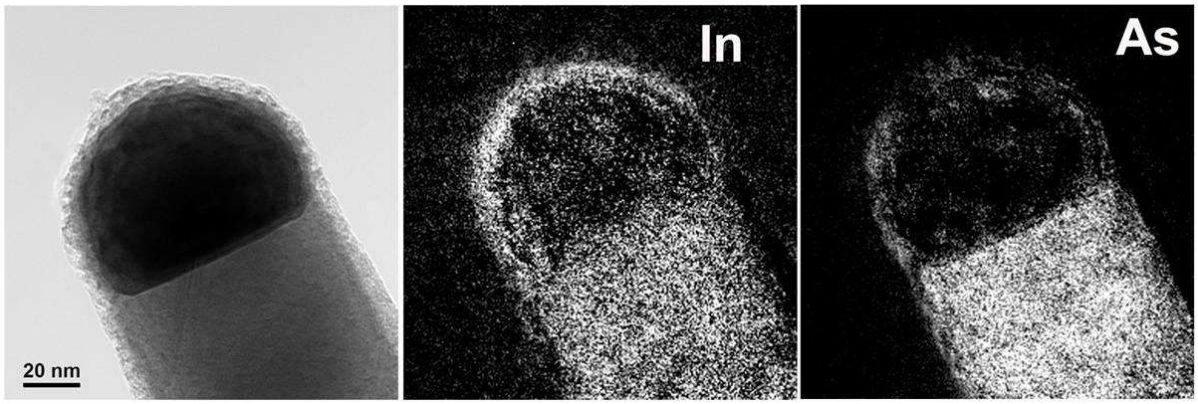

Figure 4-3. In and As distribution in nanowhiskers. Left picture is the unfiltered TEM image. Center image is the filtered TEM image showing the distribution of In atoms and right – distribution of As atoms by the bright content.

The method gave quantitative information about indium, arsenic, and gold distributions along the scan direction (figure 4-4). The EDXS confirmed the absence of gold in the semiconductor part of the wire. Also there were confirmed that the gold particle contains about 25 % of In atoms. Furthermore, the interface between gold and the wire is very sharp. The indium concentration is not reduced near the interface. Most probably the gold particle attracts indium from the substrate during the annealing step [17], [33].

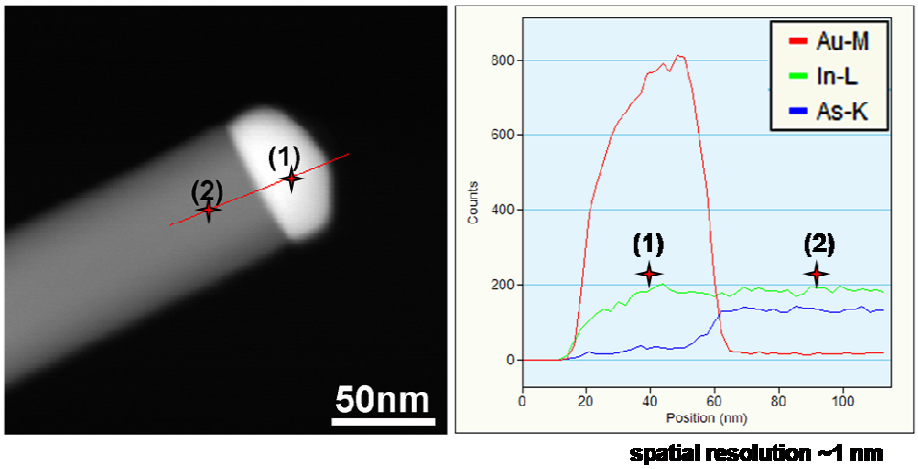

	Element	Atomic (%)
(1)	As	4.24
	In	24.87
	Au	70.88
(2)	As	50.49
	In	49.51
	Au	0.0

Figure 4-4. EDXS scan along the nanowire. In the left picture Red line shows the scan direction. A dependence of X-Ray counts for different elements of beam position along scan direction is in the right picture. Element distribution in point 1 and 2 are given in the table.

This result can provide some ideas about how to improve the synthesis method. Perhaps, it is better to use AuIn nanoparticles instead of pure Au to avoid the annealing step in the synthesize procedure. It supposed that without annealing step the wires will grow more homogeneous and only along one direction due to during the annealing nanoparticles are used to immerse in the substrate therefore nucleation process can occur in different directions.

To determine atomic the structure of the nanowires High Resolution Transmission Electron Microscopy and Fast Fourier Transform techniques were used. For this experiment wires were cut from the substrate and then deposited on the TEM grid. Wires of three different atomic structures were found in the same sample. The first type is wires with cubic Zinc-Blende structure, without stacking-faults and defect-free. These wires grow along the <001> cubic direction, supposed to be perpendicular to the substrate (figure 4-5).

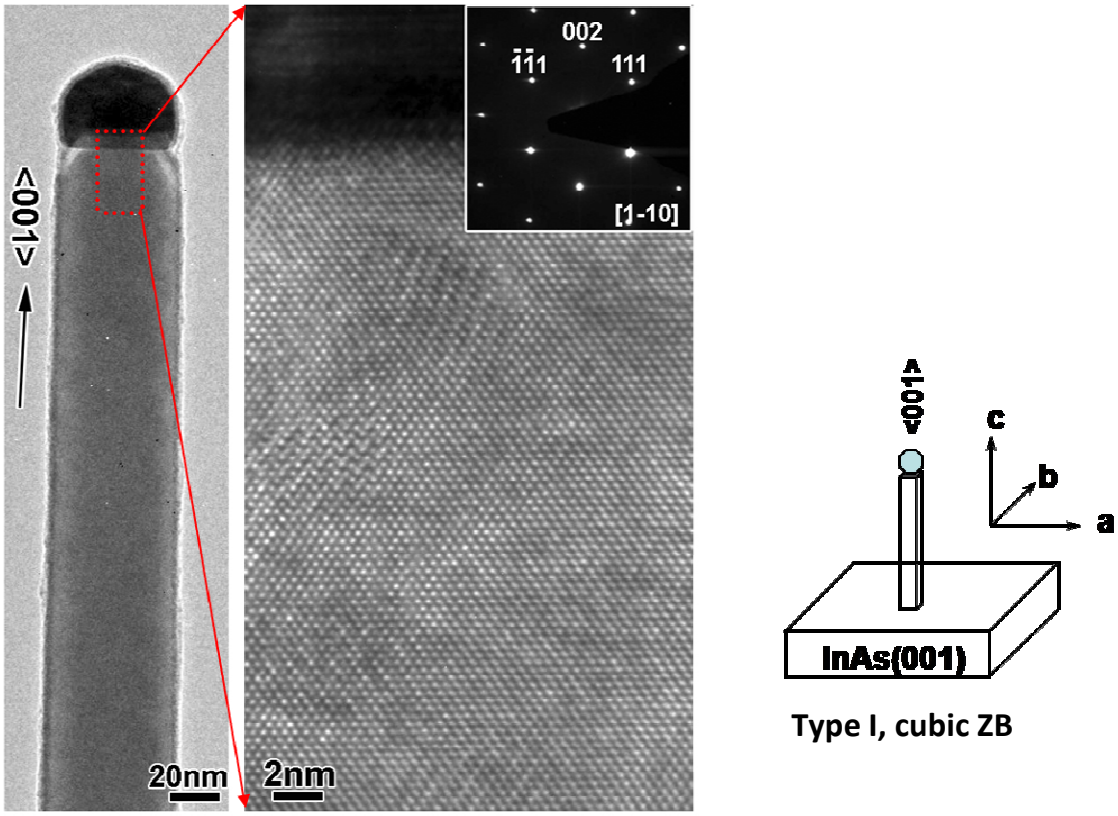

Figure 4-5. A low magnification TEM image of InAs nanowhiskers with the first type of structure (left). A corresponding HR-TEM image (center). FFT pattern for the same area (insertion in central image), characteristic spacing and angles below: a = 0.6055 nm, b = 0.6055 nm, c = 6.055 nm, $\alpha = 90^0$, $\beta = 90^0$, $\gamma = 90^0$ – typical for fcc Zinc-blende structure. Scheme of InAs nanowhiskers with the first type of structure is on the right-hand side.

The second type of the wires has hexagonal Wurtzite structure also without stacking-faults and defect-free. This wires grow along the <-12-10> hexagonal direction, i.e. with an angle of 57.4^0 to the substrate (figure 4-6).

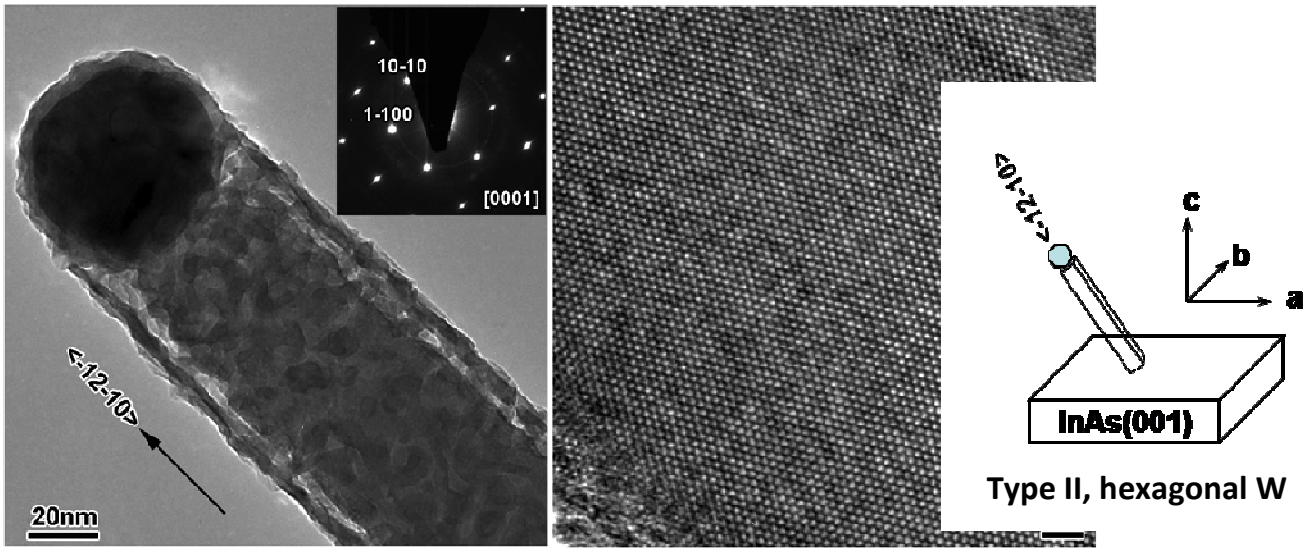

Figure 4-6. Low magnification TEM image of the InAs nanowhiskers with the second type of structure (left). Corresponding HR-TEM image (center). A SAED pattern for the same area is inserted on the left, characteristic spacings and angles are: a = 0.4245 nm, b = 0.4245 nm, c = 0.6990 nm, $\alpha = 90^0$, $\beta = 90^0$, $\gamma = 120^0$ – typical for hexagonal Wurtzite structure. Scheme of the InAs nanowhiskers with the second type of structure given on the right-hand side.

The third type of structure is the most interesting object to study. It is a mixture of Zinc-blende and Wurtzite structures, or one can say that it is cubic Zinc-blende structure with hexagonal Wurtzite stacking-faults defects. In the Zinc-blende lattice some plains are replaced by planes of the Wurtzite cell (figure 4-7, 4-8). A presence of 180 degrees rotation twins was also found. It means that the Zinc-blende plates are rotated against each other at an angle of 180 degrees. This kind of wires grow along the <111> cubic direction (equal to the <0001> hexagonal) at an angle of 35.3 degrees with respect to the substrate.

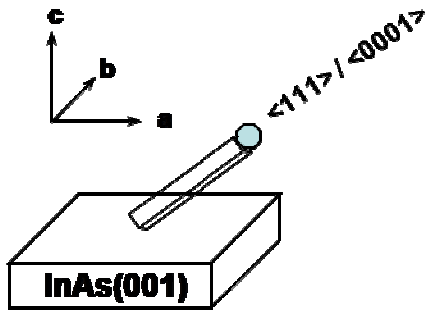

Figure 4-7. Scheme of the InAs nanowhisker with the third type of structure.

The characteristic TEM images of the wires with type III structure (figure 4-7) have a specific stripe contrast. The contrast appears due to twinning defects.

Summarizing the structural data it should be noted that in the same growth process three different types of wires are formed. The wires have a different crystalline structure and grow in different directions (figure 4-9).

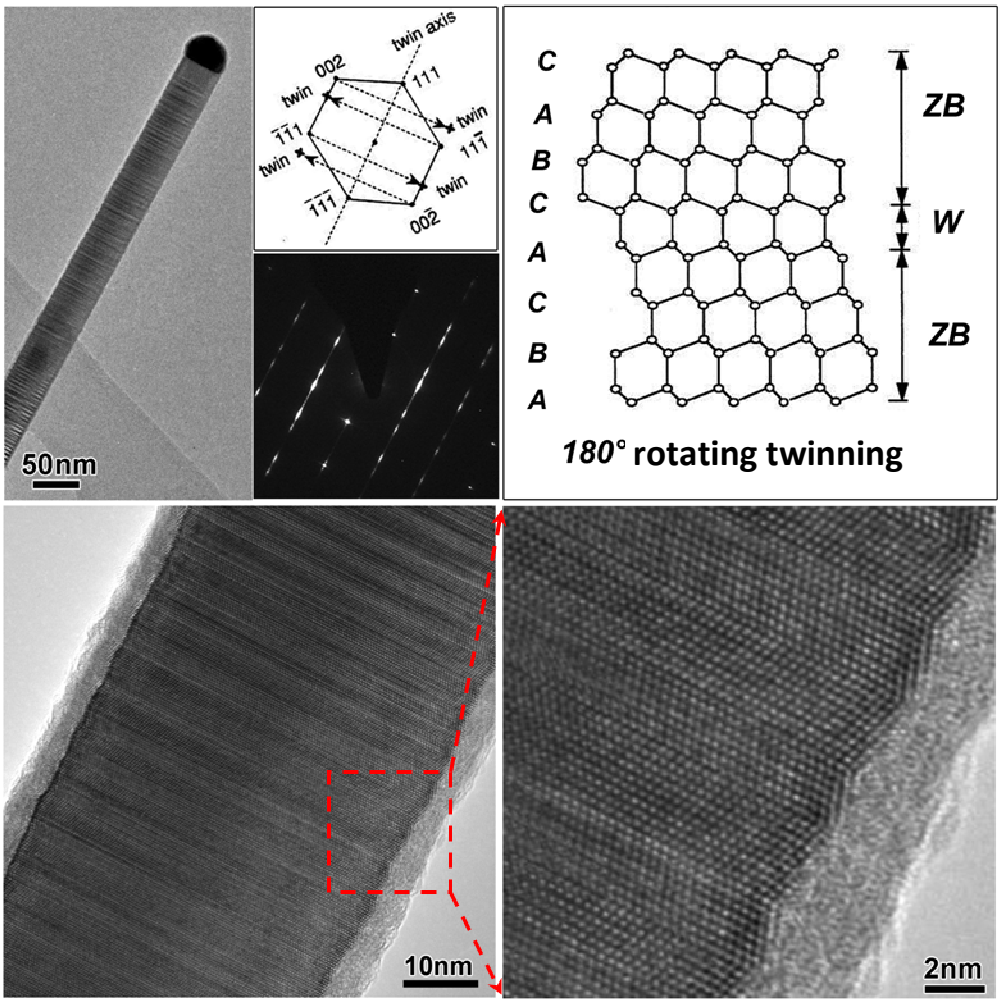

Figure 4-8. Upper part: Low magnification TEM image of the InAs nanowhiskers with the third type of structure (left). It is easy to see the stripe contrast inside the wire corresponding to the twin defects. A SAED pattern (centre bottom) and a scheme of the pattern (centre top). The double spots on the diffraction pattern correspond to rotation twin defects. Scheme of crystal planes in the wire (right). From bottom to top: usual order of planes for Zinc Blende (ZB) structure is: A-B-C-A. But instead of B plane C appears and planes C-A-C are the Wurtzite structure. It switches back to ZB structure but in the wrong order C-B-A-C, it is a typical rotation twin defect.
Lower part: Medium magnification picture with the stripe contrast (left) and the corresponding HR-TEM image (right). The rotation twin defects can be easily seen.

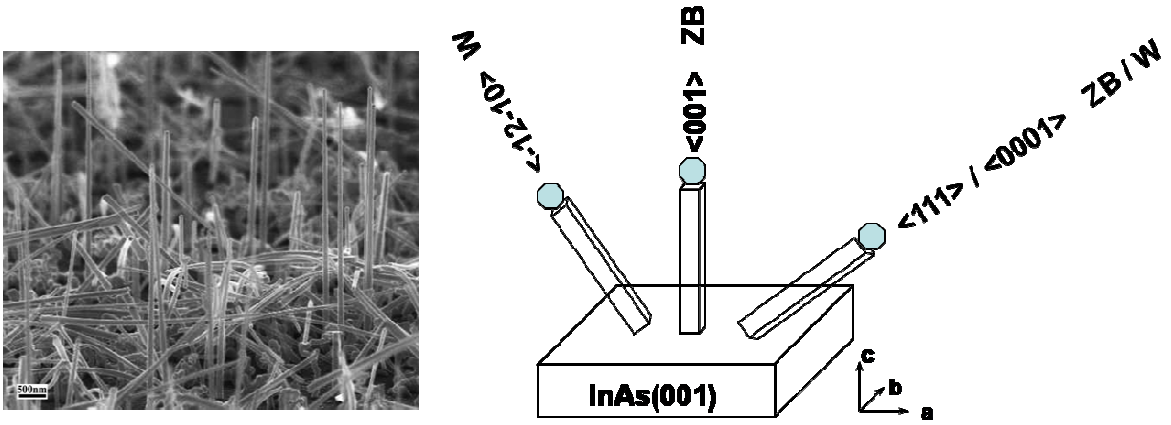

Figure 4-9. Three different types of the wires grown on one sample. The wires grown along the <001> direction have cubic Zinc-blende structure, along <-12-10> - hexagonal Wurtzite, along <111> cubic direction – Zinc-blende structure with the Wurtzite stacking-faults.

Wires with three different crystallographic structures appear in the same sample and are supposed to have different electrical properties. The next chapter will address the in-situ STM-TEM electrical and structural characterization of InAs nanowhiskers. This method gives a unique possibility to correlate each electrical measurement of a wire with its structure.

Chapter 5. Transport properties of InAs nanowhiskers

5.1 Standard procedure to study the transport properties of nanowires

The usual method to study electrical properties of nanowires is the so-called four point measurement. In this technique wires are first cut from a substrate, dispersed in a solution and deposited on a non-conductive substrate. After these operations, a wire is selected by SEM imaging and using Electron Beam Lithography four contacts are written on the wire (figure 5-1).

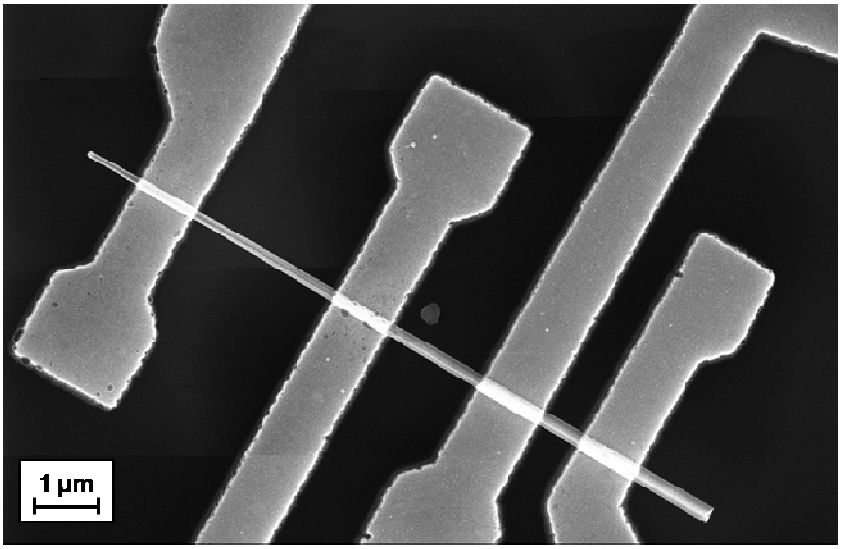

Figure 5-1. SEM image of four contacts made on an InAs nanowire (taken from the group of Prof. Tegude). Two outer contacts are used to apply the current, two inner ones are to measure the voltage.

There are some obvious disadvantages of this method. First, the wires must be cut from the substrate that can principally cause some change in structure or morphology. Second, the wire with the applied contacts is lying on the thick substrate which is not transparent to an electron beam of TEM. In this case the likely morphological changes or a deformation cannot be detected and it is impossible to perform high resolution structural studies. This is very critical in our case, when in the same sample there are wires with three different types of crystallographic structure. Obviously the electrical properties will depend on the atomic structure of the nanowhiskers. In our approach we have the opportunity to correlate the crystal structure and morphology with the electrical properties.

The next two sections will be dedicated to the experiments on the InAs nanowires done with a novel method which provides this new possibility.

5.2 Probing an individual nanowire with tungsten STM tip

In this section I will discuss how to probe the individual nanowire grown on the substrate with an STM tip in-situ in a TEM.

When the STM holder with sample and tip is installed in the TEM, the tip and the nanowires can be seen in the TEM at low magnification. The TEM is used image the approach of the tip to the InAs nanowire. The main difficulty is that the tip and the wire are at different height. A TEM image is formed as a two-dimension projection of the objects on the screen (more details were provided in section 2.3) (figure 5-2). That means the TEM image cannot provide information about the tip height. Consequently, the first step is to bring the sample at the eucentric position, which is the focus position of the microscope when no defocus current is applied. The next step is to bring the tip at the same height as the sample. The best way was found to use a defocus to measure the distance between the sample and the tip in Z direction. It means, first to bring the sample in the focus and press the “reset defocus” button. In this case the defocus value will be zero. Then one brings the tip into the focus. Here a sharp tip will make the operation much easier. The defocus value will give the distance between the tip and the sample.

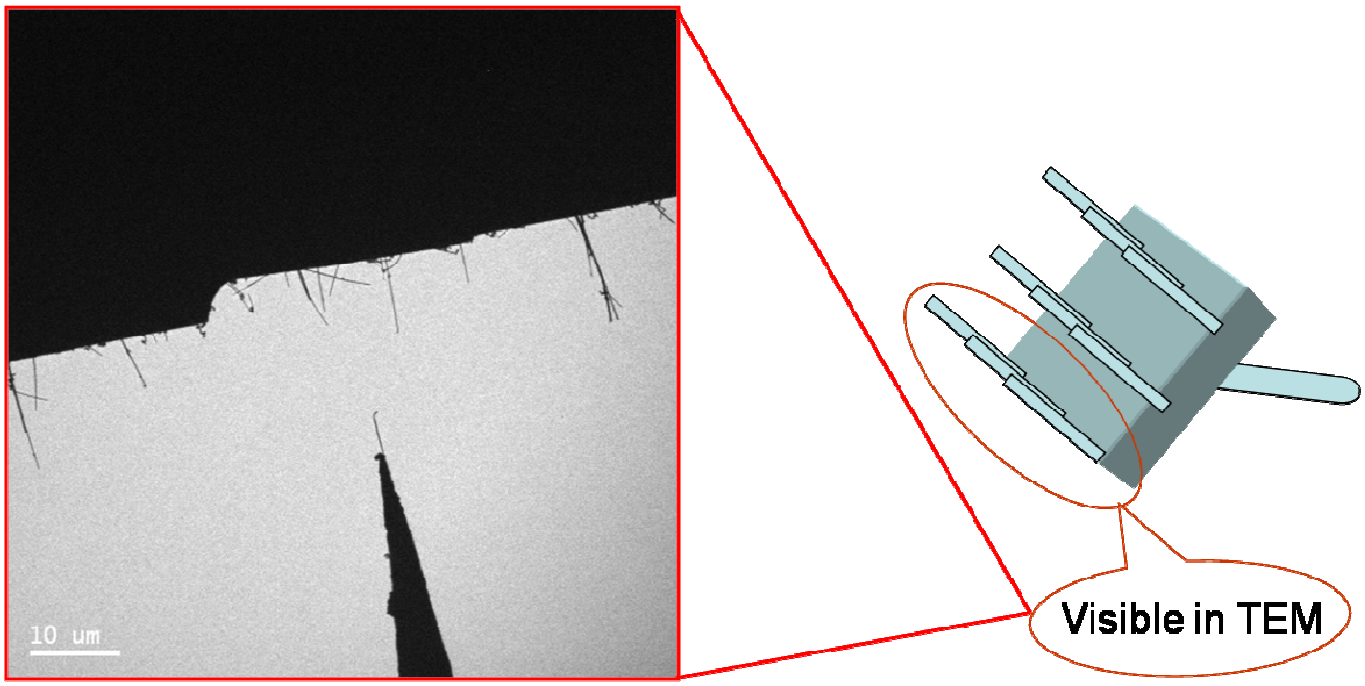

Figure 5-2. TEM image of the InAs nanowhiskers sample and the STM tip (left image). From top to bottom: InAs substrate, InAs nanowhiskers grown on the substrate, gold STM tip. On the right hand side is a scheme of the setup. Only wires on the edge of the substrate could be seen in the TEM. To install the sample into the setup the substrate should be glued with conductive glue to the copper wire at some angle (as described in section 3.5).

One should note that a positive defocus value means that the tip is below the sample. If the defocus value is negative, the tip is above the sample and should be moved downwards. The best procedure is to make the approach step by step. Focus on the tip, move it a bit, focus again and then move it again. When the distance is in the range of fine movement of the tip it is possible to move the tip quite precisely with the piezo and position it at the same height as the wire. After the tip is very close to the sample the electrical contact between the tip and the wire can be made. If the tip height is correct it is easy to touch the wire moving the tip straight ahead. The appearance of the contact is easily identified by a slight wire movement. When the tip and the wire are in contact some mechanical force and electrical pulses should be applied to achieve the best electrical contact. Afterwards, the I-V curves can be recorded.

The first series of experiments on the electrical properties of InAs nanowhiskers was performed with tungsten tips. The nanowire sample was not a good one to study due to the fact that the diameter of the wire changed along the wire growth direction and almost all wires were without a gold particle on the top and tungsten tip was in direct contact with the semiconducting nanowire. That gives an additional undetermined resistance – contact tip-to-wire resistance.

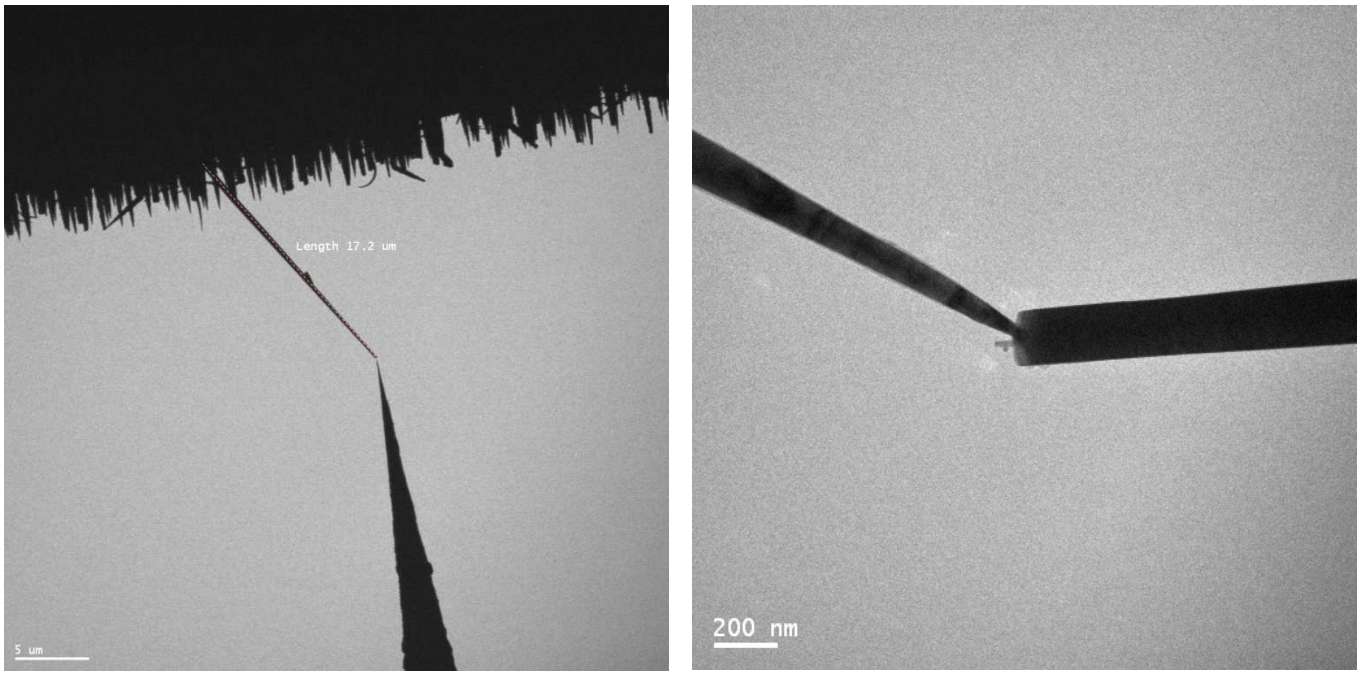

Figure 5-3. Low magnification TEM image of the tungsten tip (at the bottom) approaching the InAs nanowire (at the top) (left figure). A high magnification TEM image of the tip (left) in contact with the InAs nanowire (right figure). Notice the absence of the gold nanoparticle on the top of the wire (compare with figure 4-6).

A characteristic TEM image of the tungsten tip in contact with the wire is shown in figure 5-3. The tungsten tip sometimes has a smaller diameter than the wire, this gives a rise to constriction resistance (see section 2.6) which value estimated as R_C = (15±5) kOhm and excluded from the resistances of the nanowires. A big bias voltage of 3 V was applied for 10 ms to improve the contact between the tip and the wire. Afterwards the I-V curves were recorded. The characteristic I-V curve for InAs wires probed with a tungsten tip is shown in figure 5-4. The I-V curve is not linear due to one of the reasons: 1) presence of Schottky barriers between the InAs wire and the tungsten tip and between the InAs substrate and copper wire; 2) ohmic heating (with dissipated power of 24.7 μW) and consequently increase of the conductivity of the wire (see section 2.2). The resistances of the wires were calculated by a linear approximation of the low-voltage part of the data from -200 V to 200 V and extraction of the resistance due to the constriction at the interface. Resistance R = (77±6) kOhm was calculated for InAs nanowire with a diameter of (175±3) nm and a length of (17±2) μm approximately. It is a typical value for the first sample probed with the tungsten tip. Unfortunately, this first session of experiments couldn't be used to extract any quantitative information on the resistivity since the wires had a conical shape.

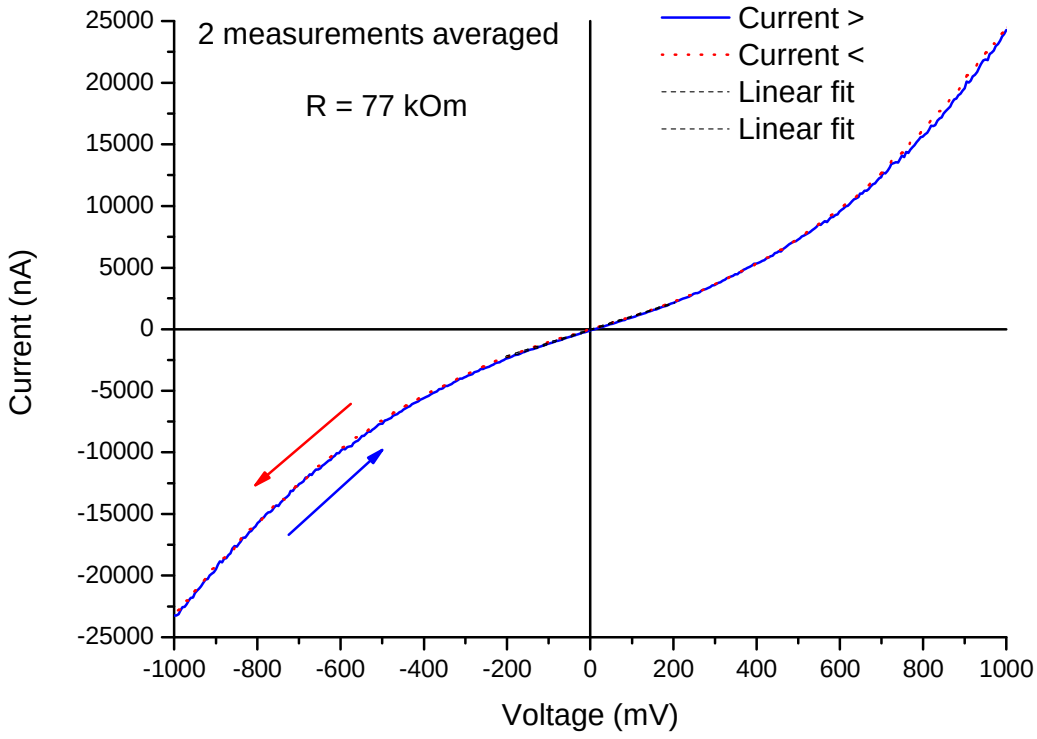

Figure 5-4. Characteristic I-V curve for the InAs nanowire (without a gold nanoparticle on the top) probed with the tungsten tip. The curves were recorded with increasing bias voltage (blue solid line) and decreasing bias (red dotted line). The data are linearly fitted between -200 V and 200 V (black dashed lines).

As a side product an interesting type of new nanowire consisting mostly of carbon was created. Initially, a contact was established between the InAs nanowire and the tungsten tip (figure 5-5) and the usual spectroscopy measurement was made (figure 5-6).

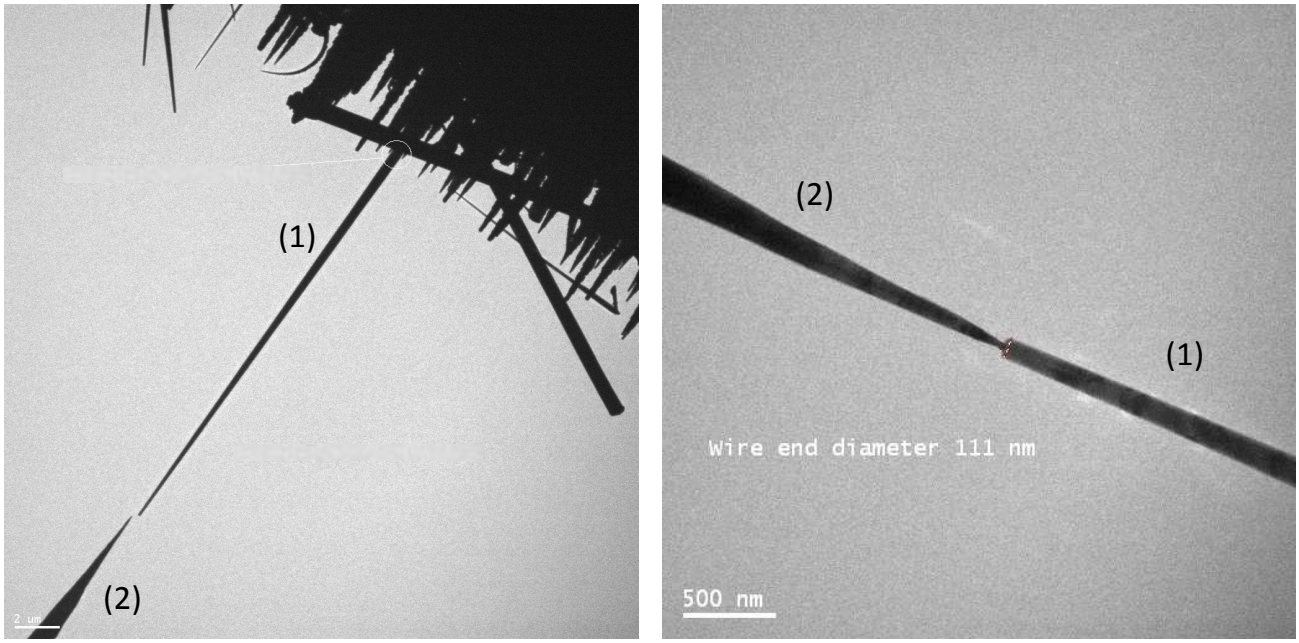

Figure 5-5. The nanowire (1) and the tungsten tip (2) are seen at low magnification (left image, the scale bar is 2 µm). The wire length is more than 25 µm. The tip (2) in contacting to the wire (1) is shown in the right high magnification TEM image. The wire end diameter is about 111nm.

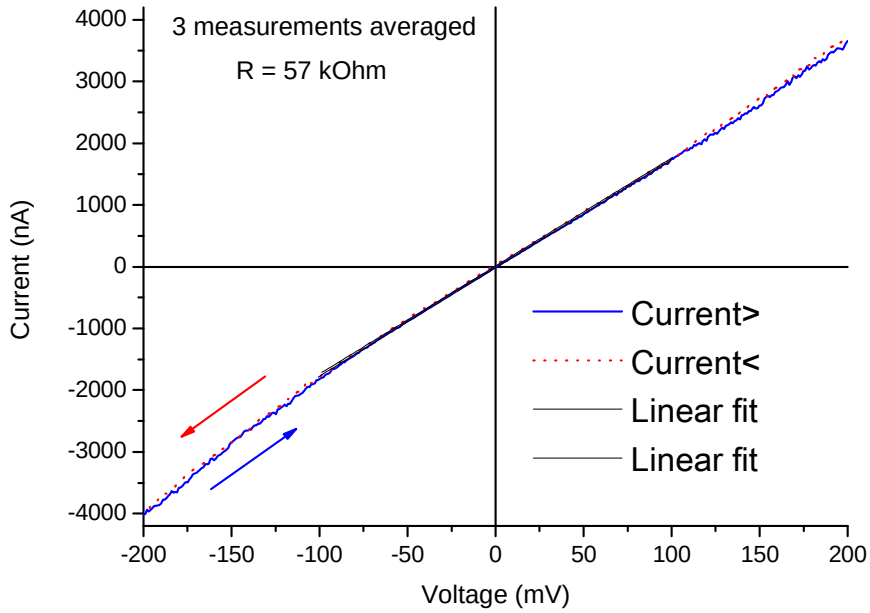

Figure 5-6. I-V curve for the wire probed by tungsten tip taken in two directions: increasing bias (blue solid line) and decreasing bias (red dotted line). The wire resistance was extracted from linear fit of -100 mV to +100 mV part of the curve.

The measurements were performed in the following way. The voltage was varied between a lower and upper bias voltages, which were step by step (0.2 V) increased to values of -1.2 V and 1.2 V respectively. Below the range of -1.2 V to 1.2 V the I-V curves were similar like in figure 5-4. The measurement from -1.2 V to +1.2 V was performed starting at -1.2 V, increasing voltage until 1.2V and then decreasing until -1.2 V. The current first rapidly increased at 1000 mV and then more rapidly decreased at voltage 1200 mV shown in figure 5-7. After switching the electron beam on it was observed that the InAs wire was destroyed in the middle and only a fiber with smaller diameter of 20 to 70 nm was left (figure 5-8). It supposed that the nanowire was melted at the voltage of 1200 mV and the power applied in this case was 36.2 µW. The current increase at 1000 mV probably corresponds to structural change of the wire due to the ohmic heating or the electron migration.

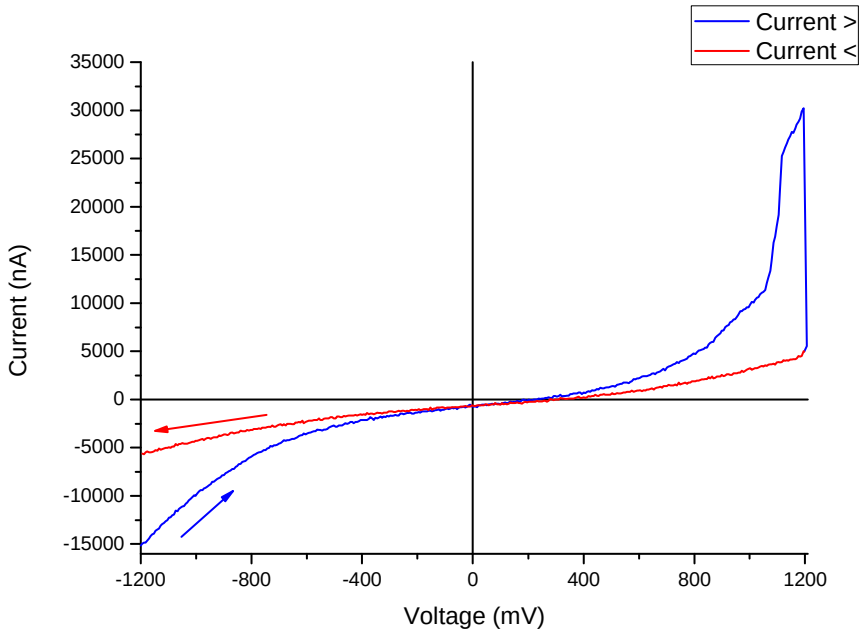

Figure 5-7. "Last" I-V curve for the wire starting at -1200 mV (blue curve), reaching 1200 mV and ending at -1200 mV (red curve). Here a sudden decrease of the current at 1200 mV corresponding to a destruction of the wire. A critical current value was 30.2 μA.

To check the chemical composition of the fiber EDXS was performed on all parts of the fiber and residual pieces (figure 5-8). It was found that the fiber consisted of 80% carbon mixed with 20% arsine. So the most probably mechanism of carbon fiber formation is that some carbon layer was present on the surface of the wire before its destruction. After big voltage was applied, arsine from the wire evaporated and indium atoms self-organized on the ends of wire and formed onion-like parts. EDXS shows that these parts (closest to the fiber) of wire consist mostly of indium (In : As = 80% : 20%). As a result, only a carbon fiber which might be a tube is left between the two pieces of the wire.

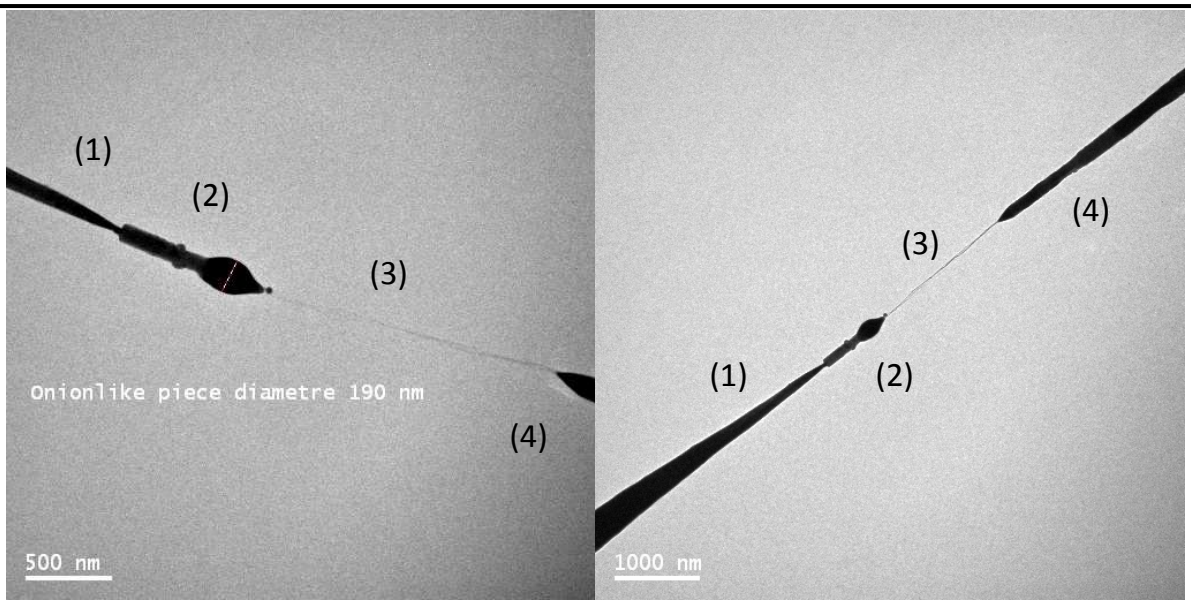

Figure 5-8. TEM images of the destroyed wire, with two different magnifications. In both pictures the tungsten tip (1) is in contact with end part of the original InAs nanowhisker (2) which is still connected to the bottom part of the InAs wire (4) with a thin carbon fiber (3).

The other parts of the original wire remain like they were before – InAs: 50% to 50%. The origin of this fiber formation may have been that the wire was heated locally to a temperature above 723 K. Possibly, the heating happened on some local defect because the rest of the wire remained unchanged. The other possible mechanism of the destruction is a diffusion of the nanowire atoms due to electron migration. An interesting point in this experiment is that the system (figure 5-8) was still conductive after the destruction. Before the contact with the tip was lost, two I-V curves were recorded and averaged (figure 5-9). The resistance has ohmic behavior in the range of -100 to 100 mV. But the resistance R_F = (2.0 ± 0.3) MOhm of the wire with the carbon fiber insert is 35 times larger ($R_{original}$ = (57 ± 5) kOhm), most likely, due to the high resistance of the wire-fiber interface resistance included serially in the wire resistance.

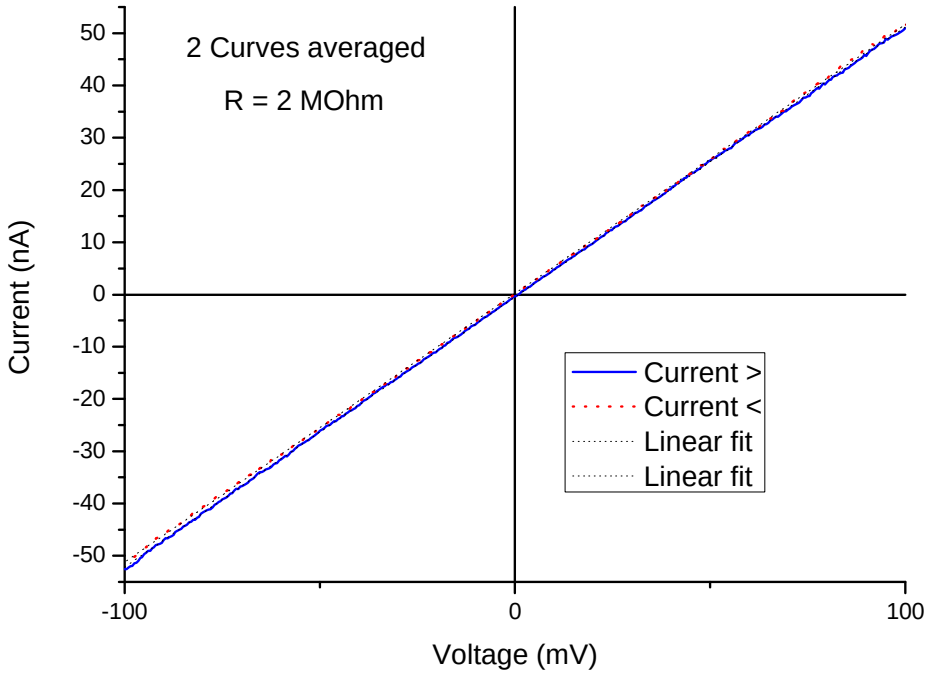

Figure 5-9. I-V curve for the tip-wire-fiber-wire system. It still has an ohmic behavior. The resistance increases 35 times against initial resistance.

Another significant experiment important for the understanding of the correlation of transport properties and mechanical strength in InAs nanowire was done with tungsten tip using the following scheme: approach tip to the wire, get a contact and improve it using the current pulses (described above), make I-V measurements without a force applied to the wire, move tip until the wire bends, make I-V measurements on the bended wire. It was found a huge difference between I-V curves of deformed and not deformed wires (figure 5-10). Almost no current flows through the deformed wire, while some current flows through the not deformed wire. The electronic structure and consequently the wire conductivity strongly influenced by lattice spacing changing during the deformation.

Here the goal was not to study the dependence of electrical properties of InAs nanowhiskers as a function of the strain. Therefore further studies in this direction were not done in this master thesis.

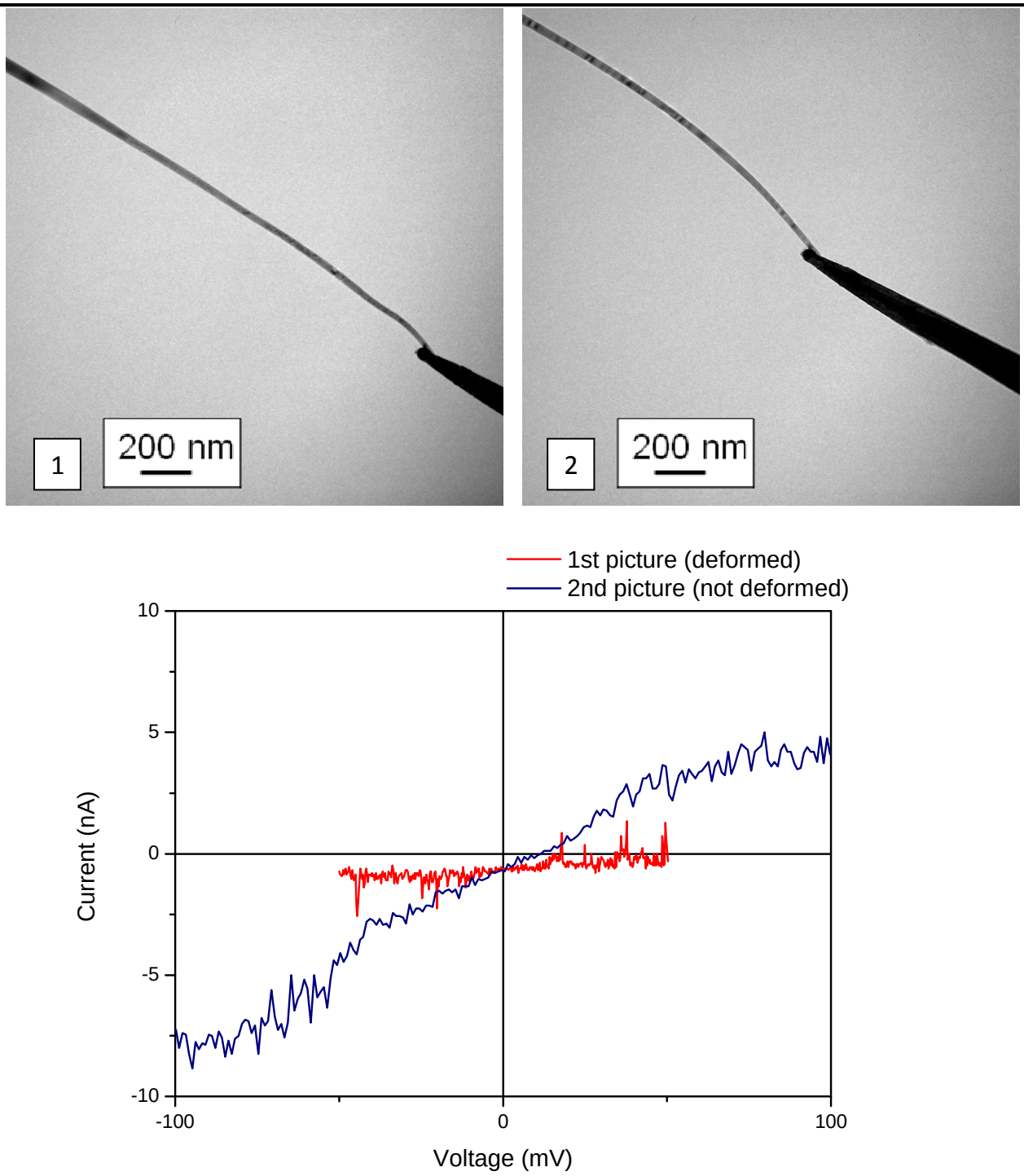

Figure 5-10. 1) TEM image of the deformed wire in contact with the STM tip. 2) TEM image of not deformed wire in contact with the STM tip. Corresponding I-V curves are shown below. There is no current through deformed wire (red line) and little current going through not deformed wire (blue line).

In this section the STM-TEM investigations of InAs nanowhiskers with tungsten tips were described. This initial test results were not suitable for a further detailed analysis due the big unknown tip-wire interface resistance and the sample

inhomogeneity. Therefore, further experiments with new uniform InAs nanowhiskers capped with gold were done and are described in the next section.

5.3 Probing an individual InAs nanowire with gold STM tip

In this part we will discuss the second series of experiments which was done with another InAs nanowhiskers sample and a gold STM tip. The new sample consisted of InAs nanowires with a uniform diameter of 50-60 nm and a gold particle on the top of each wire. The main advantage to use gold tips is that gold tips will form the low resistance contact (R_C = 2.3 Ohm approximately) with the gold particle on the top of the nanowhisker. Also as it was discussed before this kind of contact forms no oxide layer this yields ideally a zero contact resistance. Unfortunately the preparation of sharp gold tips is not easy. The etching process usually requires some luck to get a sharp tip and the preparation takes much longer time then for the tungsten tip. One has to check the tip sharpness before each experiment, then if it is not sharp make the new one, check again, then leave it in the microscope at least for four hours to prevent contaminations as described in section 3.6. Structural correlation studies were added to the experimental procedure. Selected Area Electron Diffraction was performed before the tip was approached the wire as described in previous section. Below, first results are presented for InAs nanowhiskers with a gold tip (figures 5-11, 5-12).

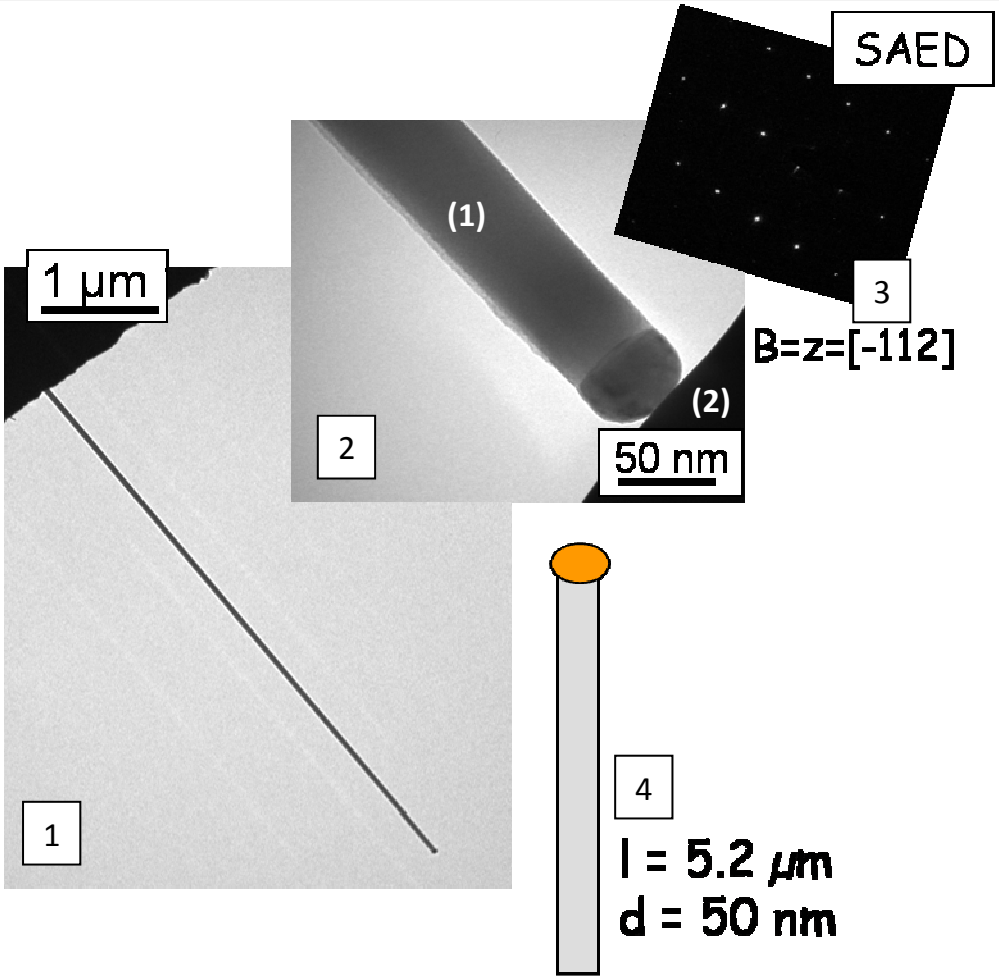

Figure 5-11. 1) InAs nanowhisker with a gold cap. 2) The wire (1) in contact with the gold tip (2). 3) Selected Area Electron Diffraction pattern: the incident electron beam is along [-112] direction and the wire has a mixed Wurtzite and Zinc-Blende atomic structure and grows along the <111> direction. This means that the wire has the third type of structure described in section 4.3. 4) Scheme of the wire and its characteristic dimensions. The wire length *l* = 5.2 µm is approximate due to the bottom part of the wire is closed by the substrate shadow.

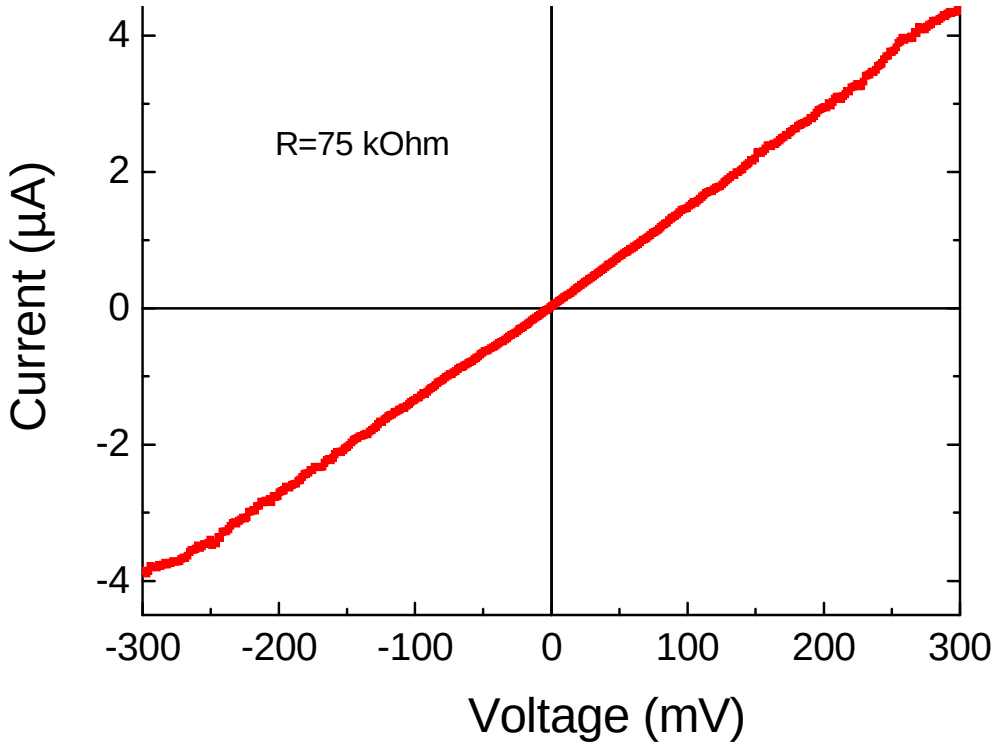

Figure 5-12. I-V curve of Au capped the InAs nanowire (figure 5-11). The linear behavior low voltage part yields a resistance of the wire and the gold particle-wire interface of 75 kOhm.

The wire has a mixed Wurtzite and Zinc-Blende atomic structure with stacking faults and rotation twin defects. A characteristic resistance of 75 kOhm was determined which is small for the 50 nm diameter wire in comparison to the first measurements (section 5.2). The result confirms the suggestion that the gold tip forms a better contact then the tungsten one.

Nevertheless, not for every wire SAED could be performed. To make this kind of structural study the electron beam of the microscope should be in the Bragg conditions means (section 2.3). For this one needs to be able to tilt the sample to get one of the crystallographic directions parallel to the beam. The STM sample holder can be tilted only in one direction which is sometimes not enough to satisfy the Bragg condition. The next experiment was made on a wire which could not be tilted into the Bragg conditions (figure 5-13).

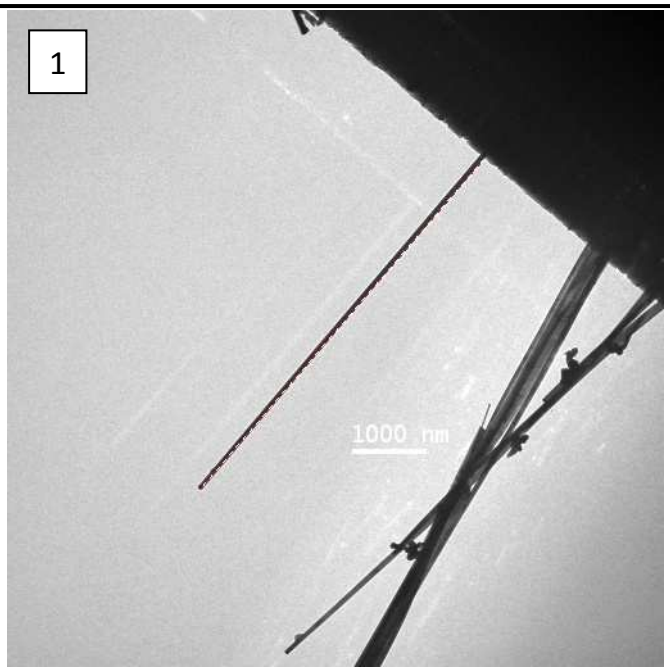

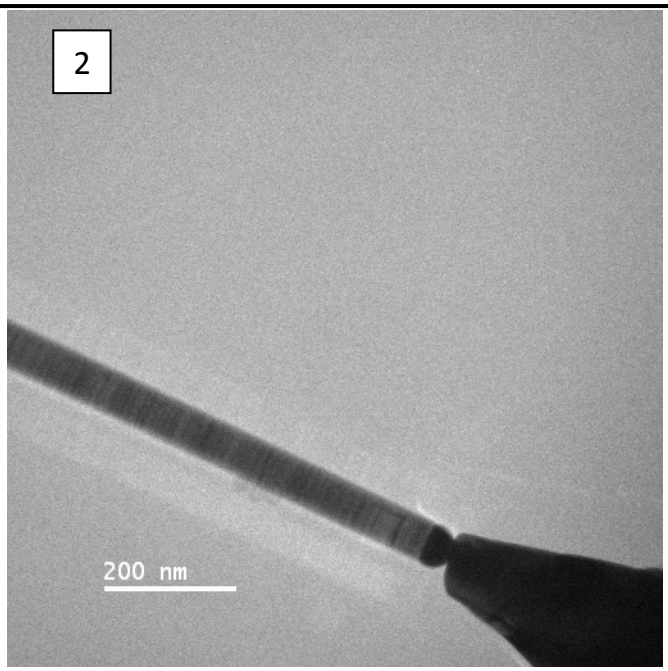

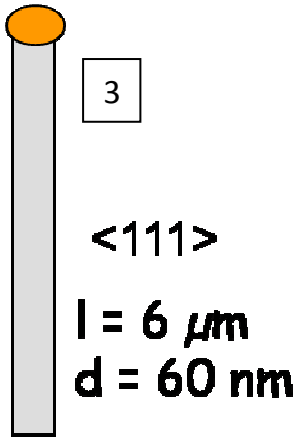

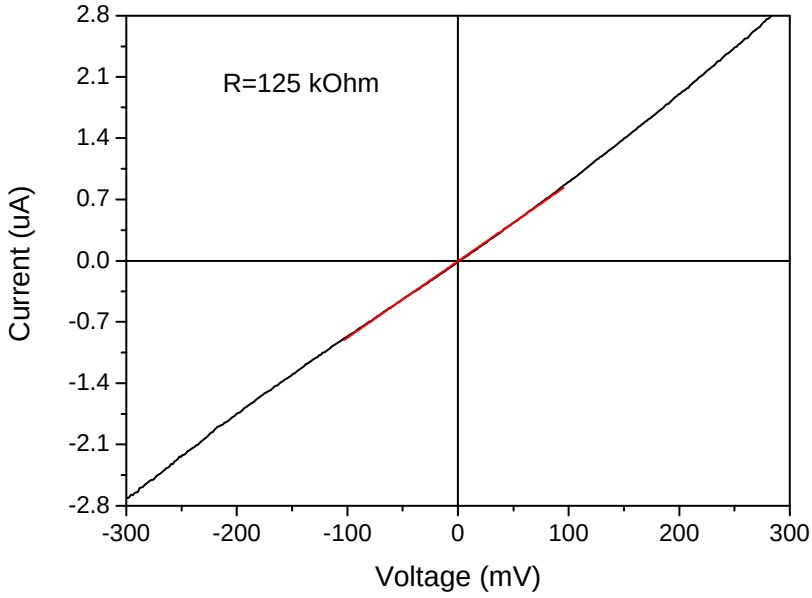

Figure 5-13. 1) The overview. 2) The wire in a contact with the gold tip. Some stripe contrast appears in the wire due to stacking-faults defects. 3) The wire growth scheme with its dimensions and 4) corresponding I-V curve The resistance value of 125 kOhm was extracted by linear fit (red line) of low voltage part of the curve between -100 mV and 100mV.

Looking at figure 5-13(2), it is should be noted that the wire show a stripe contrast. It is good evidence that stacking-faults are presented in the wire, as described in section 4.3. The nanowire has the third type of structure (Zinc-blende with Wurtzite stacking-faults). An interesting point is to compare the two last wires (figures 5-11(2)

and 5-13(2)). They both have the same structure, but on the TEM picture the first wire (figure 5-11) shows no stripe contrast. The point here is that the stripe contrast could be observed only when the beam direction nearly coincides with the <011> crystal direction. The wire for which no stripe contrast is observed could have one of the three types of structure described above in section 4.3.

In the presented section two nanowires (figures 5-11 – 5-13) with the same atomic structure were characterized. Specific resistivities are in order of several mOhms·cm, whereas, for the wires probed with tungsten tips resistivities are on the order of 0.1 Ohms·cm. It confirms that the contact with a gold tip is better than that with a tungsten tip, furthermore, this result provides a possibility to extract interface gold particle-wire resistance. The rest part of presented chapter will concern to additional experiments were made to find out different influences on the electron transport properties of InAs nanowhiskers.

5.4 Dependence of electrical properties on electron beam irradiation

The electron transport properties of InAs nanowhiskers may likely depend on the electron beam irradiation inside the TEM. All previous experiments were done with the electron beam switched off during the experiments. To study the effect of the electron beam irradiation several I-V curves were recorded with the electron beam on or off (figure 5-14). A thick nanowire growing from substrate was selected and contacted with a tungsten STM tip. The electron beam of the microscope was concentrated on the wire near the place of contact. After several I-V curves were taken (figure 5-15), afterwards the beam was switched off. Interestingly the current increased but not rapidly. It takes about a minute to achieve a constant current after the electron beam was switched off. After several minutes I-V curves “without beam” were recorded. The I-V curves show a strong increase of the resistance of the system under electron beam irradiation. There are probably several reasons for such increase of the resistance: 1) strong electrical field induced by the beam influences the band structure; 2) even local magnetic fields of the electrons can yield the change in the wire electron structure; 3) also it is possible that the nanowire was ionized by the beam which decreases the carrier concentration. To understand more particularly what really happens under the electron beam one more experiment was made on free standing tungsten tip irradiated by the electron beam. An I-V measurement was performed (figure 5-15).

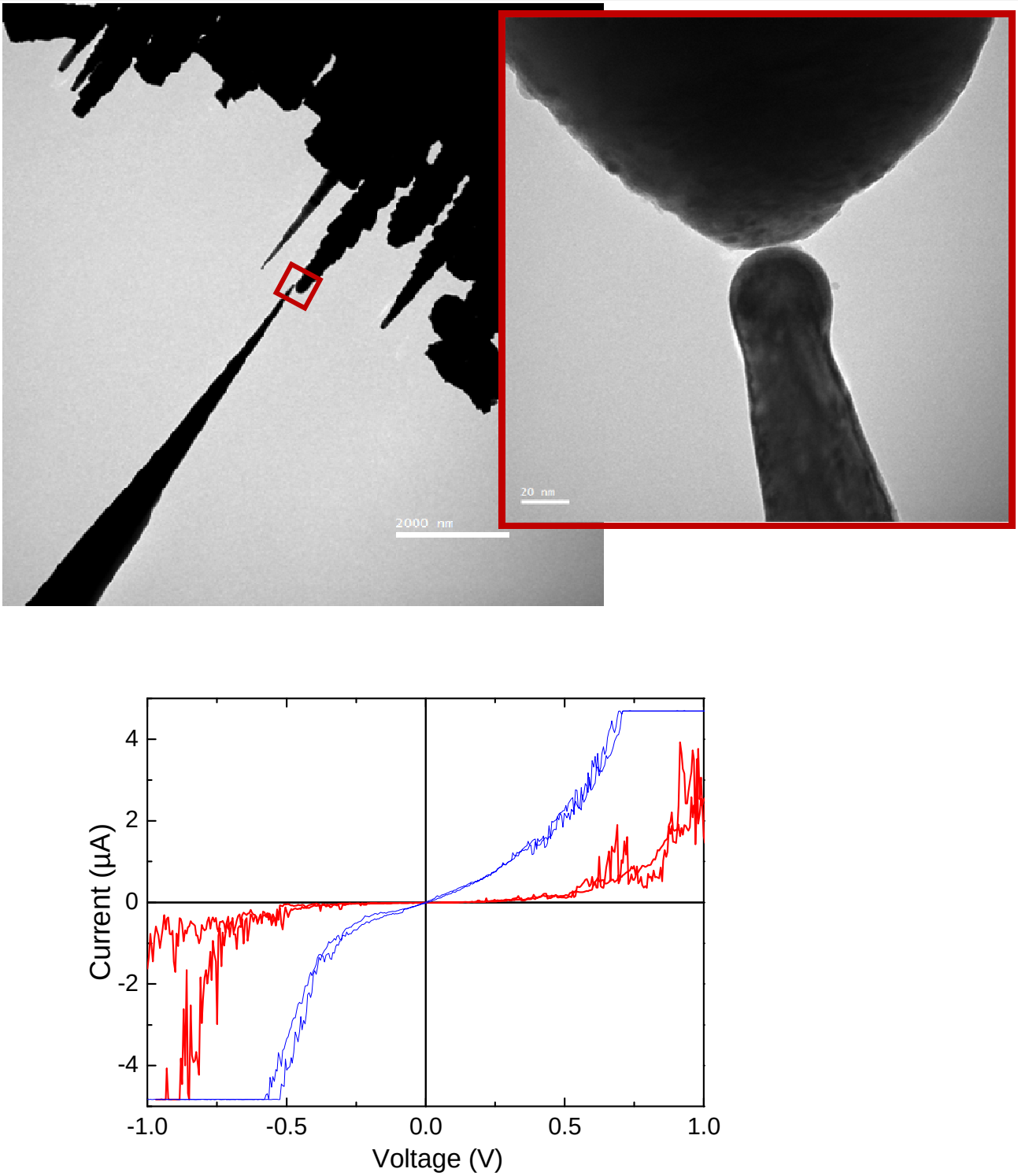

Figure 5-14. (Bottom) Dependence of the electrical properties of InAs nanowhiskers of electron beam irradiation.(Top left) Low magnification TEM image of a tungsten tip in approach to the thick InAs wire. (Top right). High magnification image of the area marked in the left picture, the tip is in contact with the wire. I-V curves under electron beam irradiation (red curve) and without the beam (blue curve) are shown in the bottom graph.

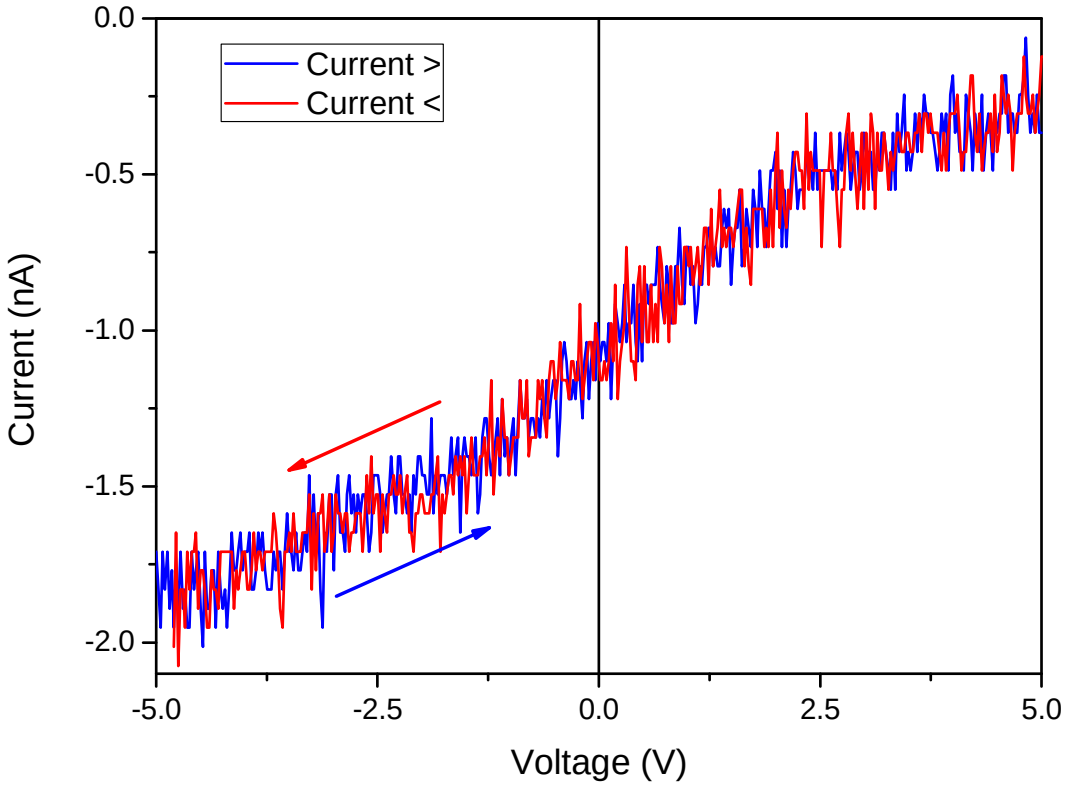

Figure 5-15. I-V measurement made with a free standing tungsten tip (several microns away from the sample) under high energy (120 keV) electron beam irradiation. The bias voltage was first increased from -5V to 5V (blue curve) and then decreased (red curve). No hysteresis was found. Curves have a non-linear and non-symmetric behavior and maximal current is about -2nA.

The I-V curve of the tungsten tip irradiated by the electron beam shows that a small negative current (about -2 nA) flows through the tip for positive as well as negative bias voltage and it is increasing with voltage increase. The reason for this effect can be in charging of the sample under electron beam irradiation.

5.5 Dependence of electrical properties on an applied magnetic field.

For future experiments it was necessary to determine how a magnetic field changes the resistivity of the InAs nanowires. In theoretical work on InAs nanowires magnetoconductivity oscillations were predicted [80]. Here a first test experiment with presence of magnetic field was performed (figure 5-16). The wire sample was installed and the previously described procedure was used to establish a contact between the tip and the wire.

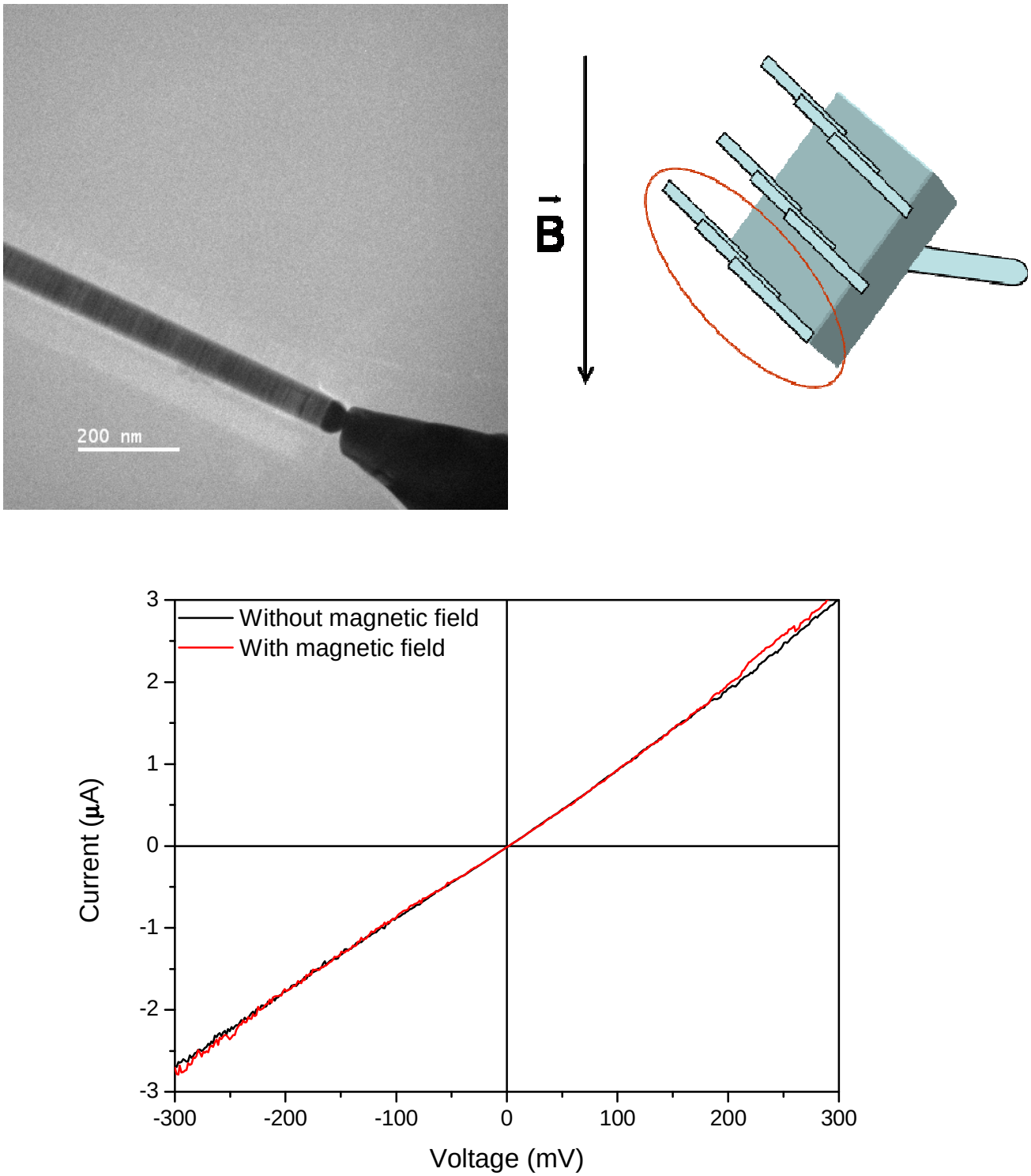

Figure 5-16. Magnetic field dependent experiment with InAs nanowires. TEM image of the wire in contact with a gold tip (left picture). Scheme of magnetic field applied (right picture). Two I-V curves are on the graphic. Black curve corresponds to lowest magnetic field (ca 700 Gauss). Red one corresponds to the biggest magnetic field applied (ca 1 Tesla). The curves couldn't be distinguished. Perhaps, no effect was found due to a huge error of the current measurement.

The microscope was switched to the low magnification mode in which the magnetic field of the objective lens system is about 700 Gauss in the sample area. Under these conditions several I-V Curves were recorded. After this, the microscope was switched to the medium magnification mode in which the magnetic field is about 1 Tesla. Several I-V curves were taken. These two cases (0.07 and 1 Tesla) could not be distinguished within the experiment error bar. Perhaps, if some magnetic effect existed in the wires it is not possible to determine it due to of large current error of about 4 nA (for current range 5 uA). Also it is possible that the effect is observable only at low temperatures, whereas the experiment was done at the room temperature.

In the following chapter these experimental observations will be discussed.

Chapter 6. Discussion

6.1 Achieving quantitative information on InAs nanowires.

To obtain quantitative information from the experimental data (chapter 5) the following model is suggested. In the case of the nanowires grown epitaxially on the substrate the resistance of the interface between wire and substrate is negligibly small. The resistance of the InAs-gold particle interface is supposed to be ohmic, since the I-V curves are symmetric. Under these conditions the InAs nanowire can be described as two ohmic resistances in series – the wire resistance and the gold-InAs interface resistance. The last interface resistance is inversely related to the area of the interface [67]. On the other hand the wire resistance is proportional to the length of the wire and inversely proportional to the cross-sectional area. In this case the measured resistance is given by the following expression:

$$R = \frac{\rho \cdot l}{A} + \frac{R_{[]}}{A},$$

where ρ is the resistivity of the InAs wire, l is the wire length, A is the cross-section area of the interface, $R_{[]}$ is a specific contact resistance. This resistance possibly depends on the thickness of the nanowire. It means that to extract the resistivity and the contact resistance the best way is to use the so called Transfer Length Measurement. This method was developed to determine the contact resistance of semiconductors by making two point contacts and varying only the length of the wire in between. In this case the dependence of the resistance (normalized to the cross-section) versus the wire length will give the specific contact resistance at the intercept with length axis. The slope is the wire resistivity. Unfortunately, in our experiments quantitative information could not be obtained due to problems with the determination of the wire length. In the TEM experiments the wires are orientated on the substrate with some angle to the electron beam. The picture in the TEM forms a 2-dimensional projection on the screen (figure 6-1). Thus on the image we can see the edge of the substrate and the wires growing near the edge but the bottom of the wires is not visible due to the substrate shadow. To solve the problem one should mark the wire with gold from the tip and then measure its length in the SEM. Unfortunately this method could not be realized in this master thesis (chapter 5). The failure motivates to develop another method which general idea is to image

with the secondary electron detector of the microscope which is situated above the sample and measure the length of the wire.

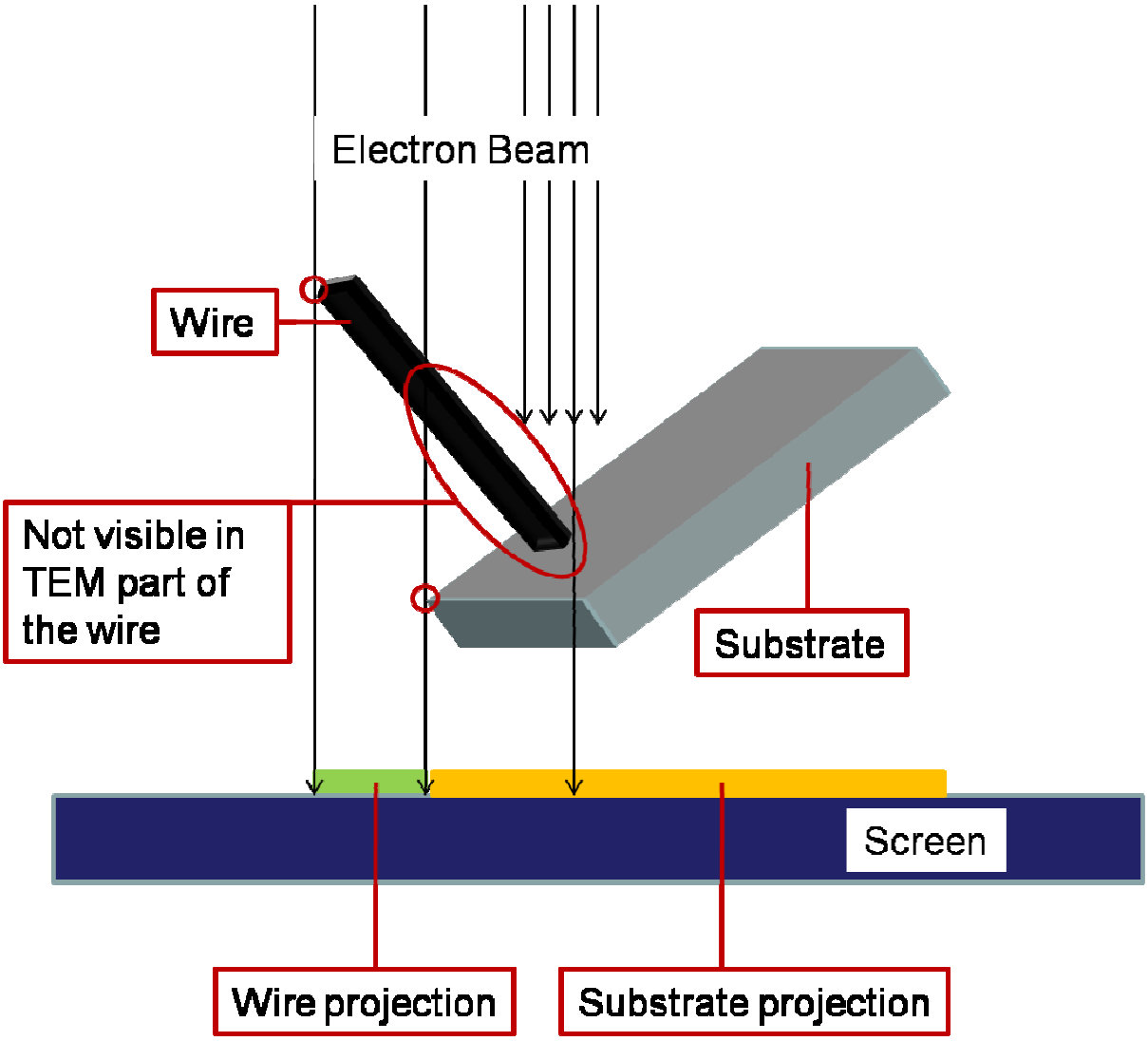

Figure 6-1. Scheme for the formation of an TEM image. The electron beam images the projection of the wire and the substrate onto the screen. A part of the wire between its base and the substrate edge is not visible because of the substrate shadow.

6.2 Summary of the experimental data.

As a result of the experiments presented here (chapter 5) we concluded that InAs nanowires in the low bias voltage range show ohmic behavior (figure 5-12). This is most probably due to the effect of pinning of the Fermi level at the surface into conduction band and the formation of a 2 dimensional electron gas (section 2.2). When higher bias voltages are applied distortions of the linearity of the I-V curves characteristics were found (figure 5-13). They appear most probably due to the ohmic

heating of the wires, which have a very strong temperature dependence of the conductivity near room temperature. To study this effect more precisely one needs to know the heat dissipation in the wires. Up to now we considered two possible reasons of such a distortion: first, the presence of the defects which gives additional electron levels. The electrons from these levels could be excited by increasing the bias voltage and give an addition to the current. Second mechanism is, nevertheless, the formation of a Schottky barrier between the InAs nanowire and the gold cap and another Schottky barrier between the InAs substrate and silver glue which connects the substrate to a copper wire (figure 5.2). Using the low voltage part of the I-V data (from -200 mV to 200 mV) the resistances of the wires were obtained. All the experimental data concerning to resistivity of the wires are summarized and given in table 6-2.

Wire, contact	Tip material	Direction of growth	Resistivity, Ohm·cm	Diameter, nm
1	W	?	**< 5.2**	19-85
2, 1	W	?	**< 0.8**	175-580
2, 2	W	?	**< 0.47**	175-560
3	W	?	**< 0.25**	156-518
4	W	?	**< 0.17**	7-150
5	Au	111	**< 2.8 e-3**	50 ± 1
6	Au	111	**< 5.9 e-3**	60 ± 1
Bulk, intrinsic	-	-	**0.16**	-
Typical, 4point	-	100	**0.88 e-3**	40

Table 6-2. Table of experimental data of InAs nanowires. The resistivity given is maximal estimation with an error of 40% in the wire length measurements. Also there was no structural analysis done for the first series of experiments with the tungsten tip. The typical four point measurement value is adopted from article [18].

The resistivity with the same order of magnitude can be divided into three groups (marked with different colors in table 6-2). The first group consists of the first wire data (section 5.2; marked with red color in the table). The second consists of the second, third and fourth wires data (section 5.2; marked with green color in the table). And the third contains the data obtained with the gold STM tip (fifth and sixth wires; section 5.3; marked with blue color in the table). The first group contains the largest resistivity value which looks unreasonable and most probably is the result of the low quality of the wire to tip contact. The values in the second group are two orders of magnitude larger than in the third group. It seems to be a result of the formation of a Schottky barrier formation between the tungsten tip and the InAs nanowires resulting in an increase of the resistances. The values in the third group are in a good agreement with the measurements performed on the InAs nanowires before. One can conclude that the resistivity of the wires with mixed Wurtzite and Zinc Blende atomic structures (the <111> growth direction) is above the resistivity of the pure Wurtzite wires (the <100> growth direction). This effect arises due to the stacking fault defects in the <111> nanowires.

A huge dependence of the transport properties of the wires on the deformation was also found. The effect is a product of changing the lattice spacing of the InAs crystal and consequent change of the band structure.

The transport properties of the nanowires also depend on the electron beam irradiation – the irradiated wire shows less conductivity than non-irradiated one. It is supposed that electric field of the electron beam influences the band structure strongly, increasing the band gap.

Chapter 7. Conclusions

A novel experimental method combining STM and TEM techniques was presented in the master thesis. The method is suited to study correlations of transport and structural properties of a single nanoscale object. Preparations of the STM tips, the samples and the whole setup were described.

The aim of the thesis was to study structural correlations of transport properties of InAs nanowhiskers grown by the MOCVD method in the VLS approach. Simultaneous structural and electrical observations were done on the nanowires. The structure was studied by SAED method in the TEM. The electrical characterization was made in-situ using different tip materials with a NanoFactory STM-TEM sample holder. The I-V curves for the InAs nanowires were recorded and analysed (chapter 5). Also with the STM-TEM technique the dependence of transport properties on electron beam irradiation and sample deformation was studied. As a result the resistivity values for the wires were estimated (table 6-2). Comparing experimental results with the bulk resistivity value and the values provided in literature, we concluded that:
1) the STM gold tip is more suitable for study the InAs nanowhiskers with a gold cap;
2) the interface gold - InAs wire plays an important role in the electron transport;
3) the InAs nanowires with mixed Wurtzite and Zinc Blende crystal structure have smaller conductivity than the wires with pure Zinc Blende structure. From my experiments no evidence for a magnetoresistance effect in the wires was found at room temperature. However, in future more detailed studies on transport properties of InAs nanowhiskers may be done including magnetoresistance measurements at different temperatures and strain dependent transport measurements.

Acknowledgments

In conclusion I would like to thank all the people who were involved in the work:

- Dipl.-Phys. Andrey Lysov and the members of the group of Prof. Tegude for the samples and discussions.
- Dipl.-Phys. Johanes Schaffert, Dipl.-Phys. Hatice Karacuban, Dipl.-Phys. Alexander Bernhart for help with the STM preparations.
- Dr. Ralf Theissmann for discussions.

Also great thanks for all the people from the group of Prof. Farle who helped me during the work:

- Dmitry Tyutyunnikov for the help with the Hall sensor calibration.
- Dipl.-Phys. Igor Barsukov for the Hall sensor.
- Dipl.-Ing. Horst Zähres and Hans Dieter Schädel for the help with solving the technical problems.
- Dipl.-Phys. Christian Wirtz and Dipl.-Phys. Oliver Posth for the help with the SEM measurements.
- Dr. Zi-An Li for the help with the TEM analysis.
- Dr. Marina Spasova for help with the TEM analysis, coordination and discussion.
- Prof. Dr. Michael Farle for the coordination, discussion and supervision.
- All other members of the group for presence and outgoingness.

Bibliography

1. *Applied physics: Tunable supercurrent through semiconductor nanowires.* **Doh, Y.-J., Van Dam, J.A., Roest, A.L.** 2005, Science, Vol. 309, pp. 272-275.

2. *Superconducting proximity effect in the native inversion layer on InAs.* **Takayanagi, H., Kawakami, T.** 22, 1985, Physical Review Letters, Vol. 54, pp. 2449-2452.

3. *Single-crystal n-InAs coupled Josephson junction.* **Kawakami, T., Takayanagi, H.** 1985, Applied Physics Letters, Vol. 46, pp. 92-94.

4. *Electrical manipulation of magnetization reversal in a ferromagnetic semiconductor.* **Chiba, D., Yamanouchi, H., Hatsukura, F.** 2003, Science, Vol. 301, pp. 943-945.

5. *Magnetotransport properties of p-type (In,Mn)As diluted magnetic III-V semiconductors.* **Ohno, H., Munekata, H., Penney, T.** 1992, Physical Review Letters, Vol. 68, pp. 2664-2667.

6. *Lateral correlation of InAs/AlInAs nanowire superlattices on InP(001).* **Li, H., Daniels-Race, T., Hasan, M.-A.** 2001, Journal of Vacuum Science and Technology B: Microelectronics and Nanometer Structures, Vol. 19, pp. 1471-1474.

7. *Growth of nanowire superlattice structures for nanoscale photonics and electronics.* **Gudiksen, M.S., Lauhon, L.J., Wang, J.** 2002, Nature, Vol. 415, pp. 617-620.

8. *Positively charged defects associated with self-assembled quantum dot formation.* **Belyaev, A.E., Stoddart, S.T., Main, P.M.** 2000, Appl. Phys. Lett., Vol. 76, p. 3570.

9. *Epitaxial growth of InP nanowires on germanium.* **Bakkers, E.P., van Dam, J.A., De Franceschi, S.** 2004, Nature materials, Vol. 3, pp. 769-773.

10. *Determination of the epitaxial growth of zinc oxide nanowires on sapphire by grazing incidence synchrotron x-ray diffraction.* **Campos, L.C., Dalal, S.H., Baptista, D.L.** 2007, Appl. Phys. Lett., Vol. 90, pp. 181929-181931.

11. *Electronic structure of GaN nanowire studied by x-ray-absorption spectroscopy and scanning photoelectron microscopy.* **Chiou, J.W., Jan, J.C., Tsai, H.M.** 2003, Applied Physics Letters, Vol. 82, pp. 3949-3951.

12. *Chemistry and physics in one dimension: Synthesis and properties of nanowires and nanotubes.* **Hu, J., Odom, T.W., Lieber, C.M.** 1999, Accounts of Chemical Research, Vol. 32, pp. 435-445.

13. *One-dimensional nanostructures: Synthesis, characterization, and applications.* **Xia, Y., Yang, P., Sun, Y.** 2003, Advanced Materials, Vol. 15, pp. 353-389.

14. *Role of molecular surface passivation in electrical transport properties of InAs nanowires .* **Hang, Q., Wang, F., Carpenter, P.D.** 2008, Nano Letters, Vol. 8, pp. 49-55.

15. *Sulfur passivation for ohmic contact formation to InAs nanowires .* **Suyatin, D.B., Thelander, C., Björk, M.T.** 2007, Nanotechnology, Vol. 18, art. no. 105307 .

16. *Scanned electrical probe characterization of carrier transport behavior in InAs nanowires .* **Zhou, X., Dayeh, S.A., Aplin, D.** 2006, Journal of Vacuum Science and Technology B, Vol. 24, pp. 2036-2040 .

17. **Lysov, A., Gutsche, C., Regolin, I., Prost, W., Tegude, F.-J.** *Privat communication.* 2008.

18. *Probing of Individual Semiconductor Nanowhiskers by TEM-STM.* **Larsson, M.W., Wallenberg, L.R., Persson, A.I.** 2004, Microscopy and Microanalysis, Vol.10, pp. 41-46

19. **Mikhailova, M.P.** [book auth.] M. ,Rumyantsev, S., Shur, M. Levinshtein. *Handbook Series on Semiconductor Parameters, vol.1.* London : s.n., 1996.

20. *Charge accumulation at InAs surfaces.* **Olsson, L.Ö., Andersson, C.B.M., Håkansson, M.C.** 1996, Physical Review Letters, Vol.76, pp. 3626-3629 .

21. *Fermi level position at metal-semiconductor interfaces.* **Mead, C.A., Spitzer, W.G.** 1964, Physical Review, Vol. 134, pp. A713-A716.

22. *Schottky barrier height of n-InGaAs diodes.* **Kajiyama, K., Mizushima, Y., Sakata, S.** 1973, Applied Physics Letters, Vol. 22 pp. 458-459.

23. *Observation of Surface Bound State and Two-Dimensional Energy Band by Electron Tunneling.* **Tsui, D.C.** 1970, Physical Review Letters, Vol.24, pp. 303-306.

24. *Observation of Landau levels at the InAs(110) surface by scanning tunneling spectroscopy.* **Wildöer, J.W.G., Harmans, C.J.P.M., Van Kempen, H.** 1997, Physical Review B, Vol. 55, pp. R16013-R16016.

25. *Imaging of friedel oscillation patterns of two-dimensionally accumulated electrons at epitaxially grown InAs(111)A surfaces.* **Kanisawa, K., Butcher, M.J., Yamaguchi, H.** 2001, Physical Review Letters, Vol. 86, pp. 3384-3387.

26. *Electron accumulation layer on clean In-terminated InAs(0 0 1)(4 × 2)-c(8 × 2) surface.* **De Padova, P., Quaresima, C., Perfetti, P.** 2001, Surface Science, Vol. 482-485, pp. 587-592.

27. *Intrinsic electron accumulation layers on reconstructed clean InAs (100) surfaces.* **Noguchi, M., Hirakawa, K., Ikoma, T.** 1991, Physical Review Letters, Vol. 66, pp. 2243-2246.

28. *Adsorption of chlorine and oxygen on cleaved InAs(110) surfaces: Raman spectroscopy, photoemission spectroscopy, and Kelvin probe measurements.* **Smit, K., Koenders, L., Monch, W.** 1989, J. Vac. Sci. Technol. B, Vol. 7, p. 888.

29. *Virtual gap states and Fermi level pinning by adsorbates at semiconductor surfaces.* **Monch, W.** 1986, J. Vac. Sci. Technol. B, Vol. 4, p. 1085.

30. *Tight-Binding Model of Surface Donor-States Induced by Metal Adatoms on GaAs(110) Surfaces.* **Monch, W.** 1988, Europhys. Lett., Vol. 7, p. 275.

31. *Chemical and electronic properties of sulfur-passivated InAs surfaces.* **Petrovykh, D.Y., Yang, M.J., Whitman, L.J.** 2003, Surface Science, Vol. 523, pp. 231-240.

32. *Chalcogenide passivation of III-V semiconductor surfaces.* **Bessolov, V.N., Lebedev, M.V.** 1998, Semiconductors, Vol.32, pp. 1141-1156.

33. *Size, position and direction control on GaAs and InAs nanowhisker growth .* **Shimada, T., Hiruma, K., Shirai, M.** 1998, Superlattices and Microstructures, Vol. 24, pp. 453-458 .

34. *Formation of InAs wires and dots on vicinal GaAs (110) surfaces with giant steps by molecular beam epitaxy .* **Torii, Satoshi, Shim.** 1997, Japanese Journal of Applied Physics, Vol.36 pp. L1645-L1647 .

35. *Formation and characterization of GaAs quantum wires at giant step edges on vicinal (110) GaAs surfaces.* **Takeuchi, Misaichi, Shiba.** 1995, Japanese Journal of Applied Physics, Vol.34, pp. 4411-4413.

36. *Step structures during MBE growth of GaAs and AIGaAs films on vicinal GaAs(110) surfaces inclined toward (111)B.* **Hasegawa, S., Kimura, K., Sato, M.** 1992, Surface Science, Vol. 267, pp. 5-7.

37. *InAs nanowires and whiskers grown by reaction of indium with GaAs .* **He, M., Fahmi, M.M.E., Mohammad, S.N.** 2003, Applied Physics Letters, Vol. 82, pp. 3749-3751.

38. *Fabrication of GaAs and InAs wires in nanochannel glass.* **Berry, A.D., Tonucci, R.J., Fatemi, M.** 1996, Applied Physics Letters, Vol. 69, pp. 2846-2848.

39. *Synthesis of semiconductor nanowires by annealing.* **Zhi, C.Y., Bai, X.D., Wang, E.G.** 2004, Applied Physics Letters, Vol. 85, pp. 1802-1804.

40. *Crystal structure change of GaAs and InAs whiskers from zinc-blende to wurtzite type.* **Koguchi, Masanari, Kakibayashi.** 1992, Japanese Journal of Applied Physics, Vol. 31, pp. 2061-2065.

41. *Evidence of stacking-fault distribution along an InAs nanowire using micro-focused coherent X-ray diffraction .* **Chamard, V., Stangl, J., Labat, S.** 2008, Journal of Applied Crystallography, Vol. 41, pp. 272-280 .

42. *Lamellar twinning in semiconductor nanowires.* **Davidson III, F.M., Lee, D.C., Fanfair, D.D.** 2007, Journal of Physical Chemistry C, Vol. 111, pp. 2929-2935.

43. **Lind E., Persson M., Niquet Y.-M.** Band Structure effects on the scaling properties of [111] InAs nanowire MOSFETs. *IEEE Transactions on electron devices.* 2009, Vol. 56, 2, pp. 201-205.

44. **Persson M. P., Xu H. Q.** Electronic structure of [100]-orientated free-standing InAs and InP naqnowires with square and rectangular crossections. *Phys. Rev. B.* 2006, Vol. 73, 12, pp. 1-9.

45. *Direct Atomic Scale Imaging of III−V Nanowire Surfaces.* **Hilner, E., Håkanson, U., Fröberg, L. E., Karlsson, M.** 2008, Nano Letters, Vol. 8, pp. 3978–3982.

46. *Growth, structural and optical properties of III-V nanowires for optoelectronic applications.* **Joyce, H.J., Gao, Q., Kim, Y.** 2007, 2007 7th IEEE International Conference on Nanotechnology, Proceedings, pp. 866-869.

47. *Nanoscale science and technology: Building a big future from small things.* **Lieber, C.M.** 2003, MRS Bulletin, Vol. 28, pp. 486-491.

48. *Nanowire-based one-dimensional electronics.* **Thelander, C., Agarwal, P., Brongersma, S.** 2006, Materials Today, Vol. 9, pp. 28-35.

49. *Highly polarized photoluminescence and photodetection from single indium phosphide nanowires.* **Wang, J., Gudiksen, M.S., Duan, X.** 2001, Science, Vol. 293, pp. 1455-1457.

50. *Nanowires for integrated multicolor nanophotonics.* **Huang, Y., Duan, X., Lieber, C.M.** 2005, Small, Vol. 1 pp. 142-147.

51. *Fabrication, optical characterization and modeling of strained core-shell nanowires .* **Zanolli, Z., Fröberg, L.E., Björk, M.T.** 2006, Thin Solid Films, Vol. 515 pp. 793-796.

52. *Combined thermoelectric and structure characterizations of patterned nanowires.* **Mavrokefalos, A., Pertes, M.T., Saha, S.** 2006, International Conference on Thermoelectrics, ICT, Proceedings, pp. 234-237.

53. *Phonon conductivity of InAs.* **Le Guillou, G., Albany, H.J.** 1972, Physical Review B, Vol. 5, pp. 2301-2308.

54. *Optimal control over the InAs nanowire growth for system integration and their structural and transport properties.* **Dayeh, S.A., Susac, D., Chen, P.** 2008, 2008 8th IEEE Conference on Nanotechnology, pp. 576-579 .

55. *High electron mobility InAs nanowire field-effect transistors .* **Dayeh, S.A., Aplin, D.P.R., Zhou, X.** 2007, Small, Vol. 3, pp. 326-332.

56. **Dayeh S.A., Yu E. T., Wang D.** Transport coefficients of InAs Nanowires as a functio of Diameter. *Small.* 2009, Vol. 5, 1, pp. 77-81.

57. *Direct observation of ballistic and drift carrier transport regimes in InAs nanowires .* **Zhou, X., Dayeh, S.A., Aplin, D.** 2006, Applied Physics Letters, Vol. 89 art. no. 053113 .

58. **Wiesendanger, R.** *Scaning probe microscopy: methods and applications.* Cambridge : Cambridge University Press, 1994.

59. *Cross-sectional scanning tunneling microscopy studies of novel III-V semiconductor structures.* **Mikkelsen, A., Lundgren, E.** 2005, Progress in Surface Science, Vol. 80, pp. 1-25.

60. **Watt, Ian M.** *The priciples and practice of electron microscopy.* Cambridge : Cambridge University Press, 1997.

61. **Weirich T., Labar J., Zou X.** *Electron Crystallography.* s.l. : Springer, 2006.

62. **Grundy P.J., Jones G.A.** *Electron microscopy in the study of materials.* London : Edward Arnold, 1976.

63. **Williams D. B. and Carter C. B.** *Transmission Electron Microscopy*. New York. Springer, 1996.

64. **Guentherodt H.-J., Wiesendanger, R.** *Scanning Tunneling Microscopy I.* Berlin : Springer-Verlag, 1992.

65. **Julian Chen, C.** *Introduction to Scanning Tunneling Microscopy.* NY : Oxford University Press, 1993.

66. **Dwayne Miller, R.J., Mizes H.A., Samsavar A.** *Instructional Scanning Tunneling Microscope, Workbook.* NY : Burleigh Instruments, Inc., 1992.

67. **Slade, Paul G.** *Elecrical Contacts: Principles and Application.* New York : CRC Press, 1999.

68. **Timsit, Roland S.** Electrical contact resistance: properties of stationary interfaces. *IEEE transaction on components and packagingtechnology.* 1999, Vol. 22, 1, pp. 85-98.

69. **Timsit, Roland S.** Electrical conduction through small contact spots. *IEEE Transaction on components and packaging technologies.* 2006, Vol. 29, 4, pp. 727-734.

70. **Y.V., Sharvin.** *Sov. Phys.* 1965, Vol. 21, p. 655.

71. **Wang, F.** *Introduction to solid state electronics.* Amsterdam : Elsiver Science Publishers, 1989.

72. **Balkanski, M., Wallis, R.** *Semiconductor Physics and Applications.* Oxford : Oxford University Press, 2000.

73. *The art and science and other aspects of making sharp tips.* **Melmed, A., J.** 1991, Journal of Vacuum Science & Technology B, Vol. 9, pp. 601-608.

74. *Very sharp gold and platinum tips to modify gold surfaces in scanning.* **Libioulle, L., Houbion, Y., Gilles, J.-M.** 1995, J. Vac. Sci. Technol. B, Vol. 13, pp. 1325-1331.

75. **Schaffert, J., Karacuban, H.** *Privat communication.* 2008.

76. **Grovenor, C.** *Microelectronic materials.* CRC Press, 1989.

77. *High transconductance MISFET with a single InAs nanowire channel.* **Do, Q.-T., Blekker, K., Regolin, I., Prost, W., Tegude, F. J.** 2007, IEEE electron device letters, Vol. 28, pp. 682-684.

78. **Ernst, F., Rühle, M.** *High-Resolution Imaging and Spectrometry of Materials.* Verlag, Berlin, Heidelberg : Springer, 2003.

79. *Quantitative Energy-Filtering Transmission Electron Microscopy (EFTEM).* **Hofer, F., Grogger, W., Warbichler, P., Papst, I.** 2000 Mikrochim. Acta, Vol. 132, pp. 273-288.

80. *Magnetoconductance oscillations in quasiballistic multimode nanowires.* **Tserkovnyak, Y., Halperin, B.** 2006, Physical Review B, Vol. 74, art. no. 245327